About Entrez
Text Version

Entrez PubMed
Overview
Help | FAQ
Tutorial
New/Noteworthy
E-Utilities

PubMed Services
Journals Database
MeSH Database
Single Citation Matcher
Batch Citation Matcher
Clinical Queries
Special Queries
LinkOut
My NCBI (Cubby)

Related Resources
Order Documents
NLM Catalog
NLM Gateway
TOXNET
Consumer Health
Clinical Alerts
ClinicalTrials.gov
PubMed Central

1: Prog Retin Eye Res. 2003 Jan;22(1):1-29. Related Articles, Links

Vascular endothelial growth factors and angiogenesis in eye disease.

Witmer AN, Vrensen GF, Van Noorden CJ, Schlingemann RO.

Ocular Angiogenesis Group, Department of Ophthalmology, University of Amsterdam, Amsterdam, The Netherlands.

The vascular endothelial growth factor (VEGF) family of growth factors controls pathological angiogenesis and increased vascular permeability in important eye diseases such as diabetic retinopathy (DR) and age-related macular degeneration (AMD). The purpose of this review is to develop new insights into the cell biology of VEGFs and vascular cells in angiogenesis and vascular leakage in general, and to provide the rationale and possible pitfalls of inhibition of VEGFs as a therapy for ocular disease. From the literature it is clear that overexpression of VEGFs and their receptors VEGFR-1, VEGFR-2 and VEGFR-3 is causing increased microvascular permeability and angiogenesis in eye conditions such as DR and AMD. When we focus on the VEGF receptors, recent findings suggest a role of VEGFR-1 as a functional receptor for placenta growth factor (PlGF) and vascular endothelial growth factor-A (VEGF)-A in pericytes and vascular smooth muscle cells in vivo rather than in endothelial cells, and strongly suggest involvement of pericytes in early phases of angiogenesis. In addition, the evidence pointing to distinct functions of VEGFs in physiology in and outside the vasculature is reviewed. The cellular distribution of VEGFR-1, VEGFR-2 and VEGFR-3 suggests various specific functions of the VEGF family in normal retina, both in the retinal vasculature and in neuronal elements. Furthermore, we focus on recent findings that VEGFs secreted by epithelia, including the retinal pigment epithelium (RPE), are likely to mediate paracrine vascular survival signals for adjacent endothelia. In the choroid, derailment of this paracrine relation and overexpression of VEGF-A by RPE may explain the pathogenesis of subretinal neovascularisation in AMD. On the other hand, this paracrine relation and other physiological functions of VEGFs may be endangered by therapeutic VEGF inhibition, as is currently used in several clinical trials in DR and AMD.

Design, Synthesis, and Evaluations of Substituted 3-[(3- or 4-Carboxyethylpyrrol-2-yl)methylidenyl]indolin-2-ones as Inhibitors of VEGF, FGF, and PDGF Receptor Tyrosine Kinases

Li Sun,* Ngoc Tran, Congxin Liang, Flora Tang, Audie Rice, Randall Schreck, Kara Waltz, Laura K. Shawver, Gerald McMahon, and Cho Tang*

SUGEN, Inc., 230 East Grand Avenue, South San Francisco, California 94080-4811

Received August 23, 1999

Receptor tyrosine kinases (RTKs) have been implicated as therapeutic targets for the treatment of human diseases including cancers, inflammatory diseases, cardiovascular diseases including arterial restenosis, and fibrotic diseases of the lung, liver, and kidney. Three classes of 3-substituted indolin-2-ones containing propionic acid functionality attached to the pyrrole ring at the C-3 position of the core have been identified as catalytic inhibitors of the vascular endothelial growth factor (VEGF), fibroblast growth factor (FGF), and platelet-derived growth factor (PDGF) RTKs. Some of the compounds were found to inhibit the tyrosine kinase activity associated with isolated vascular endothelial growth factor receptor 2 (VEGF-R2) [fetal liver tyrosine kinase 1 (Flk-1)/kinase insert domain-containing receptor (KDR)], fibroblast growth factor receptor (FGF-R), and platelet-derived growth factor receptor (PDGF-R) tyrosine kinase with IC_{50} values at nanomolar level. Thus, compound **1** showed inhibition against VEGF-R2 (Flk-1/KDR) and FGF-R1 tyrosine kinase activity with IC_{50} values of 20 and 30 nM, respectively, while compound **16f** inhibited the PDGF-R tyrosine kinase activity with IC_{50} value of 10 nM. Structural models and structure−activity relationship analysis of these compounds for the target receptors are discussed. The cellular activities of these compounds were profiled using cellular proliferation assays as measured by bromodeoxyuridine (BrdU) incorporation. Specific and potent inhibition of cell growth was observed for some of these compounds. These data provide evidence that these compounds can be used to inhibit the function of these target receptors.

Introduction

Many growth factors and cytokines mediate cellular signaling through the activation of tyrosine kinases. In human disease, tyrosine kinases have been implicated as potential therapeutic targets for cancers, cardiovascular disease, inflammatory diseases, fibrotic diseases, and other diseases resulting from chronic tissue injury. More recently, synthetic compounds have been identified that can block the function of specific tyrosine kinases and preclinical data are emerging to support the use of these compounds in clinical studies. In the area of cancer, receptor tyrosine kinases play important roles in the process of tumor development and spread.[1-3] In this regard, RTKs have been involved in tumor growth, survival, metastasis, and angiogenesis.[4,5]

We previously reported a series of 3-substituted indolin-2-ones with potent and selective inhibitory activity toward different RTKs.[6] The selectivity of these compounds against particular RTKs depended on the substituents on the indolin-2-one core, especially at the C-3 position. Of particular interest, 3-[(substituted pyrrol-2-yl)methylidenyl]indolin-2-ones showed selective inhibitory activity against the VEGF-R2 (Flk-1/KDR) tyrosine autophosphorylation at the cellular level.[6] From this series of compounds, SU5402 (compound **1** in Table 1) and SU5416 (compound **2** in Table 3) have been utilized as specific inhibitors of the FGF-R and VEGF-R, respectively.

Compound **1** was cocrystallized with the catalytic domain of FGF-R1 (flg-1)[7] and was found to inhibit tyrosine phosphorylation of VEGF-R2 (Flk-1/KDR) and PDGF-R in NIH 3T3 cells with IC_{50} values of 0.4 and 60.9 μM, respectively.[6] The cocrystal structure revealed that the indolin-2-one core occupied the adenine binding site of ATP and that **1** induced receptor conformational changes as a result of interactions between the propionic acid moiety of **1** and Asn568 in the sugar binding region.[7] This study suggested that the substitution on the core might confer kinase selectivity of these ATP mimetic 3-substituted indolin-2-ones. The information deduced from this study is useful for further modification of 3-[(substituted pyrrol-2-yl)methylidenyl]indolin-2-ones as inhibitors against FGF-R1 and other highly homologous RTKs, such as VEGF-R2 (Flk-1/KDR).

In addition, compound **2** was derived from a previous chemical series and is currently under clinical evaluation for the treatment of human cancers.[8] Compound **2** was found to inhibit tyrosine autophosphorylation of VEGF-R2 (Flk-1/KDR) and PDGF-R tyrosine kinases (TKs) in NIH 3T3 mouse fibroblast cells with IC_{50} values of 1.04 and 20.26 μM, respectively.[6] Preclinical studies have indicated that **2** did not inhibit tumor cell growth in vitro but did specifically inhibit endothelial cell proliferation facilitated by VEGF (IC_{50} = 40 nM). Consistent with its anti-angiogenic properties, compound **2** also inhibited tumor growth in vivo in a wide range of tumor models.[8]

Our goal in the present study was to explore the

* To whom correspondence should be addressed.

10.1021/jm9904295 CCC: $18.00
Published on Web 11/19/1999

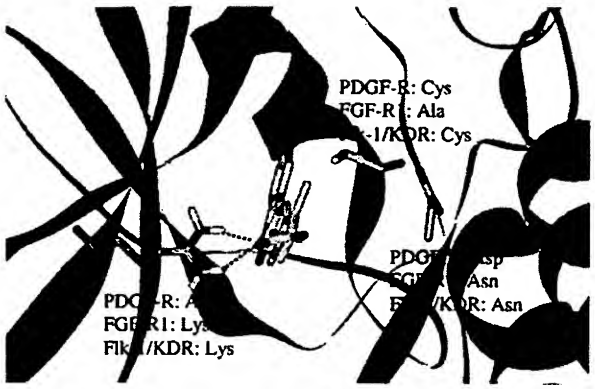

Figure 1. Compound **11a** is shown to be docked within a homology model of the PDGF-R. The receptor peptide backbone is represented by ribbons. Key nonconserved residues surrounding **11a** are shown with carbon atoms colored gray. Corresponding residues of the FGF-R1 and VEGF-R2 (Flk-1/KDR) are indicated. Compound **11a** is designated with carbon atoms colored yellow. Hydrogen bonds are denoted between **11a** and arginine (dotted lines).

influence of various chemical modifications of 3-[(substituted pyrrol-2-yl)methylindenyl]indolin-2-ones on their inhibitory activity and selectivity against VEGF, FGF, and PDGF RTKs. The structure–activity relationship of these compounds with respect to both kinase activity and ligand-dependent events in cells is discussed.

Design

All of the compounds included in this study were based, in part, on chemical features of **1**. The cocrystallographic structure of **1** and the catalytic domain of FGF-R1 revealed important ligand–receptor interactions as well as areas for further modifications.[7] First, it showed the presence of three crystallographic water molecules in proximity to the C-5 position of the indolin-2-one core, suggesting that there is more space in this area for hydrophilic substitutions (such as carboxylic acid and aminosulfonyl functionalities). Second, a comparison of a cocrystallographic study with FGF-R1 and PD173074[9] suggested that introduction of a lipophilic phenyl (or substituted phenyl) substituent at the C-6 position of the **1** core might enhance inhibitory activity against FGF-R1.

For VEGF-R and PDGF-R, homology models were built based on the FGF-R1 crystal structure. Since VEGF-R like FGF-R1 also has an asparagine residue in the sugar binding region (Figure 1), the propionic acid–asparagine interaction observed in the **1** cocrystal structure would likely be preserved upon binding to the VEGF-R. In the case of PDGF-R, the corresponding residue in the sugar-binding region is aspartic acid (Figure 1). Although favorable interaction between the propionic acid of **1** and the aspartic acid of PDGF-R could exist if one of the acids is deprotonated, such interaction would be less favorable than the propionic acid–asparagine interaction observed in the **1**/FGF-R1 cocrystal. On the other hand, PDGF-R has a basic arginine residue in proximaty to the C-4′ position on the pyrrole ring of **1**. Thus, to enhance PDGF-R inhibitory activities, the propionic acid side chain of **1** could be moved to the C-4′ position. In this manner, three types of 3-substituted indolin-2-ones containing propionic acid functionality were designed. First, modification of the substitutions at the C-4, C-5, or C-6 positions resulted in a series of **1** analogues (**9a–d** in Table 1). Second, swapping the propionic acid moiety at the C-3′ position with the methyl group at the C-4′ position of **1** gave the corresponding regioisomer, compound **11a** (Table 2). In addition, analogues of **11a** with different substitutions on the indolin-2-one core were also prepared (compounds **11b–h** in Table 2). Third, combining the structural features of **2** (a potent VEGF-R inhibitor) and compound **11a** yielded compound **16a** and its analogues (Table 3).

Chemistry

In general, compounds were prepared following condensation of substituted indolin-2-ones with aldehydes in the presence of base as described previously.[6] Indolin-2-one and 6-methoxy-indolin-2-one are commercially available, whereas 4-methyl-, 5-bromo-, 5-aminosulfonyl-, 6-aryl-, and 5-carboxyindolin-2-ones and all of the aldehydes were prepared using the following methods. 4-Methyl- and 5-bromoindolin-2-one were prepared by the method described previously.[6] 5-(Aminosulfonyl)-indolin-2-ones (compounds **4** in Scheme 1) were prepared by amidation of 5-(chlorosulfonyl)indolin-2-one (compound **3** in Scheme 1) that was prepared by sulfonylation of indolin-2-one with chlorosulfonic acid (Scheme 1). 6-Arylindolin-2-ones (**8a–e**) were prepared from 5-bromo-2-fluoronitrobenzene. Suzuki coupling of the commercially available aryl boronic acid with 5-bromo-2-fluoronitrobenzene gave 5-aryl-2-fluoronitrobenzene (compounds **5a–e** in Scheme 1). Displacement of *o*-fluoro substitution of **5a–e** with dimethyl malonate followed by hydrolytic decarboxylation with 6 N aqueous hydrochloric acid and reductive cyclization gave 6-arylindolin-2-ones (**8a–e**) (Scheme 1).[10] 5-Carboxyindolin-2-one was synthesized according to the reported method.[11]

Analogues of **1** (**9a–d**, Table 1) were prepared as depicted elsewhere.[12] Compound **11a** analogues (Scheme 2 and Table 2) were prepared by condensing the substituted indolin-2-ones with 4-carboxyethyl-3-methylpyrrol-2-carboxaldehyde (**10**), which was prepared as described previously (Scheme 2).[13] Analogues of compound **16a** (Scheme 3 and Table 3) were synthesized by condensing substituted indolin-2-ones and 3-(5-formyl-2,4-dimethyl-1*H*-pyrrol-3-yl)propionic acid (compound **15** in Scheme 3), which was prepared from 4-(2-methoxycarbonylethyl)-3,5-dimethyl-1-*H*-pyrrole-2-carboxylic acid benzyl ester via hydrogenolysis, decarboxylation, formylation, and hydrolysis (Scheme 3). As reported in our previous report, analogues of 3-[(substituted pyrrol-2-yl)methylidenyl]indolin-2-ones were shown to exist exclusively as cis isomers (*Z*-isomer).[6] We suggested that this may be due in part to intramolecular hydrogen bonding between the NH-1′ and C=O at the C-2 position of the indolin-2-one core. All of the compounds in this study are assumed to preferably exist as cis isomers.

Results and Discussion

Compounds were evaluated for their inhibitory activity toward tyrosine phosphorylation activity associated with isolated VEGF-R2 (Flk-1/KDR), FGF-R1, PDGF-R, and epidermal growth factor receptor (EGF-R) ty-

Table 1. Inhibition of Tyrosine Kinase Activities and Ligand-Dependent Cell Proliferation Using **1** Analogues

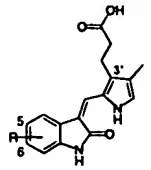

compounds		inhibition of tyrosine kinase activity (IC_{50}, μM)[a]				inhibition of cell proliferation (IC_{50}, μM)[b]			
ID	R	VEGF-R2	FGF-R1	PDGF-Rβ	EGF-R	VEGF	FGF	PDGF	EGF
1	H	0.02	0.03	0.51	>100	0.05	2.80	28.4	>50
9a	4-CH_3	0.20	0.03	2.11	>100	0.10	0.25	46.4	28.8
9b	5-Br	0.35	0.08	0.62	>100	0.04	0.49	6.70	>50
9c	6-(3-OCH_3phenyl)	28.3	1.2	0.45	>100	0.61	0.14	8.29	49.2
9d	6-(3-OC_2H_5phenyl)	1.0	4.5	2.38	>100	0.46	0.27	11.3	>50

[a] IC_{50} values for VEGF-R2 (Flk-1/KDR) and FGF-R1 were determined by at least two separate tests and reported as mean values. [b] IC_{50} values for PDGF- and EGF-dependent cell proliferations were determined by at least two separate tests and reported as mean values.

Table 2. Inhibition of Tyrosine Kinase Activities and Ligand-Dependent Cell Proliferation Using Compounds **11a–h**

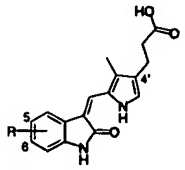

compounds		inhibition of tyrosine kinase activity (IC_{50}, μM)[a]				inhibition of cell proliferation (IC_{50}, μM)[b]			
ID	R	VEGF-R2	FGF-R1	PDGF-Rβ	EGF-R	VEGF	FGF	PDGF	EGF
11a	H	2.14	3.68	0.14	>100	0.40	10.1	58.4	>50
11b	5-COOH	0.24	0.77	4.19	>100	>50	>50	>50	>50
11c	5-SO_2NH_2	0.92	0.46	5.98	>100	>50	>50	>50	>50
11d	6-OCH_3	1.35	3.89	0.14	>100	1.20	31.6	1.40	>50
11e	6-phenyl	0.30	1.05	0.16	>100	0.81	1.00	0.15	21.8
11f	6-(3-OCH_3phenyl)	0.09	0.36	0.17	>100	0.18	0.13	0.18	30.5
11g	6-(2-OCH_3phenyl)	1.47	2.13	1.42	>100	0.04	0.04	0.65	19.2
11h	6-(4-OCH_3phenyl)	0.45	1.54	3.08	>100	1.80	1.60	2.78	22.8

[a] IC_{50} values for VEGF-R2 (Flk-1) and FGF-R1 were determined by at least two separate tests and reported as mean values. [b] IC_{50} values for PDGF- and EGF-dependent cell proliferations were determined by at least two separate tests and reported as mean values.

Table 3. Inhibition of Tyrosine Kinase Activities and Ligand-Dependent Cell Proliferation Using Compounds **16a–i**

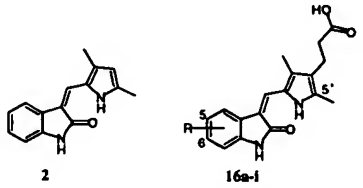

2 **16a-i**

compounds		inhibition of tyrosine kinase activity (IC_{50}, μM)[a]				inhibition of cell proliferation (IC_{50}, μM)[b]			
ID	R	VEGF-R2	FGF-R1	PDGF-Rβ	EGF-R	VEGF	FGF	PDGF	EGF
2		0.70	7.08	10.50	>100	0.04	50.0	4.54	>50
16a	H	2.43	3.04	0.06	>100	0.41	9.30	16.5	>50
16b	5-Br	1.73	2.05	0.06	>100	0.07	3.60	3.65	>50
16c	5-COOH	0.07	0.28	1.21	>100	>50	>50	>50	>50
16d	5-SO_2NH_2	1.26	0.28	1.53	84.8	42.8	>50	>50	>50
16e	6-OCH_3	8.29	5.40	0.55	>100	0.67	25.1	2.35	>50
16f	6-phenyl	0.14	2.29	0.01	>100	10.0	10.0	0.11	21.9
16g	6-(3-OCH_3phenyl)	0.30	1.40	0.10	>100	0.99	1.50	0.23	24.1
16h	6-(2-OCH_3phenyl)	4.37	7.33	2.22	>100	3.0	4.00	0.94	31.3
16i	6-(4-OCH_3phenyl)	0.52	5.76	1.0	>100	4.20	5.64	0.68	>50

[a] IC_{50} values for VEGF-R2 (Flk-1) and FGF-R1 were determined by at least two separate tests and reported as mean values. [b] IC_{50} values for PDGF- and EGF-dependent cell proliferations were determined by at least two separate tests and reported as mean values.

rosine kinases. Tyrosine autophosphorylation assays were used to assess the inhibitory activities of compounds toward PDGF-R and EGF-R tyrosine kinases, whereas peptide–base transphosphorylation assays were performed for VEGF-R2 (Flk-1/KDR) and FGF-R1 kinase activity. Compounds were also evaluated in ligand-stimulated cell proliferation assays using human umbilical vein endothelial cells (HUVECs) and NIH3T3

Scheme 1. Synthesis of Substituted Indolin-2-ones[a,b]

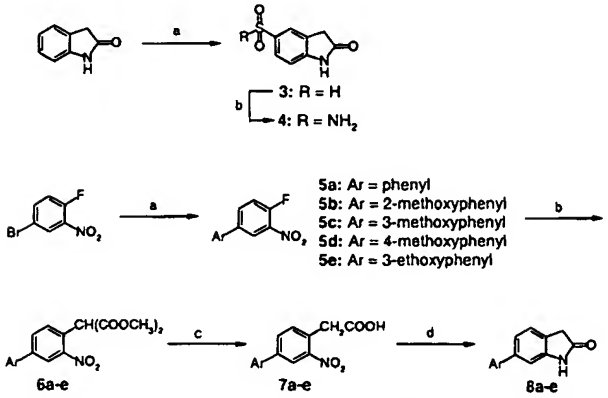

[a] **4**: (a) HSO_3Cl, room temperature to 68 °C, 2.5 h. (b) NH_4OH, ethanol, room temperature, overnight. [b] **8a–e**: (a) $ArB(OH)_2$, $(Ph_3P)_4Pd$, $NaHCO_3$, toluene–ethanol, reflux, 2 h. (b) $CH_2(COOCH_3)_2$, NaH, DMSO, 100 °C, 2 h. (c) 6 N HCl_{aq}, overnight. (d) Fe, HOAc, reflux, 2 h.

Scheme 2. Synthesis of Compounds **11a–h**[a]

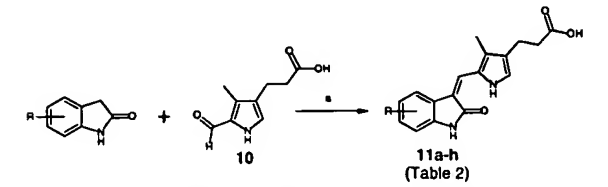

[a] (a) Piperidine, ethanol, reflux, 4 h, then 2 N HCl_{aq}.

Scheme 3. Synthesis of Compounds **16a–i**[a]

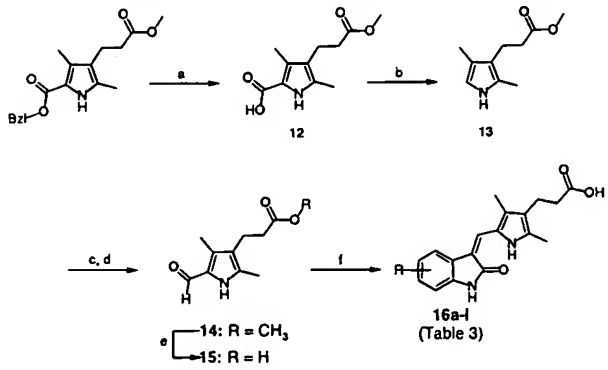

[a] (a) Pd/C, H_2, methanol, room temperature, 2 h. (b) NaOAc, 100 °C, 3 days. (c) $ClCH{=}N^+(CH_3)_2Cl^-$, $ClCH_2CH_2Cl$, room temperature, 2 h. (d) $NaOH_{aq}$, room temperature. (e) $NaOH_{aq}$, reflux, 2 h. (f) Substituted indolin-2-ones, piperidine, ethanol, reflux, overnight, then 2 N HCl_{aq}.

mouse fibroblast cells. IC_{50} values were defined as the concentration of a compound required to achieve 50% inhibition of tyrosine kinase activity or the ligand-stimulated growth compared to vehicle-treated controls (DMSO). Compounds with IC_{50} values greater than 50 μM were considered inactive. The results from these assays are summarized in Tables 1–3. The SAR analyses are discussed separately for each class of compounds in this report.

1. Analogues of Compound 1. Compound **1** is a prototype compound that exhibits good potency against VEGF-R2 (Flk-1/KDR), FGF-R1, and PDGF-R tyrosine kinases with IC_{50} values of 0.02, 0.03, and 0.51 μM, respectively (Table 1). Since VEGF-R2 (Flk-1) also has an Asn at the position similar to Asn568 in FGF-R1, it is not surprising that **1** has been shown to exhibit similar potency for this receptor kinase as well (Figure 1). In the case of PDGF-R, the corresponding residue is either aspartic acid or aspartate, depending on the ionization status of **1** (Figure 1). Nonetheless, the interaction between the propionic acid of **1** and aspartic acid would be less favorable than that between this propionic acid and asparagine. The reduced potency of **1** toward PDGF-R tyrosine kinase is consistent with this model. Methylation at the C-4 position (**9a** in Table 1) of **1** retained potency against FGF-R1 but led to 10- and 4-fold decrease in potency toward VEGF-R2 (Flk-1/KDR) and PDGF-R, respectively. Bromination at the C-5 position of **1** had little effect on inhibitory activity against either PDGF-R or FGF-R, but considerably decreased the potency toward VEGF-R2 (Flk-1) (**9b** in Table 1). These results have supported a model where FGF-R1 can better accommodate substitutions at both the C-4 and C-5 positions of the indolin-2-one core than either VEGF-R2 (Flk-1) or PDGF-R. In this model, FGF-R1 contains an alanine residue in the vicinity of the C-5 position of indolin-2-one, whereas VEGF-R2 (Flk-1) and PDGF-R contain larger cysteine residues at the comparable position (Figure 1).

Aryl substitutions at the C-6 position of the **1** core retained or slightly decreased the potency against PDGF-R but led to a significant decrease in potency toward VEGF-R2 (Flk-1) and FGF-R1 (compounds **9c** and **9d** in Table 1). The decreased activity of **9c** and **9d** against FGF-R1 was unexpected since superposition of **1** with PD173074, which is a highly potent and selective inhibitor of FGF-R1,[9] suggested that such phenyl substitution might enhance FGF-R1 inhibitory activity by increasing further side chain interactions.

All of these **1** analogues showed potent inhibitory activity against VEGF- and FGF-induced cell proliferation but weak potency toward PDGF-induced cell proliferation. However, these results were not correlated to the data from kinase assays. For instance, compound **9a** was found to be 141- and 40-fold more potent than **9c** when tested against VEGF-R2 (Flk-1) and FGF-R1, respectively. However, both compounds showed comparable potencies in the cell proliferation assays. This is probably due to other factors such as cell membrane penetration, chemical stability, metabolic stability, or the ability to affect other cellular targets including protein kinases. Therefore, advance of these compounds for in vivo assessment will largely rely on clarifying the role of the above factors in the cellular inhibitory activity for these inhibitors. Compound **9b** was the best compound from this series that showed high potency against all three targets in both kinase and cell proliferation assays when compared to EGF-R.

2. Analogues of Compound 11a. The regioisomer of **1**, **11a** (Table 2), was found to be 107- and 123-fold less potent than **1** toward VEGF-R2 (Flk-1) and FGF-R1, respectively, and 4-fold more potent when tested against the PDGF-R (IC_{50} = 0.14 μM, Table 2). Modeling studies have suggested that differences in the inhibitory target profiles of **11a** and **1** may be attributed to different compound–receptor interactions. Specifically, the propionic acid moiety of **1** can interact with asparagine within the catalytic domain of VEGF-R2 (Flk-1)

or FGF-R1 as has been observed previously in the 1/FGF-R1 cocrystal structure.[7] Also it may interact, though less favorably, with the aspartic acid/aspartate of PDGF-R as discussed previously. On the other hand, the propionic acid moiety of **11a**, attached to the C-4′ position of the core, might interact with a lysine within the catalytic domain of VEGF-R2 (Flk-1) or FGF-R1 and an arginine residue of PDGF-R (Figure 1). In particular, the guanidine group of the arginine residue in PDGF-R is aligned to interact with the carboxylate of **11a** with hydrogen bond distance of about 2 Å. For VEGF-R2 (Flk-1) and FGF-R1, the lysine residue exhibiting a shorter side chain than arginine in PDGF-R would be in a less favorable position to interact with the carboxylate of **11a** (the hydrogen bond distance would be about 2.8 Å). These considerations may help to explain, in part, the finding that **11a** was found to be more potent against PDGF-R than against VEGF-R or FGF-R.

Hydrophilic substituents at the C-5 position of **11a** (i.e., carboxyl or aminosulfonyl group in **11b** or **11c**, respectively) were shown to lead to increased potency toward both VEGF-R2 (Flk-1) and FGF-R1 and decreased the potency against the PDGF-R tyrosine kinase (Table 2). It is conceivable that these substitutions may displace water molecules in the vicinity of the C-5 position that were observed in the 1/FGF-R1 cocrystal structure[7] and hence might lead to increased potencies toward these RTKs.

In addition, lipophilic substituents at the C-6 position on the indolin-2-one core maintained or reduced the inhibitory activity against the PDGF-R as in the case of **1** series. In this regard, methoxy, phenyl, and 3-methoxyphenyl groups at the C-6 position of the indolin-2-one core (compounds **11d–f**) retained the potency against the PDGF-R, whereas C-6 substituents of **11g** and **11h** led to 10- and 22-fold decreased potency, respectively, when compared to **11a**. However, the effect of a C-6 aryl substitution in the **11a** series with respect to potency toward the VEGF-R2 (Flk-1) and FGF-R1 kinases (compounds **11e–h**) was found to be opposite that observed for the **1** series. In this regard, C-6 aryl substitutions in the **11a** series increased the inhibitory activity as it relates to VEGF-R2 (Flk-1) and FGF-R1 (Table 2) whereas C-6 aryl substituents in the **1** series reduced the potency (Table 1). We explain these findings by suggesting that the C-6 aryl substitutions may move the indolin-2-one core slightly toward the entrance of the ATP binding site. This movement may weaken the propionic acid/asparagine interaction in **1** series, but strengthen the propionic acid/lysine interaction in the **11a** series. Compound **11f** was found to be the most potent inhibitor of this series as it relates to inhibition of all three of these RTKs with IC_{50} values of 0.09, 0.36, and 0.17 μM for VEGF-R2 (Flk-1), FGF-R1, and PDGF-R, respectively.

Most of the compounds from the **11a** series were also found to show potent inhibitory activity toward VEGF-, FGF-, and PDGF-dependent cell proliferation. The exceptions to this are compounds **11b** and **11c**, which were shown to be inactive using these cell-based assays while exhibiting potency in the kinase assays. This result may be due to poor cell permeability since these compounds are highly polar. A similar lack of correlation between kinase inhibition and inhibition of cell proliferation was observed for the **11a** series as for the **1** series. For example, **11g** was over 31- and 790-fold more potent than **11d** when tested against VEGF- and FGF-dependent cell proliferation, respectively, despite their similar kinase inhibitory profile on these RTKs. In addition, **11g** is slightly more potent against PDGF-dependent cell proliferation but 10-fold less potent in the kinase assay than **11d**. The compound **11f** was the only compound of this series that showed potent inhibitory activity against both kinase and ligand-dependent cell proliferation. In this regard, it inhibited VEGF-, FGF-, and PDGF-dependent cell proliferation with IC_{50} values of 0.18, 0.13, and 0.18 μM, respectively (Table 2).

3. Analogues of Compound 16a. Combining the chemical structural features of compounds **11a** (propionic acid at the C-4′ position of the pyrrole ring) and **2** (3,5-dimethylpyrrole side chain), the **16a** series (Table 3) was prepared. Compound **16a** showed equal potency compared to **11a** when tested against VEGF-R2 (Flk-1) and FGF-R1 but was found to be slightly more potent than **11a** toward PDGF-R (IC_{50} = 0.06 μM) (Table 3). This result suggested that the extra methyl substituent at the C-5′ position on the pyrrole ring of **16a** might provide an extra interaction to PDGF-R. In general, analogues of **16a** shared some structure–activity relationships with the **11a** series. In this regard, a small lipophilic bromo substituent at the C-5 position of **16b** did not change the kinase profile when compared to the parent compound **16a**. On the other hand, the hydrophilic substituents (i.e., carboxyl or aminosulfonyl group in **16c** and **16d**, respectively) increased the inhibitory potency against both VEGF-R2 (Flk-1/KDR) and FGF-R, but decreased the potency toward PDGF-R. Phenyl and 3-methoxyphenyl substitution at the C-6 position on the indolin-2-one core (**16f** and **16g** in Table 3) increased potency toward VEGF-R2 (Flk-1) and FGF-R1 and retained or slightly decreased the potency against PDGF-R. Compound **16f** represented the most potent inhibitor of PDGF-R in this study (IC_{50} = 0.01 μM). In addition, 2-methoxyphenyl substitution in compound **16h** exhibited decreased inhibitory activity against all three RTKs when compared to **16a**.

Lastly, most of the compounds from the **16a** series were found to have inhibitory activity against ligand-dependent cell proliferation stimulated by VEGF, FGF, and PDGF. This is in contrast to their low activity when tested against EGF-dependent cell proliferation. A comparison of this series to the corresponding analogues of **11a** indicated that the **16a** series showed decreased potency toward VEGF- and FGF-dependent cell proliferation and retained similar inhibitory activity against PDGF-dependent cell proliferation. Compounds **16c** and **16d** were inactive in all cell–base assays due to their poor membrane permeability. Similarly, there is no correlation between the kinase and cell proliferation results.

Conclusion

In this report, we described a series of 3-substituted indolin-2-ones containing a propionic acid functionality and their inhibitory activities toward VEGF-R2 (Flk-1/KDR), FGF-R1, and PDGF-R tyrosine kinases. These in vitro results suggest potential utilities for the treat-

ment of cancers, inflammatory diseases, cardiovascular diseases, and fibrotic diseases of the lung, liver, and kidney. The chemical structural requirements for inhibiting these RTKs have been explored.

Our previous report has indicated that **2** showed good potency toward inhibition of VEGF-R2 (Flk-1), whereas **1**, unlike **2**, was also a potent inhibitor of FGF-R1.[6,7] In this case, potency of **1** toward FGF-R1 tyrosine kinase activity was attributed, in part, to the presence of a propionic acid side chain of **1** at the C-3′ position on the pyrrole ring.[7] In this report, we designed, synthesized, and evaluated a series of analogues possessing structural features contained in these two prototype compounds in order to assess the impact of these structural modifications on the profile of kinase inhibitory activities. As described above, the compounds were classified into three groups, **1**-related compounds (Table 1), analogues of **1** regioisomer, **11a** (Table 2), and hybrid compounds (**16a** series in Table 3) containing structure features of both **2** and **11a**.

The following chemical structural requirements for these 3-substituted indolin-2-ones to inhibit VEGF-R2 (Flk-1), FGF-R1, and PDGF-R tyrosine kinases were deduced from the enzymatic assay results and rationalized by protein kinase structural models. First, it was shown that a solubilizing propionic acid was found to be required for high potency against these RTKs. Structural models suggested that the propionic acid side chain could interact favorably with asparagine residues in VEGF-R2 (Flk-1) and FGF-R1 for **1** analogues or with basic residues (lysine or arginine) in all three target RTKs for the **11a** and **16a** analogues. Second, regarding the location of the propionic acid, FGF-R1 and VEGF-R2 (Flk-1) clearly favor substitution at the C-3′ position, while PDGF-R prefers the C-4′ position of the pyrrole ring. Third, the hydrophilic substituent (i.e., aminosulfonyl or carboxyl group) at the C-5 position of the indolin-2-one core is favorable for the inhibitory activity against both VEGF-R2 (Flk-1) and FGF-R1 (i.e., **11b** and **11c** vs **11a** and **16c** and **16d** vs **16a**). This is in agreement with the cocrystallographic study of **1**/FGF-R1, which indicated that three water molecules localized near the C-5 position of the indolin-2-one core. Therefore, hydrophilic substituent at the C-5 position should enhance the affinity of the inhibitor to FGF-R1 as well as VEGF-R2 (Flk-1), given the high homology existing between the two RTKs. Finally, The effect of C-6 aryl substitutions depends on the location of the propionic acid side chain. For the **1** series, it reduced the inhibitory activities against FGF-R1 and VEGF-R2 (Flk-1). However, for the **11a** and **16a** analogues, it increased potency toward these receptors, especially when the substituent is phenyl or 3-methoxyphenyl.

In summary, we have prepared a series of compounds that can inhibit VEGF-R2 (Flk-1/KDR), FGF-R1, and PDGF-R tyrosine kinases. Since all three RTKs play crucial roles in many disease processes such as cancer, arterial restenoesis, diabetic retinopathies, atherosclerosis, fibrosis, and rheumatoid arthritis, inhibitors of these RTKs may have therapeutic potential. For instance, inhibitors that selectively inhibit VEGF-R2 (Flk-1) and Flt-1 could be developed for the treatment of rheumatoid arthritis whereas compounds with selective inhibitory activity against PDGF-R may be useful for arterial restenosis. On the other hand, multiple signal transduction pathways and their respective RTKs could be involved in a given disease (i.e., tumor angiogenesis). In this case, compounds inhibiting all three RTKs discussed in this report (i.e., **11f** in Table 2) may be advantageous as long as such inhibition does not compromise safety. Further evaluation of compounds from these series' for in vivo efficacy in various disease models is ongoing. In vivo efficacy of these compounds in animal models will also depend on pharmacokinetic properties including aqueous solubility, relative oral bioavailability, metabolic stability, and tissue distribution.

Experimental Section

^{1}H NMR spectra were recorded by Acorn NMR using a Nicolet NT300 or a Nicolet NT360. Tetramethylsilane (TMS) was used as an internal standard, and chemical shifts are reported in parts per million (δ) downfield from TMS. Coupling constants are reported in hertz. Mass spectra (electron spray) were recorded by SYNPEP CORP, using an API I PLUS spectrometer. Elemental analyses were performed by Galbraith Laboratories, Inc. Elemental analysis results are within +0.4% of the theoretical values.

5-Aminosulfonyl-2-indolin-2-one (4). To a 100 mL flask charged with 27 mL of chlorosulfonic acid was added slowly 13.3 g (100 mmol) of indolin-2-one. The reaction temperature was maintained below 30 °C during the addition. After the addition, the reaction mixture was stirred at room temperature for 1.5 h, heated to 68 °C for 1 h, cooled, and poured into water. The precipitate was washed with water and dried in a vacuum oven to give 11.0 g of 5-chlorosulfonyl-2-indolin-2-one (**3**) (50% yield), which was used without further purification. Compound **3** (2.1 g, 9.1 mmol) was added to 10 mL of ammonium hydroxide in 10 mL of ethanol and stirred at room temperature overnight. The mixture was concentrated and the solid collected by vacuum filtration to give 0.4 g (20% yield) of 5-aminosulfonyl-2-indolin-2-one as an off-white solid (**4**): ^{1}H NMR (360 MHz, DMSO-d_6) δ 10.67 (s, 1H, NH-1), 7.63–7.66 (m, 2H, H-4,6), 7.13 (s, 2H, H_2NSO_2-5), 6.91 (d, J = 8.04 Hz, 1H, H-7), and 3.56 (s, 2H, CH_2-3); MS *m/z* (relative intensity, %) 211 ([M − 1]$^+$, 100).

6-Phenyl-2-indolin-2-one (8a). Tetrakis(triphenylphosphine)palladium (0.8 g, 0.7 mmol) was added to a mixture of 3.1 g (25.4 mmol) of benzeneboronic acid, 5 g (22.7 mmol) of 5-bromo-2-fluoronitrobenzene and 22 mL of 2 M sodium carbonate solution in 50 mL of toluene and 50 mL of ethanol. The mixture was refluxed for 2 h, concentrated, and the residue extracted twice with ethyl acetate. The ethyl acetate layer was washed with water and brine, dried, and concentrated to give a yellow oil. The oil was chromatographed on silica gel eluting with 5% ethyl acetate in hexane to give 4.75 g (96% yield) of 4-fluoro-3-nitrobiphenyl (**5a**) as a yellow oil.

Dimethyl malonate (10 mL, 87.5 mmol) in 25 mL of dimethyl sulfoxide was added dropwise to 3.5 g (145.8 mmol) of sodium hydride suspended in 25 mL of dimethyl sulfoxide and the mixture was heated at 100 °C for 10 min. The mixture was cooled to room temperature and 4.7 g (21.6 mmol) of **5a** in 25 mL of dimethyl sulfoxide was added. The mixture was heated at 100 °C for 2 h, cooled, and quenched with 300 mL of saturated ammonium chloride solution. The mixture was extracted three times with ethyl acetate and the combined organic layers washed with water and brine and evaporated to give crude dimethyl-3-nitrobiphenyl-4-malonate (**6a**) as a yellow oil.

Crude **6a** was refluxed in 30 mL of 6 N hydrochloric acid for 24 h. The precipitate was collected by filtration, washed with water, and dried to give 4.5 g (80% based on **6a**) of 3-nitrobiphenyl-4-acetic acid (**7a**) as a cream-colored solid.

Iron chips (2.6 g, 46.6 mmol) was added all at once to 4.5 g (17.5 mmol) of **7a** in 40 mL of acetic acid. The mixture was refluxed for 2 h, concentrated to dryness, and taken up in ethyl

acetate. The solids were removed by filtration and the filtrate was washed twice with 1 N hydrochloric acid and brine and dried over anhydrous sodium sulfate. The filtrate was concentrated to give 3.4 g (93% yield) of 6-phenyl-2-indolin-2-one (**8a**) as a light brown solid: ^{1}H NMR (360 MHz, DMSO-d_6) δ 10.40 (s, br, 1H, NH-1), 7.57–7.60 (m, 2H, H-2′,6′), 7.42–7.46 (m, 2H, H-3′,5′), 7.34 (dt, J = 1.96, 7.23 Hz, 1H, H-4′), 7.27 (d, J = 7.69 Hz, 1H, H-4), 7.19 (dd, J = 1.59, 7.69 Hz, 1H, H-5), 7.01 (d, J = 1.59 Hz, 1H, H-7), 3.49 (s, 2H, CH_2-3); MS *m/z* (relative intensity, %) 210 ([M + 1]$^+$, 100).

6-(2-Methoxyphenyl)-2-indolin-2-one (8b). Tetrakis-(triphenylphosphine)palladium (1 g, 0.9 mmol) was added to a mixture of 5 g (32.9 mmol) of 2-methoxyphenylboronic acid, 6.6 g (30 mmol) of 5-bromo-2-fluoronitrobenzene, and 30 mL of 2 M sodium carbonate solution in 50 mL of toluene and 50 mL of ethanol. The mixture was refluxed for 2 h, concentrated, and the residue extracted twice with ethyl acetate. The ethyl acetate layer was washed with water and brine, dried, and concentrated to give dark green oil which solidified on standing to give 6 g of crude 4-fluoro-2′-methoxy-3-nitrobiphenyl (**5b**).

Dimethyl malonate (14 mL, 122.5 mmol) was added dropwise to 2.9 g (120.8 mmol) of sodium hydride suspended in 50 mL of dimethyl sulfoxide. The mixture was heated at 100 °C for 15 min and cooled to room temperature. Crude **5b** in 60 mL of dimethyl sulfoxide was added, and the mixture was heated at 100 °C for 2 h. The reaction mixture was cooled and quenched with 300 mL of saturated ammonium chloride solution and extracted twice with ethyl acetate. The extracts were combined, washed with saturated ammonium chloride, water, and brine, dried over anhydrous sodium sulfate, and concentrated to give crude dimethyl 2′-methoxy-3-nitrobiphenyl-4-malonate (**6b**) as a yellow oil.

Crude **6b** was heated at 100 °C in 50 mL of 6 N hydrochloric acid for 24 h and cooled. The precipitate was collected by filtration, washed with water and hexane, and dried to give 9.8 g of 2′-methoxy-3-nitrobiphenyl-4-acetic acid (**7b**) as a light tan solid.

Iron chips (5 g, 89.6 mmol) was added in one portion to 9.8 g (34.1 mmol) of **7b** in 50 mL of glacial acetic acid was heated to 100 °C for 3 h. The reaction mixture was concentrated to dryness, sonicated in ethyl acetate and filtered to remove the insolubles. The filtrate was washed twice with 1 N hydrochloric acid, water, brine, dried over anhydrous sodium sulfate and concentrated. The residue was chromatographed on silica gel eluting with ethyl acetate–hexane (1:2) to give 5.4 g (75% yield based on 5-bromo-2-fluoronitrobenzene) of 6-(2-methoxyphenyl)-2-indolin-2-one (**8b**) as a rose-colored solid: ^{1}H NMR (360 MHz, DMSO-d_6) δ 10.32 (s, br, 1H, NH-1), 7.31 (dt, J = 1.86, 7.39 Hz, 1H, H-4′), 7.23 (dd, J = 1.86, 7.39 Hz, 1H, H-6′), 7.28 (d, J = 7.65 Hz, 1H, H-4), 7.08 (dd, J = 1.16, 7.39 Hz, 1H, H-3′), 6.70 (dt, J = 1.16, 7.39 Hz, 1H, H-5′), 6.98 (dd, J = 1.69, 7.65 Hz, 1H, H-5), 6.91 (d, J = 1.69 Hz, 1H, H-7), 3.74 (s, 3H, OCH_3-2′), 3.47 (s, 2H, CH_2-3); MS *m/z* (relative intensity, %) 240 ([M + 1]$^+$, 100).

6-(3-Methoxyphenyl)-2-indolin-2-one (8c). Tetrakis-(triphenylphosphine)palladium (0.7 g, 0.6 mmol) was added to a mixture of 5 g (32.9 mmol) of 3-methoxyphenylboronic acid, 3.8 g (17.3 mmol) of 5-bromo-2-fluoronitrobenzene and 11 mL of 2 M sodium carbonate solution in 100 mL of toluene. The mixture was refluxed for 2 h, diluted with water, and extracted with ethyl acetate. The ethyl acetate was washed with saturated sodium bicarbonate, brine, dried, and concentrated to give an oily solid. The solid was chromatographed on silica gel eluting with ethyl acetate–hexane to give 4.3 g of crude 4-fluoro-3′-methoxy-3-nitrobiphenyl (**5c**).

Dimethyl malonate (9.7 mL, 84.9 mmol) was added dropwise to 2.0 g (83.3 mmol) of sodium hydride suspended in 50 mL of dimethyl sulfoxide. The mixture was heated to 100 °C for 35 min and cooled to room temperature. Compound **5c** (4.2 g, 17.0 mmol) in 50 mL of dimethyl sulfoxide was added and the mixture was heated at 100 °C for 1 h. The reaction mixture was cooled and quenched with 300 mL of saturated ammonium chloride solution and extracted twice with ethyl acetate. The extracts were combined, washed with brine, dried over anhydrous sodium sulfate, and concentrated to give crude dimethyl 3′-methoxy-3-nitrobiphenyl-4-malonate (**6c**) as a pale yellow solid.

Crude **6c** was heated at 110 °C in 45 mL of 6 N hydrochloric acid for 4 days and cooled. The precipitate was collected by filtration, washed with water and hexane, and dried to give 5.3 g of crude 3′-methoxy-3-nitrobiphenyl-4-acetic acid (**7c**) as a light tan solid.

Compound **7c** (5.2 g, 18.1 mmol) was dissolved in methanol and hydrogenated over 0.8 g of 10% palladium on carbon for 3 h at room temperature. The catalyst was removed by filtration and washed with methanol, and the filtrates were combined and concentrated to give a brown solid. The solid was chromatographed on silica gel eluting with ethyl acetate–hexaneacetic acid to give 3.0 g (73% yield based on **5c**) of 6-(3-methoxypheny)-2-indolin-2-one (**9c**) as a pink solid: ^{1}H NMR (360 MHz, DMSO-d_6) δ 10.39 (s, br, 1H, NH-1), 7.35 (t, J = 7.99 Hz, 1H, H-5′), 7.26 (d, J = 7.79 Hz, 1H, H-4), 7.19 (dd, J = 1.30, 7.79 Hz, 1H, H-5), 7.51 (td, J = 0.79, 7.99 Hz, 1H, H-4′), 7.09 (t, J = 2.34 Hz, 1H, H-2′), 7.01 (d, J = 1.30 Hz, 1H, H-7), 6.92 (ddd, J = 0.79, 2.34, 7.99 Hz, 1H, H-6′), 3.80 (s, 3H, OCH_3-3′), 3.49 (s, 2H, CH_2-3); MS *m/z* (relative intensity, %) 240 ([M + 1]$^+$, 100).

6-(4-Methoxyphenyl)-2-indolin-2-one (8d). Tetrakis-(triphenylphosphine)palladium (1 g, 0.9 mmol) was added to a mixture of 5 g (32.9 mmol) of 4-methoxyphenylboronic acid, 6.6 g (30 mmol) of 5-bromo-2-fluoronitrobenzene, and 30 mL of 2 M sodium carbonate solution in 50 mL of toluene and 50 mL of ethanol. The mixture was refluxed for 2 h, concentrated, and the residue extracted twice with ethyl acetate. The ethyl acetate layer was washed with water and brine, dried, and concentrated to give a brown oily solid. The solid was chromatographed on silica gel eluting with 5% ethyl acetate in hexane to give crude 4-fluoro-4′-methoxy-3-nitrobiphenyl (**5d**) as a pale yellow solid.

Dimethyl malonate (10 mL, 87.5 mmol) was added dropwise to 2.0 g (83.3 mmol) of sodium hydride suspended in 60 mL of dimethyl sulfoxide. The mixture was heated to 100 °C for 10 min and cooled to room temperature. Crude **5d** (5.2 g, 21.0 mmol) in 50 mL of dimethyl sulfoxide was added and the mixture was heated at 100 °C for 2 h. The reaction mixture was cooled and quenched with 300 mL of saturated ammonium chloride solution and extracted three times with ethyl acetate. The extracts were combined, washed with saturated ammonium chloride, water, and brine, dried over anhydrous sodium sulfate, and concentrated to give crude dimethyl 4′-methoxy-3-nitrobiphenyl-4-malonate (**6d**) as a yellow oil.

Crude **6d** was heated at 100 °C in 60 mL of 6 N hydrochloric acid for 15 h and cooled. The precipitate was collected by filtration, washed with water and hexane, and dried to give 7.2 g of crude 4′-methoxy-3-nitrobiphenyl-4-acetic acid (**7d**) as a light tan solid.

Iron chips (3.6 g, 62.1 mmol) was added in one portion to 7.2 g (25.1 mmol) of **7d** in 50 mL of glacial acetic acid and heated at 100 °C overnight. The reaction mixture was concentrated to dryness, sonicated in ethyl acetate, and filtered to remove the insolubles. The filtrate was washed twice with 1 N hydrochloric acid, brine, dried over anhydrous sodium sulfate, and concentrated to give 2.7 g (38% yield based on 5-bromo-2-fluoronitrobenzene) of 6-(4-methoxyphenyl)-2-indolin-2-one (**8d**) as a rose-colored solid: ^{1}H NMR (360 MHz, DMSO-d_6) δ 10.38 (s, br, 1H, NH-1), 7.50–7.54 (m, 2H, H-2′6′), 7.23 (d, J = 7.72 Hz, 1H, H-4), 7.14 (dd, J = 1.38, 7.72 Hz, 1H, H-5), 6.98–7.02 (m, 2H, H-3′,5′), 6.97 (d, J = 1.38 Hz, 1H, H-7), 3.78 (s, 3H, OCH_3-4′), 3.47 (s, 2H, CH_2-3); MS *m/z* (relative intensity, %) 240 ([M + 1]$^+$, 100].

6-(3-Ethoxyphenyl)-2-indolin-2-one (8e). Tetrakis(triphenylphosphine)palladium (0.8 g, 0.7 mmol) was added to a mixture of 4.2 g (25.3 mmol) of 3-ethoxyphenylboronic acid, 5.0 g (22.7 mmol) of 5-bromo-2-fluoronitrobenzene and 22 mL of 2 M sodium carbonate solution in 50 mL of toluene and 50 mL of ethanol. The mixture was refluxed for 2 h and concentrated, water was added, and the mixture was extracted twice with ethyl acetate. The ethyl acetate layer was washed with

water and brine, dried, and concentrated. The residue was chromatographed on silica gel eluting with 5% ethyl acetate in hexane to give 5.3 g of crude 4-fluoro-3′-ethoxy-3-nitrobiphenyl (**5e**) as a yellow oil.

Dimethyl malonate (11.4 mL, 100 mmol) was added dropwise to 4.0 g (167 mmol) of sodium hydride suspended in 20 mL of dimethyl sulfoxide. The mixture was heated to 100 °C for 10 min and cooled to room temperature. Crude **5e** (5.3 g, 20.2 mmol) in 25 mL of dimethyl sulfoxide was added, and the mixture was heated at 100 °C for 2 h. The reaction mixture was cooled and quenched with 300 mL of saturated ammonium chloride solution and extracted three times with ethyl acetate. The extracts were combined, washed with water and brine, dried over anhydrous sodium sulfate, and concentrated to give crude dimethyl 3′-ethoxy-3-nitrobiphenyl-4-malonate (**6e**) as yellow oil.

Crude **6e** was heated at 100 °C in 60 mL of 6 N hydrochloric acid for a total of 4 days and cooled. The precipitate was collected by filtration, washed with water and hexane, and dried to give 4.7 g (77% yield based on 5-bromo-2-fluoronitrobenzene) of crude 3′-ethoxy-3-nitrobiphenyl-4-acetic acid as a light tan solid (**7e**).

Iron chips (2.4 g, 41 mmol) was added in one portion to 4.6 g (15.3 mmol) of **7e** in 40 mL of glacial acetic acid and refluxed for 2 h. The reaction mixture was concentrated to dryness, treated repeatedly with ethyl acetate, and filtered to remove the insoluble. The filtrate was washed twice with 1 N hydrochloric acid, brine, dried over anhydrous sodium sulfate, and concentrated to give 3.5 g (91% yield) of **8e** as a light brown solid: ^{1}H NMR (360 MHz, DMSO-d_6) δ 10.40 (s, br, 1H, NH-1), 7.33 (t, J = 7.92 Hz, 1H, H-5′), 7.25 (d, J = 7.70 Hz, 1H, H-4), 7.19 (dd, J = 1.34, 7.70 Hz, 1H, H-5), 7.13 (d, br, J = 7.92 Hz, 1H, H-4′), 7.07 (t, J = 2.62 Hz, 1H, H-2′), 7.00 (d, J = 1.34 Hz, 1H, H-7), 6.90 (dd, J = 2.62, 7.92 Hz, 1H, H-6′), 4.08 (q, J = 7.00 Hz, 2H, OCH_2CH$_3$-3′), 3.49 (s, 2H, CH$_2$-3) 1.34 (t, J = 7.00 Hz, OCH$_2$CH_3-3′); MS *m/z* (relative intensity, %) 254 ([M + 1]$^+$, 100).

3-[4-Methyl-5-(2-oxo-1,2-dihydroindol-3-ylidenemethyl)-1*H*-pyrrol-3-yl]propionic Acid (11a). 3-(5-Formyl-4-methyl-1*H*-pyrrol-3-yl)propionic acid (**10**) (9.0 g, 50 mmol), which was prepared as previously reported,[13] and 6.0 g (45 mmol) of indolin-2-one in 50 mL of ethanol were heated to 70 °C for 4 h. Acetic acid (12 mL) was slowly added, resulting in a copious precipitate. The mixture was refluxed for 5 min and cooled to room temperature, and the precipitate was collected by vacuum filtration and washed with 30 mL of ethanol. The precipitate was slurry-washed at reflux in 30 mL of ethanol, cooled to room temperature, collected by vacuum filtration, washed with 20 mL of ethanol, and dried under vacuum to give 11.9 g (89% yield) of 3-[4-methyl-5-(2-oxo-1,2-dihydroindol-3-ylidenemethyl)-1*H*-pyrrol-3-yl]propionic acid as an orange solid: ^{1}H NMR (360 MHz, DMSO-d_6) δ 13.29 (s, br, 1H, NH-1′), 12.05 (s, br, 1H, CH$_2$CH$_2$COO*H*-4′), 10.78 (s, br, 1H, NH-1), 7.73 (d, J = 7.43 Hz, 1H, H-4), 7.61 (s, 1H, H-vinyl), 7.13 (s, 1H, H-5′), 7.10 (t, J = 7.43 Hz, 1H, H-6), 6.97 (t, J = 7.43 Hz, 1H, H-5), 6.85 (d, J = 7.43 Hz, 1H, H-7), 2.65 (t, J = 7.30 Hz, 2H, CH_2CH$_2$COOH-4′), 2.46 (t, J = 7.30 Hz, 2H, CH$_2$CH_2-COOH-4′), 2.25 (s, 3H, CH$_3$-3′); MS *m/z* (relative intensity, %) 297 (M$^+$, 100). Anal. (C$_{17}$H$_{16}$N$_2$O$_3$·0.25H$_2$O) C, H, N.

3-[4-(2-Carboxyethyl)-3-methyl-1*H*-pyrrol-2-ylmethylene]-2-oxo-2,3-dihydro-1*H*-indole-5-carboxylic Acid (11b). Indolin-2-one (6.7 g, 50 mmol) was added to a stirred suspension of 23 g (172.5 mmol) of aluminum chloride in 30 mL of dichloroethane in an ice bath. Chloroacetyl chloride (11.3 g, 100 mmol) was slowly added and hydrogen chloride gas was evolved. After 10 min of stirring, the reaction was warmed to 40−50 °C for 1.5 h. The mixture was cooled to room temperature and poured into ice water. The precipitate was collected by vacuum filtration, washed with water, and dried under vacuum to give 10.3 g (98%) of 5-chloroacetylindolin-2-one as an off-white solid. A suspension of 9.3 g (44.4 mmol) of 5-chloroacetylindolin-2-one was stirred in 90 mL of pyridine at 80−90 °C for 3 h and then cooled to room temperature. The precipitate was collected by vacuum filtration and washed with 20 mL of ethanol. The solid was dissolved in 90 mL of 2.5 N sodium hydroxide and stirred at 70−80 °C for 3 h. The mixture was cooled to room temperature and acidified to pH 2 with 0.5 N hydrochloric acid. The precipitate was collected by vacuum filtration and washed thoroughly with water to give crude 5-carboxyindolin-2-one as a dark brown solid. After standing overnight, the filtrate yielded 2 g of 5-carboxy-indolin-2-one as a yellow solid. The crude dark brown product was dissolved in hot methanol, the insoluble material was removed by filtration, and the filtrate was concentrated to give another 5.6 g of 5-carboxyindolin-2-one as a brown solid. The combined yield was 85%. ^{1}H NMR (360 MHz, DMSO-d_6) δ 12.56 (s, br, 1H, COOH-5), 10.70 (s, 1H, NH-1), 7.81 (dd, J = 0.68, 8.23 Hz, 1H, H-6), 7.74 (s, br, 1H, H-4), 6.87 (d, J = 8.23 Hz, 1H, H-7), and 3.53 (s, 2H, CH$_2$-3).

The reaction mixture of 88.6 mg (0.5 mmol) of 5-carboxyindolin-2-one, 90.6 mg (0.5 mmol) of **10**, and 75 μL (0.75 mmol) of piperidine in 2.0 mL of ethanol was heated at 95 °C for 5 h and cooled to room temperature. The precipitate was filtered, washed with cold ethanol, 2 N hydrochloric acid, and water, and dried to give 42 mg (25%) of 3-[4-(2-carboxyethyl)-3-methyl-1*H*-pyrrol-2-ylmethylene]-2-oxo-2,3-dihydro-1*H*-indole-5-carboxylic acid (**11b**) as a dark yellow solid: ^{1}H NMR (360 MHz, DMSO-d_6) δ 13.27 (s, br, 1H, NH-1′), 12.28 (s, br, 2H, COOH-5 and CH$_2$CH$_2$COO*H*-4′), 11.11 (s, 1H, NH-1), 8.34 (d, J = 1.36 Hz, 1H, H-4), 7.78 (s, 1H, H-vinyl), 7.75 (dd, J = 1.36, 8.20 Hz, 1H, H-6), 7.19 (d, J = 3.07 Hz, 1H, H-5′), 6.93 (d, J = 8.20 Hz, 1H, H-7), 2.65 (t, J = 7.56 Hz, 2H, CH_2CH$_2$COOH-4′), 2.46 (t, J = 7.56 Hz, 2H, CH$_2$CH_2COOH-4′), 2.29 (s, 3H, CH$_3$-3′); MS *m/z* (relative intensity, %) 341 ([M + 1]$^+$, 7). Anal. (C$_{18}$H$_{16}$N$_2$O$_5$·0.5H$_2$O) C, H, N.

3-[4-Methyl-5-(2-oxo-5-sulfamoyl-1,2-dihydroindol-3-ylidenemethyl)-1*H*-pyrrol-3-yl]propionic Acid (11c). The reaction mixture of 106 mg (0.5 mmol) of 5-aminosulfonylindolin-2-one (**4**), 90.6 mg (0.5 mmol) of **10**, and 75 μL (0.75 mmol) of piperidine in 2.0 mL of ethanol was heated at 95 °C for 5 h and cooled to room temperature. The precipitate was filtered, washed with cold ethanol, 2 N hydrochloric acid, and water, and dried to give 132 mg (70%) of 3-[4-methyl-5-(2-oxo-5-sulfamoyl-1,2-dihydroindol-3-ylidenemethyl)-1*H*-pyrrol-3-yl]-propionic acid (**11c**): ^{1}H NMR (360 MHz, DMSO-d_6) δ 13.28 (s, br, 1H, NH-1′), 12.03 (s, br, 1H, CH$_2$CH$_2$COO*H*-4′), 11.15 (s, br, 1H, NH-1), 8.20 (d, J = 1.60 Hz, 1H, H-4), 7.73 (s, 1H, H-vinyl), 7.59 (dd, J = 1.60, 8.17 Hz, 1H, H-6), 7.23 (d, J = 2.85 Hz, 1H, H-5′), 7.10 (s, 2H, NH$_2$SO$_2$-5), 6.99 (d, J = 8.17 Hz, 1H, H-7), 2.66 (t, J = 7.41 Hz, 2H, CH_2CH$_2$COOH-4′), 2.47 (t, J = 7.41 Hz, 2H, CH$_2$CH_2COOH-4′), 2.29 (s, 3H, CH$_3$-3′). Anal. (C$_{17}$H$_{17}$N$_3$O$_5$S·H$_2$O) C, H, N.

3-[5-(6-Methoxy-2-oxo-1,2-dihydroindol-3-ylidenemethyl)-4-methyl-1*H*-pyrrol-3-yl]propionic Acid (11d). This compound was prepared using the same procedure described in the preparation of **11c** with a yield of 43%: ^{1}H NMR (360 MHz, DMSO-d_6) δ 13.10 (s, br, 1H, NH-1′), 12.04 (s, br, 1H, CH$_2$CH$_2$COO*H*-4′), 10.76 (s, br, 1H, NH-1), 7.63 (d, J = 8.29 Hz, 1H, H-4), 7.46 (s, 1H, H-vinyl), 7.07 (d, J = 3.03 Hz, 1H, H-5′), 6.55 (dd, J = 2.32, 8.29 Hz, 1H, H-5), 6.43 (d, J = 2.32 Hz, 1H, H-7), 3.74 (s, 3H, OCH$_3$-6), 2.63 (t, J = 7.31 Hz, 2H, CH_2CH$_2$COOH-4′), 2.45 (t, J = 7.31 Hz, 2H, CH$_2$CH_2-COOH-4′), 2.23 (s, 3H, CH$_3$-3′); MS *m/z* (relative intensity, %) 327 ([M + 1]$^+$, 100). Anal. (C$_{18}$H$_{18}$N$_2$O$_4$·0.5H$_2$O) C, H, N.

3-[4-Methyl-5-(2-oxo-6-phenyl-1,2-dihydroindol-3-ylidenemethyl)-1*H*-pyrrol-3-yl]propionic Acid (11e). This compound was prepared using the same procedure described in the preparation of **11c** with a yield of 78%: ^{1}H NMR (360 MHz, DMSO-d_6) δ 13.29 (s, br, 1H, NH-1′), 12.01 (s, vbr, 1H, CH$_2$-CH$_2$COO*H*-4′), 10.89 (s, br, 1H, NH-1), 7.83 (d, J = 7.92, 1H, H-4), 7.65 (s, 1H, H-vinyl), 7.63 (d, J = 7.51 Hz, 2H, H-2″,6″), 7.45 (t, J = 7.51 Hz, 2H, H-3″,5″), 7.33 (t, J = 7.51 Hz, 1H, H-4″), 7.28 (dd, J = 1.93, 7.92 Hz, 1H, H-5), 7.16 (d, J = 1.93 Hz, 1H, H-7), 7.09 (d, J = 1.71 Hz, 1H, H-5′), 2.66 (t, J = 7.47 Hz, 2H, CH_2CH$_2$COOH-4′), 2.46 (t, J = 7.47 Hz, 2H, CH$_2$CH_2-COOH-4′), and 2.27 (s, 3H, CH$_3$-3′); MS *m/z* (relative intensity, %) 373 (M$^+$, 100). Anal. (C$_{23}$H$_{20}$N$_2$O$_3$·H$_2$O) C, H, N.

3-{5-[6-(3-Methoxy-phenyl)-2-oxo-1,2-dihydroindol-3-

ylidenemethyl]-4-methyl-1*H*-pyrrol-3-yl}propionic Acid (11f). This compound was prepared using the same procedure as for preparation of **11c** with a yield of 97%: ^{1}H NMR (360 MHz, DMSO-d_6) δ 13.29 (s, br, 1H, NH-1′), 12.07 (s, br, 1H, CH_2CH_2COOH-4′), 10.88 (s, br, 1H, NH-1), 7.82 (d, J = 7.77, 1H, H-4), 7.65 (s, 1H, H-vinyl), 7.36 (t, J = 8.06 Hz, 1H, H-5″), 7.29 (dd, J = 1.40, 7.77 Hz, 1H, H-5), 7.20 (d, J = 8.06 Hz, 1H, H-6″), 7.16 (d, J = 2.23 Hz, 1H, H-2″), 7.14–7.15 (m, br, 1H, H-5′), 7.09 (d, J = 1.40 Hz, 1H, H-7), 6.91 (dd, J = 2.23, 8.06 Hz, 1H, H-4″), 3.82 (s, 3H, OCH_3-3″), 2.65 (t, J = 7.55 Hz, 2H, CH_2CH_2COOH-4′), 2.57 (t, J = 7.55 Hz, 2H, CH_2CH_2-COOH-4′), 2.27 (s, 3H, CH_3-3′); MS *m/z* (relative intensity, %) 401 (M^+, 7). Anal. ($C_{24}H_{22}N_2O_4 \cdot 0.75H_2O$) C, H, N.

3-{5-[6-(2-Methoxy-phenyl)-2-oxo-1,2-dihydroindol-3-ylidenemethyl]-4-methyl-1*H*-pyrrol-3-yl}propionic Acid (11g). This compound was prepared using the same procedure as for preparation of **11c** with a yield of 86%: ^{1}H NMR (360 MHz, DMSO-d_6) δ 13.29 (s, br, 1H, NH-1′), 11.59 (s, br, 1H, CH_2CH_2COOH-4′), 10.78 (s, br, 1H, NH-1), 7.76 (d, J = 8.13 Hz, 1H, H-4), 7.62 (s, 1H, H-vinyl), 7.29–7.34 (m, 2H), 6.99–7.15 (m, 6H), 3.76 (s, 3H, OCH_3-2″), 2.66 (t, J = 7.46 Hz, 2H, CH_2CH_2COOH-4′), 2.45 (t, J = 7.46 Hz, 2H, CH_2CH_2COOH-4′), 2.27 (s, 3H, CH_3-3′); MS *m/z* (relative intensity, %) 401 ([M − 1]$^+$, 100). Anal. ($C_{24}H_{22}N_2O_4 \cdot H_2O$) C, H, N.

3-{5-[6-(4-Methoxyphenyl)-2-oxo-1,2-dihydroindol-3-ylidenemethyl]-4-methyl-1*H*-pyrrol-3-yl}propionic Acid (11h). This compound was prepared using the same procedure as for preparation of **11c** with a yield of 59%: ^{1}H NMR (360 MHz, DMSO-d_6) δ 13.26 (s, br, 1H, NH-1′), 10.83 (s, br, 1H, NH-1), 7.78 (d, J = 8.07 Hz, 1H, H-4), 7.61 (s, 1H, H-vinyl), 7.57 (d, J = 8.95 Hz, 2H, H-2″,6″), 7.22 (dd, J = 1.44, 8.07 Hz, 1H, H-5), 7.13 (d, J = 3.09 Hz, 1H, H-5′), 7.04 (d, J = 1.44 Hz, 1H, H-7), 7.00 (d, J = 8.95 Hz, 2H, H-3″,5″), 3.79 (s, 3H, OCH_3-4″), 2.65 (t, J = 7.65 Hz, 2H, CH_2CH_2COOH-4′), 2.44 (t, J = 7.65 Hz, 2H, CH_2CH_2COOH-4′), 2.27 (s, 3H, CH_3-3′); MS *m/z* (relative intensity, %) 403 ([M + 1]$^+$, 100). Anal. ($C_{24}H_{22}N_2O_4 \cdot 0.5H_2O$) C, H, N.

3-[2,4-Dimethyl-5-(2-oxo-1,2-dihydroindol-3-ylidenemethyl)-1*H*-pyrrol-3-yl]propionic Acid (16a). 4-(2-Methoxycarbonylethyl)-3,5-dimethyl-1*H*-pyrrole-2-carboxylic acid benzyl ester (2.0 g, 6.3 mmol) was hydrogenated over 0.2 g of 10% palladium on carbon in 40 mL of methanol for 2 h at room temperature. The catalyst was removed by filtration and washed with 40 mL of methanol. The filtrate was evaporated to dryness and dried overnight in a vacuum oven to give 1.3 g (92% yield) of 4-(2-methoxycarbonylethyl)-3,5-dimethyl-1*H*-pyrrole-2-carboxylic acid (**12**).

Compound **12** (1.3 g, 5.8 mmol) was ground with 0.5 g of anhydrous sodium acetate and then heated at 100 °C for 3 days. The mixture was dissolved in water, extracted with ethyl acetate, and chromatographed on a column of silica gel in ethyl acetate–hexane to give 0.4 g (38% yield) of 3-(2,4-dimethyl-1*H*-pyrrol-3-yl)propionic acid methyl ester (**13**) as a thick, pale yellow oil.

Compound **13** (0.35 g, 1.9 mmol) and 0.5 g (3.9 mmol) of chloromethylenedimethylammonium chloride in 10 mL of dichloroethane were stirred at room temperature under nitrogen for 2 h. The reaction mixture was concentrated and treated with 10 mL of 6 M sodium hydroxide solution and then extracted three times with 10 mL of ethyl acetate. The ethyl acetate extracts were combined, dried over anhydrous sodium sulfate, and evaporated to dryness to give 0.24 g (60% yield) of 3-(5-formyl-2,4-dimethyl-1*H*-pyrrol-3-yl)propionic acid methyl ester (**14**) as a brown oil.

Compound **14** (0.23 g, 1.1 mmol) in 6 N sodium hydroxide (10 mL) was heated at 100 °C for 2 h. The reaction mixture was cooled to room temperature, acidified with 6 N hydrochloric acid, and extracted three times with 10 mL of ethyl acetate. The combined organic layers were washed with 10 mL of water and 5 mL of brine, dried over anhydrous sodium sulfate, and evaporated to dryness to give 230 mg (100%) of crude 3-(5-formyl-2,4-dimethyl-1*H*-pyrrol-3-yl)propionic acid (**15**) as a brown oil.

Compound **15** (0.22 g, 1.1 mmol), 0.15 g (1.1 mmol) of indolin-2-one, and 0.05 g (0.6 mmol) of piperidine were refluxed in 5 mL of ethanol overnight. The mixture was concentrated to dryness and chromatographed on a silica gel column eluting with ethyl acetate–hexane–acetic acid to give 80 mg (23% yield) of 3-[2,4-dimethyl-5-(2-oxo-1,2-dihydroindol-3-ylidenemethyl)-1*H*-pyrrol-3-yl]propionic acid (**16a**) as a mustard yellow solid: ^{1}H NMR (360 MHz, DMSO-d_6) δ 13.38 (s, br, 1H, NH-1′), 12.05 (s, br, 1H, CH_2CH_2COOH-4′), 10.70 (s, br, 1H, NH-1), 7.69 (d, J = 7.39 Hz, 1H, H-4), 7.53 (s, 1H, H-vinyl), 7.06 (t, J = 7.39 Hz, 1H, H-6), 6.95 (t, J = 7.39 Hz, 1H, H-5), 6.85 (d, J = 7.39 Hz, 1H, H-7), 2.63 (t, J = 7.45 Hz, 2H, CH_2CH_2-COOH-4′), 2.34 (t, J = 7.45 Hz, 2H, CH_2CH_2COOH-4′), 2.28 (s, 3H, CH_3), 2.24 (s, 3H, CH_3); MS *m/z* (relative intensity, %) 311 ([M + 1]$^+$, 100). Anal. ($C_{18}H_{18}N_2O_3$) C, H, N.

3-[5-(5-Bromo-2-oxo-1,2-dihydroindol-3-ylidenemethyl)-2,4-dimethyl-1*H*-pyrrol-3-yl]propionic Acid (16b). The reaction mixture of 106.0 mg (0.5 mmol) of 5-bromo-indolin-2-one, 97.5 mg (0.5 mmol) of **15**, and 75 μL (0.75 mmol) of piperidine in 2.0 mL of ethanol was heated at 95 °C for 5 h and cooled to room temperature. The precipitate was filtered, washed with cold ethanol, 2 N hydrogen chloride, and water, and dried to give 171 mg (88%) of 3-[5-(5-bromo-2-oxo-1,2-dihydroindol-3-ylidenemethyl)-2,4-dimethyl-1*H*-pyrrol-3-yl]-propionic acid as a dark yellow solid: ^{1}H NMR (360 MHz, DMSO-d_6) δ 12.04 (s, br, 1H, CH_2CH_2COOH-4′), 10.80 (s, br, 1H, NH-1), 8.00 (d, J = 2.06 Hz, 1H, H-4), 7.67 (s, 1H, H-vinyl), 7.19 (dd, J = 2.06, 8.50 Hz, 1H, H-6), 6.79 (d, J = 8.50 Hz, 1H, H-7), 2.64 (t, J = 7.63 Hz, 2H, CH_2CH_2COOH-4′), 2.35 (t, J = 7.63 Hz, 2H, CH_2CH_2COOH-4′), 2.29 (s, 3H, CH_3), 2.27 (s, 3H, CH_3); MS *m/z* (relative intensity, %) 389 (M^+, 100). Anal. ($C_{18}H_{17}BrN_2O_3$) C, H, N.

3-[4-(2-Carboxyethyl)-3,5-dimethyl-1*H*-pyrrol-2-yl methylene]-2-oxo-2,3-dihydro-1*H*-indole-5-carboxylic Acid (16c). This compound was prepared using the same procedure as for preparation of **16b** with a yield of 65%: ^{1}H NMR (300 MHz, DMSO-d_6) δ 13.39 (s, 1H, NH-1′), 12.31 (s, br, 2H, COOH-5 and CH_2CH_2COOH-4′), 11.07 (s, 1H, NH-1), 8.04 (s, 1H, H-4), 7.72 (d, J = 8.07 Hz, 1H, H-6), 7.70 (s, 1H, H-vinyl), 6.93 (d, J = 8.07 Hz, 1H, H-7), 2.64 (t, J = 7.37 Hz, 2H, CH_2CH_2COOH-4′), 2.34 (t, J = 7.37 Hz, 2H, CH_2CH_2COOH-4′), 2.30 (s, 3H, CH_3), 2.28 (s, 3H, CH_3); MS *m/z* (relative intensity, %) 354 (M^+, 100). Anal. ($C_{19}H_{18}N_2O_5 \cdot 0.5H_2O$) C, H, N.

3-[2,4-Dimethyl-5-(2-oxo-5-sulfamoyl-1,2-dihydroindol-3-ylidenemethyl)-1*H*-pyrrol-3-yl]propionic Acid (16d). This compound was prepared using the same procedure as for preparation of **16b** with a yield of 60%: ^{1}H NMR (300 MHz, DMSO-d_6) δ 13.40 (s, 1H, NH-1′), 12.09 (s, br, 1H, CH_2CH_2COOH-4′), 11.10 (s, 1H, NH-1), 8.16 (s, 1H, H-4), 7.65 (s, 1H, H-vinyl), 7.55 (d, J = 8.21 Hz, 1H, H-6), 7.10 (s, br, 2H, H_2NSO_2-5), 6.98 (d, J = 8.21 Hz, 1H, H-7), 2.64 (t, J = 7.22 Hz, 2H, CH_2CH_2COOH-4′), 2.38 (t, J = 7.22 Hz, 2H, CH_2CH_2COOH-4′), 2.31 (s, 3H, CH_3), 2.28 (s, 3H, CH_3); MS *m/z* (relative intensity, %) 389 (M^+, 100). Anal. ($C_{18}H_{19}N_3O_5S \cdot 0.8H_2O$) C, H, N.

3-[5-(6-Methoxy-2-oxo-1,2-dihydroindol-3-ylidenemethyl)-2,4-dimethyl-1*H*-pyrrol-3-yl]propionic Acid (16e). This compound was prepared using the same procedure as for preparation of **16b** with a yield of 76%: ^{1}H NMR (360 MHz, DMSO-d_6) δ 13.15 (s, br, 1H, NH-1′), 11.70 (s, br, 1H, CH_2CH_2COOH-4′), 10.65 (s, br, 1H, NH-1), 7.58 (d, J = 8.27 Hz, 1H, H-4), 7.39 (s, 1H, H-vinyl), 6.54 (dd, J = 2.26, 8.27 Hz, 1H, H-5), 6.43 (d, J = 2.26 Hz, 1H, H-7), 3.74 (s, 3H, OCH_3-6), 2.62 (t, J = 7.67 Hz, 2H, CH_2CH_2COOH-4′), 2.30 (t, J = 7.67 Hz, 2H, CH_2CH_2COOH-4′), 2.26 (s, 3H, CH_3), and 2.22 (s, 3H, CH_3); MS *m/z* (relative intensity, %) 341 (M^+, 100). Anal. ($C_{19}H_{20}N_2O_4 \cdot 0.5H_2O$) C, H, N.

3-[2,4-Dimethyl-5-(2-oxo-6-phenyl-1,2-dihydroindol-3-ylidenemethyl)-1*H*-pyrrol-3-yl]propionic Acid (16f). This compound was prepared using the same procedure as for preparation of **16b** with a yield of 71%: ^{1}H NMR (360 MHz, DMSO-d_6) δ 13.38 (s, br, 1H, NH-1′), 12.05 (s, br, 1H, CH_2CH_2COOH-4′), 10.81 (s, br, 1H, NH-1), 7.79 (d, J = 7.84 Hz, 1H, H-4), 7.62 (d, J = 7.51 Hz, 2H, H-2″,6″), 7.58 (s, 1H, H-vinyl), 7.44 (t, J = 7.51 Hz, 2H, H-3″,5″), 7.32 (t, br, J =

7.51 Hz, 1H, H-4″), 7.26 (dd, J = 1.13, 7.84 Hz, 1H, H-5), 7.09 (d, J = 1.13 Hz, 1H, H-7), 2.64 (t, J = 7.71 Hz, 2H, CH_2CH$_2$-COOH-4′), 2.35 (t, J = 7.71 Hz, 2H, CH$_2$CH_2COOH-4′), 2.30 (s, 3H, CH$_3$), 2.26 (s, 3H, CH$_3$); MS m/z (relative intensity, %) 387 ([M + 1]$^+$, 100). Anal. ($C_{24}H_{22}N_2O_3 \cdot 0.5H_2O$) C, H, N.

3-{5-[6-(3-Methoxy-phenyl)-2-oxo-1,2-dihydroindol-3-ylidenemethyl]-2,4-dimethyl-1*H*-pyrrol-3-yl}propionic Acid (16g). This compound was prepared using the same procedure as for preparation of **16b** with a yield of 91%: ^{1}H NMR (360 MHz, DMSO-d_6) δ 13.38 (s, br, 1H, NH-1′), 12.04 (s, br, 1H, CH$_2$CH$_2$COOH-4′), 10.79 (s, br, 1H, NH-1), 7.77 (d, J = 8.05, 1H, H-4), 7.58 (s, 1H, H-vinyl), 7.35 (t, J = 8.11 Hz, 1H, H-5″), 7.27 (dd, J = 1.49, 8.05 Hz, 1H, H-5), 7.19 (d, br, J = 8.11 Hz, 1H, H-6″), 7.14 (t, J = 2.31 Hz, 1H, H-2″), 7.09 (d, J = 1.49 Hz, 1H, H-7), 6.90 (dd, J = 2.31, 8.11 Hz, 1H, H-4″), 3.81 (s, 3H, OCH$_3$-3″), 2.65 (t, J = 7.62 Hz, 2H, CH_2CH$_2$COOH-4′), 2.35 (t, J = 7.62 Hz, 2H, CH$_2$CH_2COOH-4′), 2.30 (s, 3H, CH$_3$), 2.27 (s, 3H, CH$_3$); MS m/z (relative intensity, %) 417 ([M + 1]$^+$, 72). Anal. ($C_{25}H_{24}N_2O_4 \cdot 0.25H_2O$) C, H, N.

3-{5-[6-(2-Methoxyphenyl)-2-oxo-1,2-dihydroindol-3-ylidenemethyl]-2,4-dimethyl-1*H*-pyrrol-3-yl}propionic Acid (16h). This compound was prepared using the same procedure as for preparation of **16b** with a yield of 44%: ^{1}H NMR (360 MHz, DMSO-d_6) δ 13.38 (s, br, 1H, NH-1′), 12.00 (s, br, 1H, CH$_2$CH$_2$COOH-4′), 10.70 (s, br, 1H, NH-1), 7.71 (d, J = 7.81 Hz, 1H, H-4), 7.55 (s, 1H, H-vinyl), 7.28–7.33 (m, 2H, H-4″,6″), 7.09 (d, J = 7.60 Hz, 1H, H-3″), 7.05 (dd, J = 1.27, 7.81 Hz, 1H, H-5), 7.01 (t, J = 7.60 Hz, 1H, H-5″), 7.00 (d, J = 1.27 Hz, 1H, H-7), 3.76 (s, 3H, OCH$_3$-2″), 2.66 (t, J = 7.60 Hz, 2H, CH_2CH$_2$COOH-4′), 2.35 (t, J = 7.60 Hz, 2H, CH$_2$CH_2COOH-4′), 2.30 (s, 3H, CH$_3$), 2.26 (s, 3H, CH$_3$); MS m/z (relative intensity, %) 415 ([M − 1]$^+$, 100). Anal. ($C_{25}H_{24}N_2O_4 \cdot 0.2H_2O$) C, H, N.

3-{5-[6-(4-Methoxyphenyl)-2-oxo-1,2-dihydroindol-3-ylidenemethyl]-2,4-dimethyl-1*H*-pyrrol-3-yl}propionic Acid (16i). This compound was prepared using the same procedure as for preparation of **16b** with a yield of 57%: ^{1}H NMR (360 MHz, DMSO-$d6$) δ 13.35 (s, br, 1H, NH-1′), 12.02 (s, br, 1H, CH$_2$CH$_2$COOH-4′), 10.75 (s, br, 1H, NH-1), 7.74 (d, J = 6.75 Hz, 1H, H-4), 7.56 (d, J = 9.01 Hz, 2H, H-2″,6″), 7.54 (s, 1H, H-vinyl), 7.21 (dd, J = 1.57, 6.75 Hz, 1H, H-5), 7.04 (d, J = 1.57 Hz, 1H, H-7), 7.00 (d, J = 9.01 Hz, 2H, H-3″,5″), 3.79 (s, 3H, OCH$_3$-4″), 2.65 (t, J = 7.54 Hz, 2H, CH_2CH$_2$COOH-4′), 2.35 (t, J = 7.54 Hz, 2H, CH$_2$CH_2COOH-4′), 2.29 (s, 3H, CH$_3$), 2.26 (s, 3H, CH$_3$); MS m/z (relative intensity, %) 417 ([M + 1]$^+$, 100). Anal. ($C_{25}H_{24}N_2O_4 \cdot 0.25H_2O$) C, H, N.

Molecular Modeling. Homology models for the catalytic domains of VEGF-R2 (Flk-1/KDR) and PDGF-R were generated using the Modeler program in InsightII 95.5 released from Molecular Simulations, Inc. The "open form" of FGF-R1 cocrystallized with SU4984 (PDB code: 1agw) was used as reference, and t he sequence alignment was based on previous study[15] with slight modifications. Since the sequence homologies between FGF-R1 and VEGF-R2 (Flk-1/KDR) (62%) and between FGF-R1 and PDGF-R (51%) are very high, the overall structures were similar. The VEGF-R2 (Flk-1/KDR) and PDGF-R models were superimposed with the FGF-R1 crystal structures based on the Cα trace. Docking of substituted indolin-2-ones to these receptors were done manually based on the FGF-R1/SU4984 crystal structure followed by simple energy minimization.

PDGF-R and EGF-R Kinase Assays. Solubilized membranes derived from NIH3T3 mouse fibroblasts overexpressing human PDGF-Rβ or EGF-R were added to polystyrene 96-well microtiter plates which had been coated with a monoclonal antibody that recognized either the PDGF-R or EGF-R.[14] After a 30 min incubation with lysate, the plates were washed to remove unbound material, and serial dilutions of chemical inhibitors were added to the immunolocalized receptor. The kinase reaction was started by the addition of ATP to the wells at a final concentration of 20 μM for PDGF-Rβ and 3 μM for EGF-R, twice the experimentally determined K_m values for ATP. The kinase reaction was allowed to proceed for 30 min for PDGF-Rβ and 5 min for EGF-R at room temperature and then was stopped by addition of EDTA. The amount of phosphotyrosine present on the receptors in the individual wells was determined by incubating the immunolocalized receptor with a biotinylated monoclonal antibody directed against phosphotyrosine. After removal of the unbound anti-phosphotyrosine antibody, avidin-conjugated horseradish peroxidase H was added to the wells. A stabilized form of 3,3′,5,5′-tetramethylbenzidine dihydrochloride (TMB) and hydrogen peroxide (H_2O_2) was added to the wells. The color readout of the assay was allowed to develop for approximately 30 min and the reaction was stopped with sulfuric acid (H_2SO_4).

FGF-R1 and Flk-1/KDR Kinase Assays. The catalytic portion of FGF-R1 and Flk-1/KDR were expressed as GST fusion proteins following infection of *Spodoptera frugiperda* (sf9) cells with engineered baculoviruses. GST-FGFR1 and GST-Flk1 were purified to homogeneity from infected sf9 cell lysates by glutathione sepharose chromatography. The assays were performed in 96-well microtiter plates that had been coated overnight with 2.0 μg of a polyGlu-Tyr peptide (4:1) (Sigma P-0275) in 0.1 mL of PBS per well. The purified kinases were diluted in kinase assay buffer (100 mM Hepes pH 7.5, 100 mM NaCl, and 0.1 mM sodium orthovanadate) and added to all test wells at 5 ng of GST fusion protein per 0.05 mL volume buffer. Test compounds were diluted in 4% DMSO and added to test wells (0.025 mL/well). The kinase reaction was initiated by the addition of 0.025 mL of 40 μM ATP/40 mM $MnCl_2$, and plates were shaken for 10 min before stopping the reactions with the addition of 0.025 mL of 0.5 M EDTA. The final ATP concentration was 10 μM, which is twice the experimentally determined K_m value for ATP. Negative control wells received $MnCl_2$ alone without ATP. The plates were washed three times with 10 mM Tris pH 7.4, 150 mM NaCl, and 0.05% Tween-20 (TBST). Rabbit polyclonal anti-phosphotyrosine antiserum was added to the wells at a 1:10000 dilution in TBST for 1 h. The plates were then washed three times with TBST. Goat anti-rabbit antiserum conjugated with horseradish peroxidase was then added to all wells (Biosource Cat. No. ALI0404; 1:10000 dilution in TBST) for 1 h. The plates were washed three times with TBST, and the peroxidase reaction was detected with the addition of 2,2′-azinobis(3-ethylbenzthiazoline-6-sulfonic acid) (ABTS) (Sigma A1888). The color readout of the assay was allowed to develop for 20–30 min and read on a Dynatech MR5000 ELISA plate reader using a 410 nM test filter.

PDGF and EGF-Dependent BrdU Incorporation Assays. NIH 3T3 cells overexpressing human EGF receptors (8000/well) were added to a 96-well microtiter plate in DMEM containing 10% calf serum (Rockville, MD). The plates were incubated overnight at 37 °C, and then deprived of serum for 24 h by incubation with DMEM containing 1% BSA, followed by stimulation with PDGF-β (3.8 nM) or EGF (4 nM) in the presence of various test compounds. After 20 h of incubation, BrdU (Roche Molecular Biochemicals, Indianapolis, IN) was added for a 2 h labeling period, and the cells were fixed with Fix/Denat solution (Roche Molecular Biochemicals, Indianapolis, IN). The amount of BrdU incorporation was then determined using anti-BrdU/POD and the horseradish peroxidase substrate, ABTS (both from Roche Molecular Biochemicals, Indianapolis, IN). All experiments were performed three times, and the IC_{50} values were determined by nonlinear regression using the data analysis program PRISM (Graphpad Inc., San Diego, CA).

VEGF and FGF Cell BrdU Incorporation Assays. These cellular assays were preformed as previously described.[8]

Acknowledgment. The authors thank Robert Blake, Danny Tam, James Rodda, and Kim Lach for providing data on the enzymatic activities of the inhibitors, Zhaoyang Wen for preparing compounds **16c** and **16d**, and Kenneth E. Lipson for organizing the BrdU data.

References

(1) Kolibaba, K. S.; Druker, B. J. Protein tyrosine kinases and cancer. *Biochim. Biophys. Acta* **1997**, *1333*, F217–F248.

(2) Cantley, L. C.; Auger, K. R.; Carpenter, C.; Duckworth, B.; Graziani, A.; Kapeller, R.; Soltoff, S. Oncogenes and signal transduction. *Cell* **1991**, *64*, 281–302.

(3) Merenmies, J.; Parada, L. F.; Henkemeyer, M. Receptor tyrosine kinase signaling in vascular development. *Cell Growth Differ.* **1997**, *8*, 3–310.

(4) Shawver, L. K.; Lipson, K. E.; Fong, T. A. T.; McMahon, G.; Plowman, G. D.; Strawn, L. M. Receptor tyrosine kinases as targets for inhibition of angiogenesis. *Drug Discovery Today* **1997**, *2* (2), 50–63.

(5) Plowman, G. D.; Ullrich, A.; Shawver, L. K. Receptor tyrosine kinases as targets for drug intervention. *DN&P* **1994**, *7* (6), 334–339.

(6) Sun, L.; Tran, N.; Tang, T.; App, H.; Hirth, P.; McMahon, G.; Tang, C. Synthesis and biological evaluations of 3-substituted indolin-2-ones: a novel class of tyrosine kinase inhibitors that exhibit selectivity towards particular receptor tyrosine kinases. *J. Med. Chem.* **1998**, *41* (14), 2588–2603.

(7) Mohammadi, M.; McMahon, G., Sun, L.; Tang, P. C.; Hirth, P.; Yeh, B. K.; Hubbard, S. R.; Schlessinger, J. Structures of the tyrosine kinase domain of fibroblast growth factor receptor in complex with inhibitors. *Science* **1997**, *276*, 955–960.

(8) Fong, A. T. T.; Shawver, L. K.; Sun, L.; Tang, C.; App, H.; Powell, T. J.; Kim, Y. H.; Schreck, R.; Wang, X. Y.; Risau, W.; Ullrich, A.; Hirth, K. P.; McMahon, G. SU5416 is a potent and selective inhibitor of the vascular endothelial growth factor receptor (Flk-1/KDR) that inhibits tyrosine kinase catalysis, tumor vascularization, and growth of multiple tumor types. *Cancer Res.* **1999**, *59*, 99–106.

(9) Mohammadi, M.; Froum, S.; Hamby, J. M.; Schroeder, M. C.; Panek, R. L.; Lu, G. H.; Eliseenkova, A. V.; Green, D.; Schlessinger, J.; Hubbard, S. R. Crystal structure of an angiogenesis inhibitor bound to the FGF receptor tyrosine kinase domain. *EMBO J.* **1998**, *17* (20), 5896–5904.

(10) Quallich, G. J.; Morrissey, P. M. A general oxindole synthesis. *Synthesis* **1993**, *1*, 51–53.

(11) Ogawa, H.; Tamada, S.; Fujioka, T.; Teramoto, S.; Kondo, K.; Yamashita, S.; Yabuuchi, Y.; Tominaga, M.; Nakagawa, K. Studies on Positive Inotropic Agents. V. Synthesis of 1-Heteroaroylpiperazine Derivatives. *Chem. Pharm. Bull.* **1988**, *36*, 2253–2258.

(12) Tang, C.; Nematalla, A.; Sun, L.; Andrews, S.; Garst, M. Improved synthesis of potent tyrosine kinase inhibitor. Manuscript in preparation.

(13) Woodward, R. B.; Ayer, W. A.; Beaton, J. M.; Bickelhaupt, F.; Bonnett, R.; Buchschacher, P.; Closs, G. L.; Dutler, H.; Hannah, J.; Hauck, F. P.; Ito, S.; Langemann, A.; Goff, E. L.; Leimgruber, W.; Lwowski, W.; Sauer, J.; Valenta, Z.; Volz, H. *Tetrahedron* **1990**, *46* (22), 7599–7659.

(14) Strawn, L. M.; McMahon, G.; App, H.; Schreck, R.; Kuchler, W. R.; Longhi, M. P.; Hui, T. H.; Tang, C.; Levitzki, A.; Gazit, A.; Chen, I.; Keri, G.; Orfi, L.; Risau, W.; Flamme, I.; Ullrich, A.; Hirth, K. P.; Shawver, L. K. Flk-1/KDR as a target for tumor growth inhibition. *Cancer Res.* **1996**, *56*, 3540–3545.

(15) Hanks, S.; Quinn, A. M. Protein kinase catalytic domain sequence database: Identification of conserved features of primary structure and classification of family members. *Methods Enzymol.* **1991**, *200*, 38–62.

JM9904295

Inhibition of lymphangiogenesis with resulting lymphedema in transgenic mice expressing soluble VEGF receptor-3

TAIJA MÄKINEN[1], LOTTA JUSSILA[1], TANJA VEIKKOLA[1], TERHI KARPANEN[1], MIKKO I. KETTUNEN[2], KALEVI J. PULKKANEN[3,4], RISTO KAUPPINEN[2], DAVID G. JACKSON[5], HAJIME KUBO[6], SHIN-ICHI NISHIKAWA[6], SEPPO YLÄ-HERTTUALA[3] & KARI ALITALO[1]

[1]*Molecular/Cancer Biology Laboratory and Ludwig Institute for Cancer Research, Haartman Institute, University of Helsinki, Helsinki, Finland*
[2]*National Bio-NMR Facility and* [3]*Department of Molecular Medicine, A.I. Virtanen Institute, University of Kuopio, Kuopio, Finland*
[4]*Department of Oncology, Kuopio University Hospital, Kuopio, Finland*
[5]*University of Oxford, Molecular Immunology Group, Nuffield Department of Medicine, Headington, Oxford, United Kingdom*
[6]*Department of Molecular Genetics, Kyoto University, Japan*
Correspondence should be addressed to K.A.; email: kari.alitalo@helsinki.fi

The lymphatic vasculature transports extravasated tissue fluid, macromolecules and cells back into the blood circulation. Recent reports have focused on the molecular mechanisms regulating the lymphatic vessels. Vascular endothelial growth factor (VEGF)-C and VEGF-D have been shown to stimulate lymphangiogenesis and their receptor, VEGFR-3, has been linked to human hereditary lymphedema. Here we show that a soluble form of VEGFR-3 is a potent inhibitor of VEGF-C/VEGF-D signaling, and when expressed in the skin of transgenic mice, it inhibits fetal lymphangiogenesis and induces a regression of already formed lymphatic vessels, though the blood vasculature remains normal. Transgenic mice develop a lymphedema-like phenotype characterized by swelling of feet, edema and dermal fibrosis. They survive the neonatal period in spite of a virtually complete lack of lymphatic vessels in several tissues, and later show regeneration of the lymphatic vasculature, indicating that induction of lymphatic regeneration may also be possible in humans.

Vascular endothelial growth factor (VEGF) is a key regulator of endothelial cell functions required for vasculogenesis and for physiological and pathological angiogenesis[1,2]. The VEGF family also comprises placenta growth factor (PlGF), VEGF-B, VEGF-C, VEGF-D and VEGF-E (ref. 3), the effects of which are mediated by three endothelial cell-receptor tyrosine kinases, VEGFR-1/Flt-1, VEGFR-2/Flk-1/KDR and VEGFR-3/Flt4 (ref. 4). In addition, some VEGFs bind to the non-kinase coreceptor neuropilin-1. VEGF binds to VEGFR-1 and VEGFR-2, whereas VEGF-C and VEGF-D bind to VEGFR-2, and they are the only known ligands for VEGFR-3.

Targeted inactivation of *Flt1* (encoding VEGFR-1) or *Kdr* (encoding VEGFR-2) in mouse embryos leads to disorganized vessel formation due to enhanced production of endothelial cells, or to a block in the differentiation of both endothelial and hematopoietic cells[5,6], respectively. In contrast, *Flt4*$^{-/-}$ (encoding VEGFR-3) embryos die due to failure of remodeling and maturation of the primary capillary plexus[7]. In adult tissues, however, VEGFR-3 expression is mainly in lymphatic endothelium[8,9], and VEGF-C can induce the growth of lymphatic vessels[10,11]. We have recently reported that human hereditary lymphedema is associated with heterozygous missense mutations of *FLT4*, which inactivate the tyrosine kinase domain and lead to insufficient VEGFR-3 signaling[12,13]. The finding of germline mutations in lymphedema permits early diagnosis and treatment of the hereditary forms of this disease. However, the development of an animal model for lymphedema might also lead to more effective therapies for the more common forms of the disease caused by, for example, filariasis, surgery or radiotherapy.

A soluble form of VEGFR-1 generated by alternative RNA splicing inhibits the binding of VEGF to its cell-surface receptors and may regulate VEGF function *in vivo*[14]. Recombinant soluble VEGFR-1 or VEGFR-2 can inhibit both physiological and pathological angiogenesis, such as retinal neovascularization, *corpus luteum* angiogenesis or tumor growth[15–20]. Here we show that a chimeric protein consisting of the ligand-binding portion of the extracellular part of VEGFR-3, joined to the Fc domain of immunoglobulin (Ig) γ-chain (VEGFR-3–Ig) neutralizes the activity of VEGF-C and VEGF-D and inhibits the formation of the dermal lymphatic vasculature when expressed in mouse epidermis under the keratin-14 (K14) promoter. As the blood vessel network remained normal in these mice, the inhibition appears to be specific to the lymphatic vessels. VEGFR-3–Ig induced regression of lymphatic vessels during embryonic development, indicating that continuous signaling by this receptor is essential for the maintenance of the lymphatic vasculature. In addition, the phenotype of K14-VEGFR-3–Ig mice has features of human lymphedema. Here we show that considerable loss of lymphatic tissue need not prevent neonatal survival and that lymphatic regeneration can occur in adult tissues.

Soluble VEGFR-3 inhibits VEGF-C–mediated signaling *in vitro*

To investigate the inhibition of VEGF-C signaling by soluble VEGFR-3, we tested *in vitro* a fusion protein consisting of the first

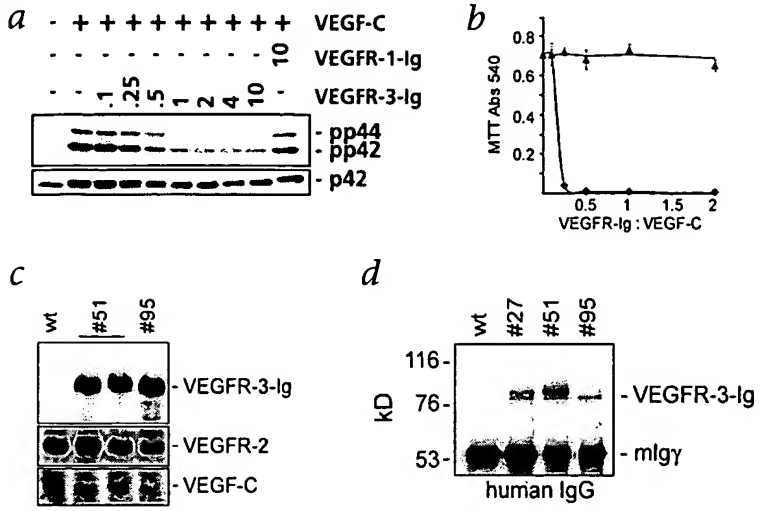

Fig. 1 Soluble VEGFR-3 inhibits ligand-dependent receptor signaling. *a*, Blocking of VEGF-C–induced p42/p44 MAP kinase activation in PAE/VEGFR-3 cells by VEGFR-3–Ig or VEGFR-1–Ig as measured by a western blot using a phospho-MAPK antibody. The VEGFR-Ig concentrations are indicated as molar ratios with VEGF-C. *b*, Inhibition of the VEGF-C–induced viability of Ba/F3 cells expressing a chimeric VEGFR-3/EpoR by VEGFR-3–Ig (◆) or by VEGFR-1-Ig (▲). Data represent the mean values from triplicate assays (mean ± s.d.). *c*, Transgene expression analyzed by northern blotting of total RNA isolated from the skin of K14-VEGFR-3–Ig or wild-type mice. *d*, Detection of transgene-encoded protein (around 90 kD) from the skin extracts of three different founder lines by immunoblotting using anti-human IgG antibodies. The antibodies cross-reacted with the murine Ig γ-chain (band at around 55 kD).

three Ig-homology domains of VEGFR-3 and the IgG Fc domain. VEGFR-3–Ig bound VEGF-C and VEGF-D with the same efficiency as the full-length extracellular domain (data not shown) and inhibited VEGF-C–induced VEGFR-3 phosphorylation (data not shown) and subsequent p42/p44 mitogen-activated protein kinase (MAPK) activation in VEGFR-3 expressing endothelial cells (Fig. 1*a*). In contrast, a similar VEGFR-1–Ig fusion protein, which does not bind VEGF-C, did not affect p42/p44 MAPK activation.

We also determined the effect of soluble VEGFR-3 on VEGF-C signaling in a bioassay using a chimeric VEGFR-3/erythropoietin (Epo) receptor capable of transmitting VEGF-C dependent survival and proliferation signals for the IL-3 dependent Ba/F3 cells in the absence of IL-3 (ref. 21). In this cellular assay, we observed complete inhibition of VEGF-C–dependent cell survival at a 0.5:1 molar ratio (VEGFR-3–Ig:VEGF-C), whereas VEGFR-1–Ig had no effect (Fig. 1*b*). Similarly, VEGFR-3–Ig also abolished VEGF-D–induced survival of the VEGFR-3/EpoR cells (data not shown). In contrast, even a two-fold molar excess of VEGFR-2–Ig only partially abolished VEGF-C dependent viability, perhaps because of lower affinity of VEGF-C to VEGFR-2 (data not shown).

Soluble VEGFR-3 inhibits the formation of lymphatic vessels

To test the inhibitory effect of VEGFR-3–Ig *in vivo*, we expressed the fusion protein under the K14 promoter, which directs transgene expression to the basal epidermal cells of the skin. We detected VEGFR-3–Ig expression in transgenic mice by northern blotting of skin RNA (Fig. 1*c*) and by western blotting of protein extracts from the skin (Fig. 1*d*). These mice appeared healthy and fertile and had a normal lifespan, but histological examination of the skin revealed a thickened dermis and subcutaneous layer (Fig. 2*a* and *b*). Antibody staining confirmed VEGFR-3–Ig expression in the basal keratinocytes (Fig. 2*c* and *d*). When the skin sec-

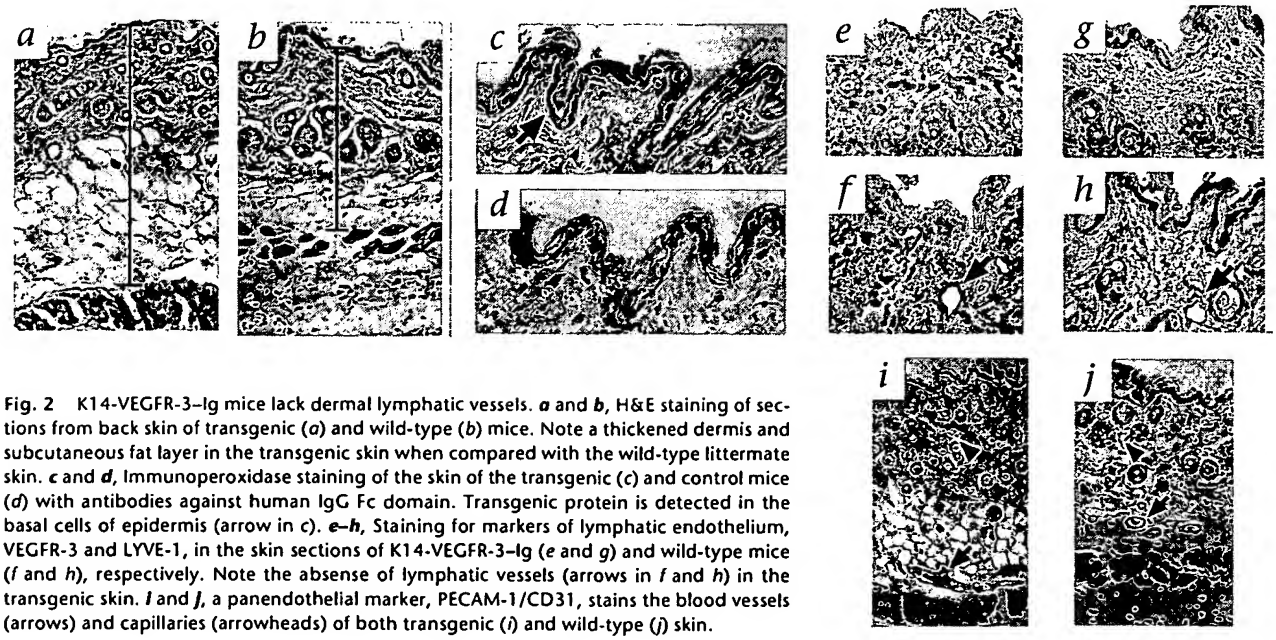

Fig. 2 K14-VEGFR-3–Ig mice lack dermal lymphatic vessels. *a* and *b*, H&E staining of sections from back skin of transgenic (*a*) and wild-type (*b*) mice. Note a thickened dermis and subcutaneous fat layer in the transgenic skin when compared with the wild-type littermate skin. *c* and *d*, Immunoperoxidase staining of the skin of the transgenic (*c*) and control mice (*d*) with antibodies against human IgG Fc domain. Transgenic protein is detected in the basal cells of epidermis (arrow in *c*). *e–h*, Staining for markers of lymphatic endothelium, VEGFR-3 and LYVE-1, in the skin sections of K14-VEGFR-3–Ig (*e* and *g*) and wild-type mice (*f* and *h*), respectively. Note the absense of lymphatic vessels (arrows in *f* and *h*) in the transgenic skin. *I* and *J*, a panendothelial marker, PECAM-1/CD31, stains the blood vessels (arrows) and capillaries (arrowheads) of both transgenic (*i*) and wild-type (*j*) skin.

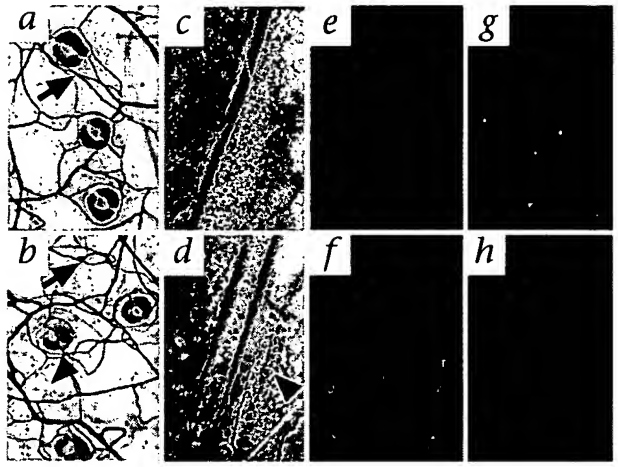

Fig. 3 Soluble VEGFR-3 inhibits lymphangiogenesis specifically. Top panel are transgenic; bottom panel are wild-type. ***a*** and ***b***, Lectin perfusion staining of the ear vasculature (arrows) of the transgenic (*a*) and control (*b*) mice in the VEGFR-3$^+$/LacZ background followed by whole mount staining of the lymphatic vessels with X-gal (arrowhead). ***c*** and ***d***, Ischiatic veins in wild-type (*d*) and transgenic (*c*) mice. The lymphatic vessels (arrowhead) were visualized by injection of Evans blue dye into the footpad of the hindlimb. ***e–h***, Visualization of the lymphatic vessels using fluoresence microscopy after intradermal TRITC-dextran injection into the ear or tail of wild-type (*f* and *h*) or K14-VEGFR-3–Ig (*e* and *g*) mice, respectively.

tions were stained for markers of the lymphatic endothelium, VEGFR-3 (refs. 22,23) and LYVE-1 (ref. 24), we observed no lymphatic vessels in the transgenic mice (Fig. 2*e* and *g*), though lymphatics were stained in the skin of control mice (Fig. 2*f* and *h*). In contrast, blood vessels were stained for the panendothelial marker PECAM-1/CD31 in both transgenic and wild-type skin (Fig. 2*i* and *j*).

Suppression of lymphangiogenesis but not angiogenesis

In order to better visualize the lymphatic vessels, the K14-VEGFR-3–Ig mice were mated with heterozygous VEGFR-3$^+$/LacZ mice that express β-gal in the *Flt4* locus[7]. When whole-mount tissue preparations of the ear skin were stained using the substrate X-gal, no lymphatic vessels were detected (Fig. 3*a*), whereas, in the control mice, blue-staining lymphatic vessels were visualized (Fig. 3*b*, arrowhead). In vascular perfusion staining using biotin-labeled lectin[25], the blood vessels appeared normal in the K14-VEGFR-3–Ig mice (Fig. 3*a* and *b*, arrows).

We also confirmed absence of the lymphatic vessels using a functional assay, monitoring the fate of Evans blue dye injected into the skin. The dye was rapidly collected into the lymphatic vessels surrounding the ischiatic vein after injection into the hindlimb footpads of wild-type mice (Fig. 3*d*), whereas no dye was seen in such vessels in the transgenic mice (Fig. 3*c*) where collecting lymphatic vessels were either absent or rudimentary (data not shown). We also visualized the lymphatic vessels in control mice using fluorescence microscopy for TRITC-dextran injected intradermally into the ear (Fig. 3*f*) or tail (Fig. 3*h*), whereas no such vessels were seen in the transgenic mice (Fig. 3*e* and *g*).

Transient loss of lymphatic tissue in internal organs

By the age of two weeks, the VEGFR-3–Ig/VEGFR-3+/LacZ mice had only a few thin and rudimentary, if any, lymphatic vessels in organs such as heart and caecum, esophagus, mesenterium, diaphragm (Fig. 4*a–h*), lungs and pancreas (data not shown) when compared with the control VEGFR-3$^+$/LacZ littermate mice. Such findings, obtained by X-gal staining, were confirmed by immunostaining for VEGFR-3 and LYVE-1 (data not shown). In addition, the lack of lymphatic vessels in heart pericardium was associated with pericardial fluid accumulation in at least

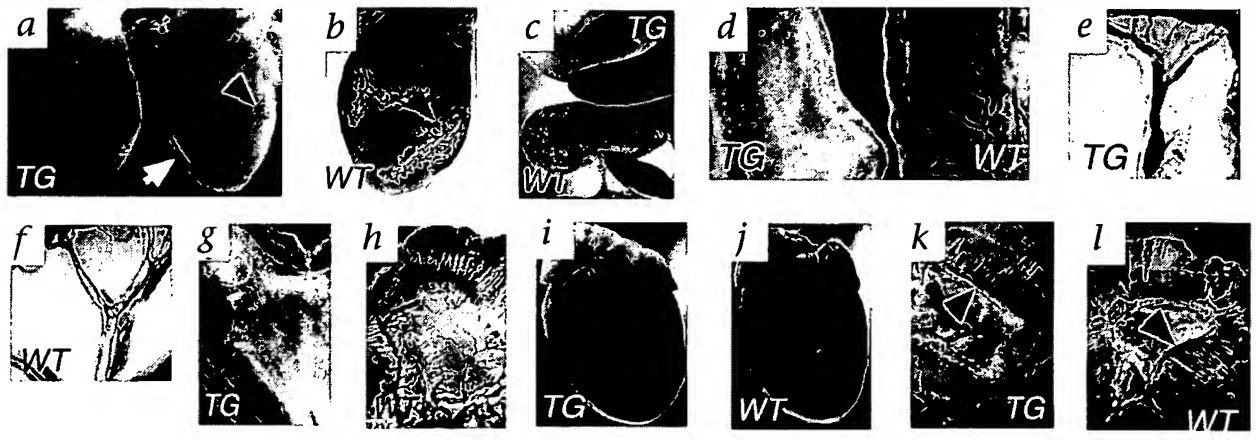

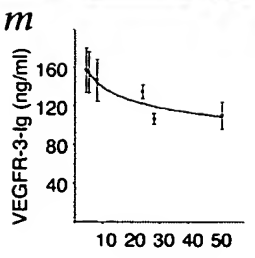

Fig. 4 Circulating levels of soluble VEGFR-3 inhibit lymphatic vessel development in internal organs. ***a***, ***c–g***, X-gal staining of the transgenic heart (*a*), caecum (*c*, upper), esophagus (*d*, on the left), mesenterium (*e*) and diaphragm (*g*) in comparison with the respective organs of wild-type mice (***b***, *c*, lower, *d*; on the right, *f* and ***h***) at the age of 2 weeks. Note the accumulation of fluid into the pericardial cavity (arrow in *a*) and a thin lymphatic vessel (arrowhead in *a*) on the surface of heart of the transgenic mouse, compared with the pericardial lymphatics of control heart (arrowhead in *b*). ***i–l***, Visualization of the lymphatic vessels in heart of transgenic (*i*) and wild type (*j*) mice at the age of 4 weeks and in the diaphragm of transgenic (*k*) and wild-type (*l*) mice at the age of 3 months. ***m***, Detection of the VEGFR-3–Ig protein in sera from two transgenic founder lines using a specific ELISA assay. Data represent mean values from 2 to 7 sera analyzed at each timepoint (mean ± s.d.).

some of the mice (Fig. 4*a*). At three weeks of age, regrowth of the lymphatic vessels was apparent (Fig. 4*i* and *j*). In adult transgenic mice, only some organs such as heart (data not shown) and diaphragm (Fig. 4*k* and *l*) had abnormally patterned and/or incompletely developed lymphatic vessels.

The effects seen in the internal organs indicate that the soluble VEGFR-3–Ig protein circulates in the bloodstream. We in fact detected the fusion protein in the sera of the transgenic mice using a specific enzyme-linked immunosorbent assay; the levels ranged between 100–200 ng/ml, being highest in younger mice (Fig. 4*m*). Based on our *in vitro* experiments, such concentrations would neutralize about 20–40 ng/ml of VEGF-C. The VEGFR-3–Ig protein was relatively stable in the bloodstream, as intravenously injected recombinant VEGFR-3–Ig was detectable in serum for at least nine hours (data not shown).

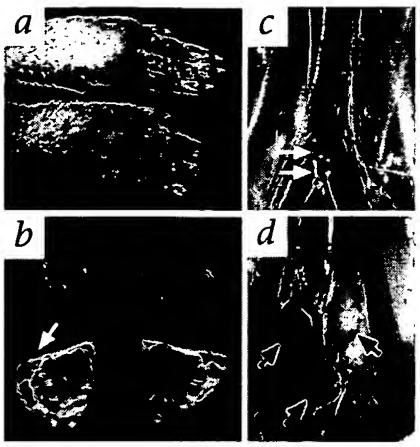

Fig. 5 Features of human lymphedema in the K14-VEGFR-3–Ig mice. ***a***, Hindlimbs of transgenic (lower) and control littermate (upper) mice. ***b***, T_2-weighted magnetic resonance imaging (MRI) of feet of transgenic (lower) and wild-type (upper) mice. Metatarsal region of a foot of a VEGFR-3–Ig mouse shows hyperintensity (arrow) that is absent in the control mouse. ***c*** and ***d***, The para-aortic lymph nodes surrounding the inferior *vena cava* in a transgenic (*c*) and wild-type littermate (*d*). Note the absence or different size of these lymph nodes (arrows) in the K14-VEGFR-3–Ig mouse.

The transgenic phenotype has features of lymphedema

The K14-VEGFR-3–Ig mice were distinguished from their wild-type littermates by the swelling of their feet (Fig. 5*a*), which was already visible at birth. Older mice showed thickening of the skin, dermal fibrosis and increased deposition of subcutaneous fat (Fig. 2*a* and *i*). Magnetic resonance imaging (MRI) revealed prominent T_2-hyperintense regions in foot skin and subcutaneous tissues of the transgenic mice indicating increased fluid accumulation, whereas similar regions were absent in littermate controls (Fig. 5*b*). The apparent diffusion coefficient (ADC) for these hyperintense areas was 1.99 [± 0.60] × 10^{-3} mm^2/s, being higher than for normal tissue where ADC was 1.32 [± 0.21] × 10^{-3} mm^2/s, and about 1–2 orders of magnitude greater than the values for fat[26]. In addition, the size and appearance of lymph nodes varied, especially in the large para-aortic lymph nodes surrounding the inferior *vena cava* (Fig. 5*c* and *d*). However, mesenteric lymph nodes and Peyer's patches were seen in the VEGFR-3–Ig mice (data not shown).

Regression of the developing lymphatic vessels

During embryogenesis, a dramatic increase in K14-driven transgene expression occurs at E14.5, and by E16.5 the expression encompasses the whole embryonic skin[27]. When analyzed in the VEGFR-3+/LacZ background by X-gal staining, the lymphatic networks of the skin were indistinguishable between transgenic and wild-type embryos at E15 (Fig. 6*a*). At E15.5–16.5, the lymphatic vessels of the transgenic embryos had regressed in some areas. At E17.5, the lymphatic vessels still formed a continuous network but were thinner than in control embryos (Fig. 6*a*). At E18.5, the whole cutaneous lymphatic network was disrupted in the transgenic embryos and after birth, no or only a few single disrupted lymphatic vessels were in the skin, mainly accompany-

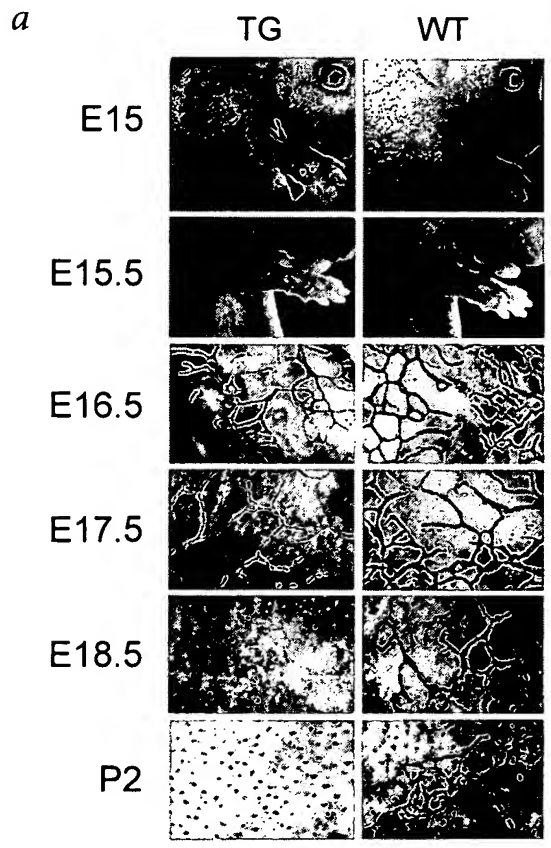

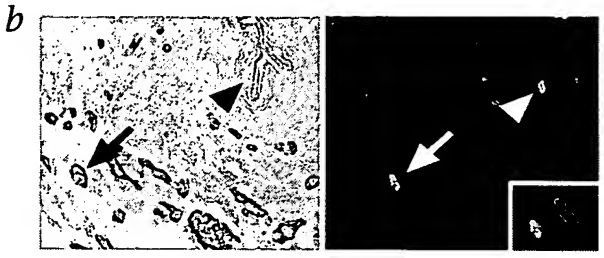

Fig. 6 Soluble VEGFR-3 leads to a regression of the lymphatic vessels in embryonic skin. ***a***, Visualization of the lymphatic vessels by X-gal staining in the skin of transgenic (TG) and wild-type (WT) embryos in the VEGFR-3$^+$/LacZ background. Note that at E15, the lymphatic networks are similar in TG and WT embryos, but the vessels regress in the TG embryos between E17.5-E18.5. ***b***, TUNEL staining for apoptotic cells (right panel) and PECAM-1 staining for endothelial cells (left panel) in skin section from a E18.5 K14-VEGFR-3–Ig embryo. Arrows indicate an apoptotic endothelial cell, arrowheads point to an apoptotic epidermal cell. Inset on the right shows a superimposed image of the TUNEL-positive vessel.

ing the large dermal blood vessels. Thus, the lymphatic vessels initially form in the skin during embryogenesis, but regress when the expression of the transgene is turned on. However, the formation of the dermal blood vasculature was not inhibited in the K14-VEGFR-3–Ig embryos as shown by X-gal staining in the Tie-promoter-LacZ background[28] (data not shown).

We used TUNEL staining to detect apoptosis in endothelial cells, which we identified by simultaneous staining for PECAM-1. We saw apoptotic endothelial cells in the dermis of the transgenic embryos beginning at E17.5 (data not shown) and E18.5 (Fig. 6*b*). No endothelial cell apoptosis was seen in wild-type embryos. The TUNEL-positive cells were detected almost exclusively in VEGFR-3 positive endothelia in the transgenic skin (data not shown), indicating that VEGFR-3–Ig mediated apoptosis was targeted to the lymphatic endothelium.

Discussion

We demonstrate here that a soluble VEGFR-3 fusion protein inhibits lymphangiogenesis and leads to regression of existing fetal lymphatic vessels *in vivo*. Continuous VEGFR-3 signaling is thus essential for the fetal development and maintenance of the lymphatic vascular system. Although soluble VEGFR-1– and VEGFR-2–Ig fusion proteins have been used *in vivo* to inhibit VEGF signaling and angiogenesis[15–19,29] and many other inhibitors of angiogenesis have been reported, soluble VEGFR-3 is the first inhibitor shown to be highly specific for lymphatic vessels without detectable effects on the blood vascular endothelium.

The absence of lymphatic vessels in the skin of K14-VEGFR-3–Ig mice was associated with a thickening of the dermis and especially the subcutaneous fat layer as in human lymphedema—a disorder caused by insufficiency of the lymphatic system and characterized by a swelling of the extremities of increasing severity[30,31,32]. In primary lymphedema, which is an inherited disease, the superficial or subcutaneous lymphatic vessels are usually hypoplastic or aplastic, and fail to transport the lymphatic fluid into the venous circulation. Noninherited secondary or acquired lymphedema develops when the lymphatic vessels are damaged by surgery, radiation, infection or trauma. In lymphedema, a protein-rich fluid accumulates in the interstitial space, leading to tissue fibrosis and adipose degeneration, interference with wound healing, and susceptibility to infections. In K14-VEGFR-3–Ig mice, we observed a lack of macromolecular transport in the dermis and, especially in older mice, signs of dermal fibrosis. Moreover, the swelling of the feet and increased fluid accumulation in the skin and subcutaneous tissue in the transgenic mice were similar to symptoms of human lymphedema. The skin phenotype of the K14-VEGFR-3–Ig mice thus shares several features with human lymphedema.

In studies of some lymphedema families, heterozygous inactivating missense mutations have been detected in the tyrosine kinase-encoding region of *Flt4* (refs. 12,13). Thus, at least some lymphedema patients have dysfunctional lymphatics due to defective VEGFR-3 signaling. Our results concur, as we show here that the disruption of VEGFR-3 signaling by the soluble VEGFR-3 protein can completely destroy the lymphatic network and lead to a lymphedema-like phenotype. Moreover, as in some cases of lymphedema, the size and appearance of certain regional lymph nodes was variable, indicating that lymph flow and a functional lymphatic vasculature are essential for the formation of normal lymph nodes.

VEGFR-3–Ig also induced regression of the already-formed lymphatics. Thus, inhibition of VEGF-C and/or VEGF-D binding to VEGFR-3 during development leads to apoptosis of the lymphatic endothelial cells and disruption of the lymphatic network, which indicates that continuous VEGFR-3 signaling is required for the survival of the lymphatic endothelial cells. In cell culture, VEGFR-3 activates biochemical signaling cascades associated with endothelial cell survival (T.M. *et al.*, unpublished data). Although transgenic mice that overexpress either VEGF-C (ref. 10) or VEGF-D (T.V. *et al.*, unpublished data) in the skin develop a hyperplastic dermal lymphatic vasculature, their dermal lymphatic vessels also regress when mated with K14-VEGFR-3–Ig mice (T.V. *et al.*, unpublished data). As both VEGFR-3 ligands are also expressed in the skin, the phenotype observed in K14-VEGFR-3–Ig mice might be due to a simultaneous inhibition of both VEGF-C and VEGF-D.

Inhibition of VEGF by soluble VEGFR-1–Ig inhibited angiogenesis during *corpus luteum* development and retinal neovascularization[15,16]. Moreover, in early post-natal life, VEGF inactivation led to apoptosis of endothelial cells, failure to thrive and lethality[29]. In adult animals, however, the suppression of VEGF was no longer able to induce endothelial cell apoptosis[29], probably due to pericyte coverage of the vasculature, which is thoughtto be the critical event determining whether endothelial cells remain dependent on VEGF for their survival[33]. For the lymphatic vessels, such criteria for vessel maturation have not been determined. For example, the lymphatic vessels have a discontinuous basement membrane and lack the pericyte coating typical of mature blood vessels. We are currently investigating if administration of recombinant VEGFR-3–Ig or an adenovirus encoding the same can induce the regression of lymphatic vessels in neonatal or adult mice.

Although VEGF-C and VEGF-D are mitogenic for blood vascular endothelial cells both *in vitro* and *in vivo*[34–38], VEGFR-3–Ig did not seem to affect the blood vessels. The late onset of K14-promoter expression may explain the lymphatic specificity of the VEGFR-3–Ig protein. A substantial increase in K14-promoter activity is not seen until around E14.5–16.5 (ref. 27). Although the expression of endogenous VEGFR-3 is first detected at E8.5 in developing blood vessels, by E14.5–16.5 it has been largely downregulated in blood vascular endothelia[7,8]. Therefore, during the developmental period when VEGFR-3 no longer occurs in the blood vessel endothelium, VEGFR-3 signaling does not seem to be important for angiogenesis in the skin.

In young VEGFR-3–Ig mice, several internal organs were almost completely devoid of lymphatic vessels, but they regrew in adult mice, although into an abnormal pattern in some organs. The growth and maintenance of lymphatic vasculature can therefore be reactivated in adult organs. Decreasing levels of VEGFR-3 inhibition, or independent signals from, for example, maturing connective tissue matrix might have reactivated lymphangiogenesis, but we obtained no evidence that increased VEGF-C or VEGF-D levels were responsible for the regrowth. However, administration by an adenovirus vector of VEGF-C in quantities exceeding those usually found in interstitial fluids can lead to lymphatic growth in adult tissues (B. Enholm *et al.*, unpublished data). The use in gene therapy of a modified VEGF-C that no longer binds VEGFR-2 (ref. 39) might prevent its potential effects on the blood vascular endothelium.

VEGFR-3 levels are increased in the vascular endothelia of various types of solid tumors[22,40,41] and VEGF-C has been detected in tumor cells[42–44]; two indications that VEGF-C may stimulate tumor angiogenesis and/or lymphangiogenesis. VEGFR-3–Ig could therefore be used therapeutically to inhibit

these processes. Recently, monoclonal antibodies blocking VEGFR-3 activation were reported to inhibit the growth of glioblastoma or prostatic carcinoma cells in mice[23]. In addition, soluble VEGFR-1 and VEGFR-2 proteins have already been shown to suppress tumor growth in mice[17–20]. Many tumors metastasize through the lymphatic vessels and VEGF-C and/or VEGF-D expression in tumor cells has been linked to lymphangiogenesis associated with tumors, invasion of cancer cells into the lymphatic vessels and lymph node metastasis[43–47]. Therefore, lymphatic eradication by molecular tool, such as soluble forms of VEGFR-3 could also provide a novel mechanism for the inhibition of tumor metastasis. We in fact have preliminary results indicating that the growth of VEGF-C expressing tumors and the induction of lymphangiogenesis in such tumors can be inhibited by VEGFR-3–Ig (T.K., M. Egeblad *et al.*, unpublished data).

In conclusion, we have shown that soluble VEGFR-3 is a potent and specific inhibitor of lymphangiogenesis *in vivo*. In addition, we have created a mouse model that has features of human lymphedema. As lymphedema always involves the skin, our mouse model is useful in understanding and characterizing this disease and in testing of new therapies that could be applied to human patients.

Methods

Production of VEGF-C, VEGF-D and VEGFR Ig-fusion proteins. We produced the mature form of human VEGF-C as described[34]. VEGF-D was from R&D Systems (Minneapolis, Minnesota).The expression plasmids encoding human VEGFR-1-Ig and VEGFR-3-Ig were constructed by PCR-amplification of the first three Ig homology domains of the extracellular portions of VEGFR-1 and VEGFR-3 using the primer pairs 5′-TCTCGGATC CTCTAGTTCAGGTTCAAAATT-3′/5′-GATGAGATCTTTATCATATATATG-CACTGA-3′ and 5′-CCTGGGATCCCTGGTGAGTGGCTACTCCATGAC -3′/ 5′-GATGAAGAGATCTTCATGCACAATGACCTCGG-3′, respectively. The products were cloned into the *Bgl*II site of pMT/BiP·V5·*His* C vector (Invitrogen) and the cDNA encoding the Fc-tail of human IgG1 was cloned in frame into the same vector. The stable Drosophila S2 cell (Invitrogen) pools were generated and after 4 d of induction using 500 mM $CuSO_4$ in serum-free DES medium (Invitrogen). The Ig-fusion proteins were purified from the conditioned medium by protein A affinity chromatography (Amersham Pharmacia).

VEGFR-3 bioassay. We seeded Ba/F3 cells expressing the VEGFR-3/EpoR chimera[21] in 96-well microtiter plates at 15,000 cells/well in triplicates supplied with 100 ng/ml of VEGF-C and with indicated concentrations of VEGFR-Ig proteins. After 48 h, the viability of the cells was determined by adding MTT (3-(4,5-dimethylthiazol-2-yl)-2,5-diphenyl tetrazolium bromide (Sigma), 0.5 mg/ml), followed by further 2 h of culture, addition of an equal volume of cell lysis solution (10% SDS, 10 mM HCl) and incubation overnight at 37 °C. Measurement of the absorbance was at 540 nm.

Generation of the transgenic mice. Using PCR, we amplified sequence encoding human VEGFR-3 Ig-homology domains 1–3 using the primers 5′-TACAAAGCTTTTCGCCACCATGCAG-3′ and 5′-TACAGGATCCTCATGCA-CAATGACCTC-3′ and cloned the product into the pIg-plus vector (Ingenius, R&D Systems) in frame with human IgG1 Fc tail. The VEGFR-3–Ig part was transferred into the human keratin-14 promoter-expression vector (gift of E. Fuchs). The expression cassette fragment was injected into fertilized mouse oocytes of the FVB/NIH and DBAxBalbC hybrid strains to create seven lines of K14-VEGFR-3–Ig mice. Transgene expression was analyzed and the phenotype was confirmed from all 3 founder lines expressing the transgene.

Analysis of transgene expression. For northern blotting, we electrophoresed 10 µg of total RNA extracted from skin in 1 % agarose, transferred it to nylon filters (Nytran), hybridized it with the corresponding [^{32}P]-labeled cDNA probes and exposed it by autoradiography. For western blotting, skin biopsies were homogenized into the lysis buffer (20 mM Tris, pH 7.6, 1 mM EDTA, 50 mM NaCl, 50 mM NaF, 1% Triton-X100) supplemented with 1 mM PMSF, 1 mU/ml approtinin, 1 mM Na_3VO_4 and 10 µg/ml leupeptin. The Ig-fusion proteins were precipitated from 1 mg of total protein and separated in SDS-PAGE, transferred to nitrocellulose and detected using the horseradish peroxidase-conjugated rabbit antibodies against human IgG (DAKO, Carpinteria, California) and the enhanced chemiluminescence detection system.

Immunohistochemistry and TUNEL staining. We stained Paraffin sections (5 µm) from 4% paraformaldehyde (PFA) fixed tissues using rat monoclonal antibodies against mouse VEGFR-3 (ref. 23) or CD31/PECAM-1 (PharMingen, San Diego, California), rabbit polyclonal antibodies against mouse LYVE-1 (ref. 24, and D. Jackson, unpublished data), or biotinylated mouse monoclonal antibodies against human IgG Fc domain (Zymed, San Diego, California). For TUNEL staining, detection of DNA fragmentation was done using *in situ* Cell Death Detection Kit (fluorescein; Roche).

Visualization of blood and lymphatic vessels. For visualization of blood vessels[25], we injected (IV) 100 µl of 1 mg/ml biotinylated *Lycopersicon esculentum* lectin (Sigma) by the femoral vein and allowed it to circulate for 2 min. After fixation by perfusion with 1% PFA/0.5% glutaraldehyde in PBS, bound lectin was visualized by the ABC-3,3′-diaminobenzidine peroxidase reaction. In VEGFR-3$^+$/LacZ mice the lymphatic vessels were then stained by the β-galactosidase substrate X-gal (Sigma). For the visualization of functional lymphatic vessels, Evans blue dye (Sigma, 5 mg/ml) was injected into the footpad of the hindlimb or TRITC-dextran (Sigma, 8 mg/ml) was injected intradermally into the ear or tail and the lymphatic vessels were analysed by light or fluorescence microscopy, respectively.

Detection of the VEGFR-3–Ig protein in serum. We coated the ELISA plates (Nunc Maxisorp, Copenhagen, Denmark) with mouse antibodies against human IgG (Zymed, 2 µg/ml in PBS) or human VEGFR-3 (clone 7B8, 4 µg/ml). The mouse sera were diluted into the incubation buffer (5 mg/ml BSA, 0.05 % Tween 20 in PBS) and allowed to bind for 2 h at room temperature. The plates were then washed 3 times with incubation buffer before addition of mouse anti-human IgG1 (Zymed, 1:500) for 1 h. Streptavidin conjugated with alkaline phosphatase (Zymed, 1:5000) was then incubated in the wells for 30 min, followed by addition of the substrate (1 mg/ml p-Nitrophenyl phosphate in 0.1 M dietanolamine, pH 10.3) and absorbance reading at 405 nm.

Magnetic resonance imaging. We acquired MRI data using a s.m.i.s. console (Surrey Medical Imaging Systems, Guildford, UK) interfaced to a 9.4 T vertical magnet (Oxford Instruments, Oxford, UK). A single loop surface coil (diameter 35 mm) was used for signal transmission and detection. A T_2-weighted (TR 2000 ms, TE 40 ms, 4 scans/line) multislice spin-echo sequence was used with an FOV of 25.6 mm^2 (matrix size: 256 × 128) and slice thickness of 1.3 mm in transverse orientation. Saturation pulses centered at 1.2 ppm were used to decrease fat signals in T_2-images. Diffusion weighted MRI was acquired using monopolar diffusion gradients (b-value ≈800 s/mm^2) along slice axis in the spin-echo sequence (TR 2000 ms, TE 40 ms), and water apparent diffusion coefficient (ADC) was computed by fitting the MRI data as function of b-values into a single exponential.

Acknowledgments

We thank G. Thurston and D. McDonald for teaching the lectin staining. J Jänne, L. Alhonen, M. Jänne and H. Rauvala for help in the generation of the transgenic mice; I. Seppälä for advice on ELISA; and T. Tainola, P. Ylikantola, S. Karttunen, R. Kivirikko and K. Makkonen for technical assistance. The K14 vector was a gift from E. Fuchs. This study was supported by grants from the Finnish Cancer Organization, Ida Montini Foundation, Finnish Cultural Foundation and Paulo Foundation.

RECEIVED 7 NOVEMBER; ACCEPTED 19 DECEMBER 2000

1. Ferrara, N. Molecular and biological properties of vascular endothelial growth factor. *J. Mol. Med.* 77, 527–543 (1999).
2. Carmeliet, P. Mechanisms of angiogenesis and arteriogenesis. *Nature Med.* 6, 389–395 (2000).

3. Eriksson, U. & Alitalo, K. Structure, expression and receptor-binding properties of novel vascular endothelial growth factors. *Curr. Top. Microbiol. Immunol.* 237, 41–57 (1999).
4. Veikkola, T., Karkkainen, M.J., Claesson-Welsh, L. & Alitalo, K. Regulation of angiogenesis via vascular endothelial growth factor receptors. *Cancer Res.* 60, 203–212 (2000).
5. Fong, G.-H., Zhang, L., Bryce, D.-M. & Peng, J. Increased hemangioblast commitment, not vascular disorganization, is the primary defect in flt-1 knock-out mice. *Development* 126, 3015–3025 (1999).
6. Shalaby, F. *et al.* Failure of blood island formation and vasculogenesis in Flk-1-deficient mice. *Nature* 376, 62–66 (1995).
7. Dumont, D.J. *et al.* Cardiovascular failure in mouse embryos deficient in VEGF receptor-3. *Science* 282, 946–949 (1998).
8. Kaipainen, A. *et al.* Expression of the *fms*-like tyrosine kinase FLT4 gene becomes restricted to lymphatic endothelium during development. *Proc. Natl. Acad. Sci. USA* 92, 3566–3570 (1995).
9. Partanen, T.A. *et al.* VEGF-C and VEGF-D expression in neuroendocrine cells and their receptor, VEGFR-3, in fenestrated blood vessels in human tissues. *FASEB J.* 14, 2087–2096 (2000).
10. Jeltsch, M. *et al.* Hyperplasia of lymphatic vessels in VEGF-C transgenic mice. *Science* 276, 1423–1425 (1997).
11. Oh, S.J. *et al.* VEGF and VEGF-C: specific induction of angiogenesis and lymphangiogenesis in the differentiated avian chorioallantoic membrane. *Dev. Biol.* 188, 96–109 (1997).
12. Karkkainen, M.J. *et al.* Missense mutations interfere with VEGFR-3 signaling in primary lymphoedema. *Nature Genet.* 25, 153–159 (2000).
13. Irrthum, A., Karkkainen, M.J., Devriendt, K., Alitalo, K. & Vikkula, M. Congenital hereditary lymphedema caused by a mutation that inactivates VEGFR3 tyrosine kinase. *Am. J. Hum. Gen.* 67, 295–301 (2000).
14. Kendall, R.L. & Thomas, K.A. Inhibition of vascular endothelial cell growth factor activity by an endogenously encoded soluble receptor. *Proc. Natl. Acad. Sci. USA* 90, 10705–10709 (1993).
15. Aiello, L.P. *et al.* Suppression of retinal neovascularization in vivo by inhibition of vascular endothelial growth factor (VEGF) using soluble VEGF-receptor chimeric proteins. *Proc. Natl. Acad. Sci. USA* 92, 10457–10461 (1995).
16. Ferrara, N. *et al.* Vascular endothelial growth factor is essential for corpus luteum angiogenesis. *Nature Med.* 4, 336-340 (1998).
17. Lin, P. *et al.* Inhibition of tumor growth by targeting tumor endothelium using a soluble vascular endothelial growth factor receptor. *Cell Growth Differ.* 9, 49–58 (1998).
18. Kong, H.L. *et al.* Regional suppression of tumor growth by *in vivo* transfer of a cDNA encoding a secreted form of the extracellular domain of the flt-1 vascular endothelial growth factor receptor. *Hum. Gene Ther.* 9, 823–833 (1998).
19. Goldman, C.K. *et al.* Paracrine expression of a native soluble vascular endothelial growth factor receptor inhibits tumor growth, metastasis, and mortality rate. *Proc. Natl. Acad. Sci. USA* 95, 8795–8800 (1998).
20. Takayama, K. *et al.* Suppression of tumor angiogenesis and growth by gene transfer of a soluble form of vascular endothelial growth factor receptor into a remote organ. *Cancer Res.* 60, 2169–2177 (2000).
21. Achen, M.G. *et al.* Monoclonal antibodies to vascular endothelial growth factor-D block its interactions with both VEGF receptor-2 and VEGF receptor-3. *Eur. J. Biochem.* 267, 2505–2515 (2000).
22. Jussila, L. *et al.* Lymphatic endothelium and Kaposi's sarcoma spindle cells detected by antibodies against the vascular endothelial growth factor receptor-3. *Cancer Res.* 58, 1599–1604 (1998).
23. Kubo, H. *et al.* Involvement of vascular endothelial growth factor receptor-3 in maintenance of integrity of endothelial cell lining during tumor angiogenesis. *Blood* 96, 546–553 (2000).
24. Banerji, S. *et al.* LYVE-1, a new homologue of the CD44 glycoprotein, is a lymph-specific receptor for hyaluronan. *J. Cell Biol.* 144, 789–801 (1999).
25. Thurston, G. *et al.* Leakage-resistant blood vessels in mice transgenically overexpressing angiopoietin-1. *Science* 286, 2511–2514 (1999).
26. Hakumaki, J.M., Poptani, H., Sandmair, A.M., Yla-Herttuala, S. & Kauppinen, R.A. ^{1}H MRS detects polyunsaturated fatty acid accumulation during gene therapy of glioma: implications for the in vivo detection of apoptosis. *Nature Med.* 5, 1323–1327 (1999).
27. Byrne, C., Tainsky, M. & Fuchs, E. Programming gene expression in developing epidermis. *Development* 120, 2369–2383 (1994).
28. Korhonen, J. *et al.* Endothelial-specific gene expression directed by the tie gene promoter in vivo. *Blood* 86, 1828–1835 (1995).
29. Gerber, H.P. *et al.* VEGF is required for growth and survival in neonatal mice. *Development* 126, 1149–1159 (1999).
30. Witte, M.H., Way, D.L., Witte, C.L. & Bernas, M. Lymphangiogenesis: Mechanisms, significance and clinical implications. in *Regulation of Angiogenesis* (eds. Goldberg, I.D. & Rosen, E.M.) 65–112 (Birkhäuser Verlag, Basel, Switzerland, 1997).
31. Mortimer, P.S. The pathophysiology of lymphedema. *Cancer* 83, 2798–2802 (1998).
32. Karkkainen, M.J., Jussila, L., Ferral, R. E., Finegold, D.N. & Alitalo, K. Molecular regulation of lymphangiogenesis and targets for tissue oedema. *Trends Mol. Med.* 7, 18–22 (2000)
33. Benjamin, L.E., Hemo, I. & Keshet, E. A plasticity window for blood vessel remodelling is defined by pericyte coverage of the preformed endothelial network and is regulated by PDGF-B and VEGF. *Development* 125, 1591–1598 (1998).
34. Joukov, V. *et al.* Proteolytic processing regulates receptor specificity and activity of VEGF-C. *EMBO J.* 16, 3898–3911 (1997).
35. Achen, M.G. *et al.* Vascular endothelial growth factor D (VEGF-D) is a ligand for the tyrosine kinases VEGF receptor 2 (Flk1) and VEGF receptor 3 (Flt4). *Proc. Natl. Acad. Sci. USA* 95, 548–553 (1998).
36. Cao, Y. *et al.* Vascular endothelial growth factor C induces angiogenesis in vivo. *Proc. Natl. Acad. Sci. USA* 95, 14389–14392 (1998).
37. Witzenbichler, B. *et al.* Vascular endothelial growth factor-C (VEGF-C/VEGF-2) promotes angiogenesis in the setting of tissue ischemia. *Am. J. Pathol.* 153, 381–394 (1998).
38. Marconcini, L. *et al.* c-fos-induced growth factor/vascular endothelial growth factor D induces angiogenesis in vivo and in vitro. *Proc. Natl. Acad. Sci. USA* 96, 9671–9676 (1999).
39. Joukov, V. *et al.* A recombinant mutant vascular endothelial growth factor-C that has lost vascular endothelial growth factor receptor-2 binding, activation, and vascular permeability activities. *J. Biol. Chem.* 273, 6599–6602 (1998).
40. Lymboussaki, A. *et al.* Expression of the vascular endothelial growth factor C receptor VEGFR-3 in lymphatic endothelium of the skin and in vascular tumors. *Am. J. Pathol.* 153, 395–403 (1998).
41. Valtola, R. *et al.* VEGFR-3 and its ligand VEGF-C are associated with angiogenesis in breast cancer. *Am. J. Pathol.* 154, 1381–1390 (1999).
42. Salven, P. *et al.* Vascular endothelial growth factors VEGF-B and VEGF-C are expressed in human tumors. *Am. J. Pathol.* 153, 103–108 (1998).
43. Yonemura, Y. *et al.* Role of vascular endothelial growth factor C expression in the development of lymph node metastasis in gastric cancer. *Clin. Cancer Res.* 5, 1823–1829 (1999).
44. Tsurusaki, T. *et al.* Vascular endothelial growth factor-C expression in human prostatic carcinoma and its relationship to lymph node metastasis. *Br. J. Cancer* 80, 309–313 (1999).
45. Mandriota, S.J. *et al.* Vascular endothelial growth factor-C-mediated lymphangiogenesis promotes tumour metastasis. *EMBO J.* in the press (2001).
46. Skobe., M. *et al.* Induction of tumor lymphangiogenesis by VEGF-C promotes breast cancer metastasis. *Nature Med.* this issue (2001).
47. Stacker, S.A. *et al.* VEGF-D promotes the metastatic spread of cancer by lymphatics. *Nature Med.* this issue (2001).

June 27, 1999, 67:12 > THE VISUALIZATION OF T CELL RESPONSES1. < Previous

ARTICLE LINKS:
Abstract | References (56) | View full size inline images

Transplantation: Volume 67(12) 27 June 1999 pp 1508-1514

THE VISUALIZATION OF T CELL RESPONSES[1]

Barbara, Jeffrey A.J.[2]; Gilot, Bryant J.[3]; Hara, Masaki; Van Maurik, Andre; Jones, Nick D.; Turvey, Stuart E.[4]; Wood, Kathryn J.[5]

Nuffield Department of Surgery, University of Oxford, The John Radcliffe Hospital, Headington Oxford OX3 9DU

[1] This research was supported by the Wellcome Trust, British Heart Foundation, and National Kidney Research Foundation.

[2] Don and Lorraine Jacquot Travelling Fellow.

[3] Morris Scholar.

[4] Rhodes Scholar.

[5] Address correspondence to: Prof. Kathryn Wood, Nuffield Department of Surgery, Nuffield Department of Surgery, University of Oxford, The John Radcliffe Hospital, Headington Oxford OX3 9DU.

Received 5 November 1998.

Accepted 9 February 1999.

Abstract TOP

Transplanting allogeneic grafts is still significantly hampered by the rejection process, despite the use of powerful immunosuppressive agents. The T cell is recognized as playing a central role in the process of rejection, and it is believed that graft tolerance will ultimately be achieved by immunological manipulation of this cell (1, 2). As immunologists strive to define the role of the T cell in the fundamental processes of immunity and tolerance, new methods are emerging that will facilitate visualization of the T cells directly involved in the rejection response (3, 4). This overview addresses the visualization of T cell responses as made possible by these technological developments.

The majority of information available on antigen-specific T cells has been accrued in vitro. T cells derived from the secondary lymphoid organs of naive or primed mice are explanted and placed in in vitro antigen stimulation assays. The assay systems employed include proliferation (tritiated thymidine incorporation), cytotoxic analysis (limiting dilution assays), and cytokine detection by ELISA,

Article Outline

enzyme-linked immunospot assay (ELISPOT*), flow cytometric analysis, and reverse transcription-polymerase chain reaction. However, these in vitro systems are often difficult to interpret because bystander T cell effects may be operating, and the data obtained seem to reflect only distantly the complex microenvironment from which the T cells came. The generation of T cell clones and lines that display a uniform response to antigen offer some advantages, but they are relatively labor intensive to produce and maintain and are still exposed to tissue culture conditions far removed from the in vivo environment. In addition, because T cell clones respond to antigen only in a set way, the complex behavior of naive T cells in vivo is not necessarily reflected. Nevertheless, the analysis of clones and lines has enabled significant advances to be made in the areas of T cell receptor (TCR) antigen recognition, costimulation, and signaling events in T cell activation.

- Figure 1
- Figure 2
- Figure 3

THE T CELL-ANTIGEN PRESENTING CELL INTERACTION TOP

The in vitro analysis of antigen-specific T cells has not been limited to a functional readout. Various groups have attempted to visualize what happens when T cells contact antigen presenting cells (APCs) in vitro. When T cells engage APCs, the cell surface proteins and cytoskeletal components on T cells become polarized (5, 6). Using fluorescent antibody reagents and fluorescence microscopic analysis, it was demonstrated that during an antigen-specific interaction between a helper T cell and a B cell, the microtubule-organizing center moves toward the area of cell-cell contact. Thus, the Golgi apparatus, with its cytokine producing capacity, is also directed to the area of contact along with the T cell receptor and CD4 molecules. The notion of a directional release of cytokines from T cells was further substantiated by Janeway and co-workers using 3 μm Nucleopore chemotaxis membranes into which cells from an interleukin (IL)4-producing T cell clone (D10) were plugged (7). They demonstrated that IL4 was selectively released into the chamber containing the stimulating antibody (anti-D10 receptor antibody 3D3).

In recent times, our knowledge of the dynamics of T cell-APC contact and activation have been enhanced by digital imaging systems that have permitted an analysis of the spatial orientation of fluoresceinated receptors and intracellular proteins that accumulate at the contact zones. It has been shown that the TCR and lymphocyte function-associated antigen (LFA-1), with their associated intracellular proteins, protein kinase C and talin, respectively, are separated into spatial domains known as supramolecular activation clusters (8). The expression and cycling of the negative T cell regulator, CTLA4, between cell surface and intracellular vesicles was studied in a similar fashion and was found to be localized toward sites of TCR activation (9). The visualization of supramolecular activation clusters has provided new insights into the mechanisms of intercellular communication and T cell activation, with undoubted consequences for all areas of T cell biology.

THE VIDEOTAPING OF T CELL ACTIVATION TOP

The full activation of T cells requires the engagement of the TCR-MHC/peptide complex and additional costimulatory interactions (10). The ligation of LFA-1 on the T cell with ICAM-1 on the APC (B cell) is one such costimulatory pathway in T cell activation (11, 12). Fluorescence video microscopic analysis has been used to visualize the dynamics of T cell activation in vitro (13). The experiments used primed T cells from the lymph nodes of 5C.C7 TCR transgenic mice that recognize the moth cytochrome C peptide 88-103 presented in the context of the MHC class II molecule I-E^k (14, 15). The system devised enabled the simultaneous examination of morphological changes, alterations in intracellular calcium concentrations, and the localization of cell surface molecules on live cells in real time in vitro. Fura-2, which reveals itself as blue with low resting concentrations and red with high intracellular calcium concentrations, was used to examine intracellular events. ICAM-1 fused to green fluorescent protein (GFP) was used to explore changes at the cell surface; the GFP fluorescence is green for low ICAM1-GFP levels, yellow for medium, and red for high. The film foot-age of these experiments can be viewed at http://cmgm.stanford.edu/hhmi/mdavis (13).

The data obtained using this system indicated that a minimal but specific signal through the TCR is required to commence the program of T cell activation, which is then supported by the accessory costimulatory molecules. The elevation of intracellular calcium in the T cell is followed by the rapid up-regulation of ICAM-1 on the B cell at the contact interface. This clustering by ICAM-1 seems T cell driven and results in a sustained elevation of intracellular calcium within the cell. Valitutti et al. (16) have demonstrated that the

serial engagement of each peptide/MHC complex with many TCR molecules is a mechanism by which T cell activation may be amplified. Wülfing et al. (13) have eloquently demonstrated that ICAM-1 clustering represents another way in which T cell activation is amplified. As illustrated, the in vitro demonstration of live T cell interactions, using fluorescent dyes and video imaging, has provided important insights into the activation mechanisms employed by T cells.

VISUALIZING COSTIMULATION IN ACTION TOP

Of the known costimulatory pathways, the CD28/B7 system seems to be the most important (17, 18). To determine how CD28 costimulation affects T cell responses, the fluorescent dye 5-(and-6)-carboxyfluorescein diacetate, succinimidyl ester (CFSE), whose concentration is reduced by half at mitotic division (see THE IN VIVO VISUALIZATION OF T CELLS: SUPERANTIGENS AND TRANSGENICS), has been used to follow (by flow cytometric analysis) the proliferative history of subgroups of T cells in a bulk population in response to soluble anti-CD3 and anti-CD28 antibodies (19). This approach allowed T cell activation, as assessed by cell surface markers, and TCR usage to be examined simultaneously. By measuring the percentage of cells under each successive CFSE peak and the total yield of T cells at specific time points, the absolute number of daughter cells present can be calculated along with the absolute number of precursors and mitotic events. The data obtained in this study showed that TCR engagement primarily regulates the frequency of T cells entering the proliferative pool, whereas CD28 costimulation regulates not only the frequency of responding cells but also the number of mitotic events that occur. It is interesting that when maximal costimulation was provided, only 60% of the original T cell population could be induced to divide, despite 95% showing evidence of early activation (CD25 and CD69 up-regulation). This effect may be the result of the stimulatory antibodies used or may represent an inherent physiological checkpoint in the activation process.

THE IN VIVO VISUALIZATION OF T CELLS: SUPERANTIGENS AND TRANSGENICS TOP

Visualizing the behavior and responses of naive T cells in vivo has, until recently, been either difficult or impossible. The frequency of antigen-specific T cells is exceedingly low, and the sensitivity of standard techniques, such as flow cytometry and immunohistochemistry, is insufficient to identify them, even when reagents such as an appropriate set of Vα or Vβ antibodies are available. One of the first successful attempts at T cell examination in vivo involved the use of superantigens. In the 1960s, Festenstein identified a mouse antigen(s) derived from the minor lymphocyte stimulatory (Mls) locus that stimulated the proliferation of MHC-identical lymphocytes in vitro: mice with the Mls^b allele responded strongly to MHC-identical cells possessing the Mls^a allele (20). In 1988, it was reported that the Mls^a/MHC ligand could be recognized by a high proportion of T cells of Vβ 8.1 specificity (21). At the same time, a dominant Vβ 6 T lymphocyte reactivity to Mls^a/MHC was also demonstrated (22). These groups showed that when Mls^a/MHC was present during T cell development, the specific Vβ populations were deleted within the thymus, verifying that tolerance to self antigens was achieved at least in part by clonal deletion. The ability of superantigens to be recognized by a high proportion of T cells of known Vβ (or Vα) specificity was a useful surrogate for the initial study of naive antigen-specific T cells in vivo, irrespective of the nonphysiological nature of this response.

The development of TCR transgenic mice has provided another system in which naive antigen-specific T cells can be tracked in vivo (23-25). In most instances, there is a clonotypic antibody that identifies the TCR in immunohistochemical or flow cytometric analysis. However, these animals have a fixed and skewed T cell repertoire that limits the assessment of a physiological T cell response in vivo, and incomplete allelic exclusion at the α-chain locus can permit the generation of T cells with undefined specificities (26). In addition, the T cell response in these TCR transgenic mice to specific a antigen is overwhelmingly large and nonphysiological, as is the case with superantigens.

Because the major difficulty perceived when TCR transgenic mice are used is the number of antigen-reactive T cells encountered, a strategy was developed in which TCR transgenic (DO11.10) T cells were adoptively transferred into syngeneic normal recipients (4, 27). This allowed an antigen-specific population big enough to be detected by flow cytometric analysis (with clonotypic antibody) but of a size within the total T cell repertoire that could be considered physiological. These TCR transgenic mice possess a TCR that is

specific for a peptide from chicken ovalbumin (cOVA) bound to IA^d class II MHC molecules (28) that can be detected with the specific monoclonal antibody, KJ1-26 (29). After the injection of antigen, with or without adjuvant, the transgenic T cells were examined by flow cytometric analysis, immunohistochemical analysis, and 5-bromodeoxyuridine (BrDu) incorporation (proliferation), enabling a comprehensive study of T cell activation and trafficking in vivo. In the presence of antigen alone, tolerance was achieved, but when adjuvant was coadministered with antigen, immunity resulted, from which it is inferred that in the absence of inflammation, antigen stimulation may result in unresponsiveness.

The transgenic adoptive transfer system has now been extended to the visualization of both T and B lymphocytes in vivo, allowing an analysis of T-B interactions (30). In this study, the TCR transgenic T cells used were the $CD4^+$ cOVA-specific DO11.10 cells and the B cells were MD4 immunoglobulin transgenic cells specific for hen egg lysozyme (HEL) (31). cOVA was coupled with HEL producing the cOVA-HEL antigen, which was recognized by both transgenic populations. This study demonstrated that T cell activation occurred in the T cell areas of lymph nodes, whereas B cells were still dispersed in B cell follicles. However, both cell groups migrated to the B cell side of the follicular margin and interacted in this location. The precise visualization of T-B interactions in vivo will allow a more detailed examination of the mechanisms involved in this major effector pathway.

CFSE TOP

TCR transgenic T cells that are identified by a clonotypic antibody or by T cell populations (i.e., clones or lines) that are recognized by Vα or Vβ antibodies can be traced effectively in adoptive transfer experiments using the appropriate monoclonal antibody. However, if these reagents are unavailable, then CFSE is a suitable alternative that can also be used in combination with the above methods for the identification and examination of antigen-specific T cells in vivo. CFSE is a fluorescein-based dye that covalently couples with intracellular macromolecules resulting in persistence in viable lymphocytes for several weeks (allowing long-term migration studies) and division equally between daughter cells at cell division (32). Through the use of the BrDu-Hoechst quenching method for cell cycle and division analysis, Lyons and Parish determined that the sequential halving of CFSE staining was indeed caused by cell division (33).

Consequently, this property of CFSE can be used to examine cell division in vitro and the division of adoptively transferred cells in vivo. Using this approach, multiple successive generations of leukocytes can be resolved using flow cytometric analysis (Fig. 1, (19, 32, 34)). The cells can also be stained with other nonfluorescein markers (e.g., phycoerythrin) to provide further immunophenotypic information with flow cytometric analysis. In addition, the fluorescent nature of CFSE allows the in vivo detection of T cells in histological sections by fluorescence microscopic analysis (Fig. 2). However, by converting in situ immunofluorescence staining into immunoenzyme staining using anti-fluorescein isothiocyanate (FITC) antibodies, Oehen et al. (35) have developed a method for tracking adoptively transferred cells by light microscopic analysis, with improved visualization of general tissue morphology when compared with fluorescence microscopic analysis, by which tissue morphology is difficult to discern.

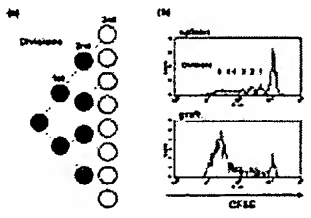

Figure 1. The labeling of T cells with 5 μM CFSE: (A) the halving of CFSE concentration with each successive division and (B) the proliferative behavior of $CD8^+$ TCR transgenic T cells (specific for K^b) in the spleen and cardiac graft after an adoptive transfer into a syngeneic host ($H2^k$) and exposure to an allogeneic K^{b+} graft. The organs were retrieved for flow cytometric analysis after 5 days; a single cell suspension of splenocytes was washed in phosphate-buffered saline containing 2% fetal calf serum; and the heart was digested with collagenase before washing.

Figure 2. CFSE-labeled T cells (5 μM) are present in the spleen 5 days after i.v. injection into a syngeneic recipient ($H2^k$) with probable localization to the marginal zone (the area between the white and red pulp containing numerous macrophages which can be identified by their red autofluoresce). After a splenectomy, the organ was placed in Tissuetek™ and frozen in liquid nitrogen. 7 μm cryosectioning was performed; the section was fixed in acetone after drying and viewed with a

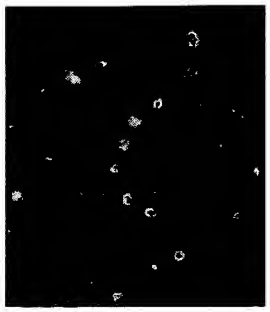

fluorescent microscope (magnification × 400).

Murine lymphocytes labeled with CFSE remain viable and proliferate to the same extent as unlabeled cells in response to the same stimulus (36), and cytotoxic T cells do not show impairment of cytotoxic activity when stained with CFSE (35). Whereas these murine T cell responses seem unaffected by CFSE labeling, human lymphocytes and granulocytes are partially inhibited by the fluorescent dye. CFSE inhibits, to varying extents, the proliferative response of human lymphocytes to phytohemaglutinin and pokeweed mitogen, and lymphocyte adhesion was also judged to be impaired. Our unpublished data in a murine system (T cell lines reactive to IA^b class II MHC) suggest that at higher concentrations of CFSE, lymphocyte proliferation in response to alloantigen, IL2, and concanavalin A supernatant is also impaired.

VISUALIZING ALLOSPECIFIC T CELLS DURING GRAFT REJECTION TOP

The adoptive transfer of transgenic T cells has provided immunologists with a marvellous opportunity to view the processes of T cell activation and trafficking. The application of this methodology to transplantation is essential if the mechanism of action of T cells in graft rejection and tolerance are to be identified. Recently, the adoptive transfer of TCR transgenic T cells has been examined in the setting of murine cardiac transplants, for which recipients are either naive (37) or immunocompromised (38). In both systems, the TCR transgenic T cells are specific for the class I MHC molecule K^b. Hara et al. adoptively transferred $CD8^+$ TCR transgenic T cells (Des $H2^k$ (39)) into syngeneic mice with intact immune systems 24 hr before they received a $H2K^{b+}$ heart. It was demonstrated that the TCR transgenic T cells, identified by the clonotypic antibody, Désiré-1 (40), and CD8-APC (allophycocyanin), proliferated in the peripheral lymphoid organs and even more extensively in the graft in a donor-specific manner (CFSE staining). The graft-infiltrating T cells were activated (up-regulated CD69 and downregulated CD62L), and when analyzed by intracellular cytokine staining, they produced high levels of interferon (IFN)γ but little IL2 on restimulation, whereas T cells present in the periphery produced significant amounts of IL2 and IFNγ.

In the immunocompromised system, Jones et al. (38) adoptively transferred $CD8^+$ T cells purified from K^b-specific TCR transgenic BM3.6 mice (41, 42) into thymectomized, T cell depleted, syngeneic mice (empty mice); a cardiac transplant with a K^{b+} graft followed. Using the clonotypic antibody Ti98 (43, 44), CFSE, and 4-color flow cytometric analysis, it was demonstrated that the TCR transgenic T cells proliferated and became activated after the transplant but then assumed a memory phenotype that rapidly produced IFNγ and IL2 after in vitro stimulation. These and other studies (45, 46) demonstrate that the fate of alloantigen-specific T cells can be tracked in vivo during the immune response to an allograft.

TETRAMERIC MHC/PEPTIDE LIGANDS TOP

It has always been suspected that T cells could be identified by the specificity of their antigen-binding properties. However, the peptide/MHC ligand binds with low affinity and fast off-rates (47), suggesting that the staining of T cells with these ligands would prove ineffective. Multimeric MHC ligands (tetramers) have now been developed that have a much greater avidity for T cell receptors, and the binding can be detected by flow cytometric analysis if streptavidin PE (phycoerythrin) or FITC is used (Fig. 3). The tetramers are constructed as follows (48, 49): An enzyme (BirA) biotinylates a lysine residue within a 15-amino acid recognition sequence that is tailored onto the COOH terminus of one chain of the MHC molecule. The tag is then labeled with biotin and bound to streptavidin. Because streptavidin has four binding sites, tetramers are

produced. The site recognized by the TCR is at the N terminal end; therefore, biotinylation at the C terminal end allows correct orientation of the MHC molecules within the tetramer.

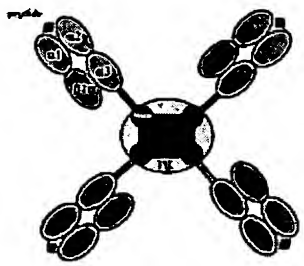

Figure 3. A phycoerythrin-labeled MHC class I/peptide tetramer. MHC class I α-chain: orange; β2-microglobulin: green; peptide: red; biotin: dark blue; streptavidin: light blue; phycoerythrin: pink.

The method was initially applied using IE^k molecules (murine class II) bound to pigeon cytochrome c peptide (50) and then to HLA class I molecules to enable estimates of the number of peptide-specific $CD8^+$ cytotoxic T cells to be made (48). HLA A2 tetramers were designed with peptides from human immunodeficiency virus (HIV) *gag* and *pol,* and these bound to T cells from the peripheral blood of patients with HIV. It was revealed that up to 1% of $CD8^+$ T cells stained with tetramers, which is very high when compared with precursor estimates determined using limiting dilution assays. Tetramers of MHC class I molecules containing viral peptides have also been used to visualize antigen-specific $CD8^+$ T cells directly during acute murine lymphocytic choriomeningitis virus (LCMV) infection (51). It was demonstrated that 50-70% of activated $CD8^+$ T cells were antigen specific and the intracellular cytokine staining and ELISPOT analysis (IFNγ) of the epitope-stimulated T cells gave similar results. Others have also demonstrated, through the use of tetramers, that antigen-specific T cells accounted for the majority of cells responding to LCMV, and similar conclusions have been reached by adoptively transferring TCR transgenic $CD8^+$ T cells specific for an epitope of LCMV (52, 53). The same phenomenon is also known to occur in human Epstein-Barr Virus infection (54). The significance of limiting dilution assays needs to be reconsidered in light of the tetramer findings because the procedure seems to grossly underestimate the true frequency of precursor cells.

The difficulty with applying this technology to transplantation research is that in the vast majority of instances, the identity of the allogeneic HLA peptides presented in the context of donor or recipient MHC class II (or class I: cross-presentation) are unknown. However, in some MHC combinations, the alloreactive T cells may recognize a wide spectrum of peptides presented in the context of a particular allo-MHC molecule or the response may be against the allo-MHC molecule itself and independent of the bound peptides (55). This remains a controversial area, but it suggests that tetramers of MHC molecules could be constructed without a peptide and may indeed prove to be generally applicable in transplantation. Specifically, an experimental model has been developed that should be suited to tetramer technology (56). B6 and K^{bm1} mice differ in that there is a 3-amino acid disparity at positions 152, 155, and 156 of the MHC class IK molecule, and it has been shown that a natural peptide derived from the K^{bm1} MHC class I molecule is presented by MHC class II IA^b molecules and recognized by Bm1-specific $CD4^+$ T cells of B6 origin.

CONCLUSIONS TOP

The field of immunology as applied to transplantation is evolving rapidly parallel with the technological advances thrust upon immunology in general. Although in vitro experiments seem far removed from the complexities of the in vivo setting, they have provided essential information about T cell activation, costimulation, and signaling, and they have laid the foundation for future advances. The initial difficulties with the visualization of T cells in vivo have been overcome to a large extent by the adoptive transfer of identifiable transgenic T cells and/or by CFSE labeling when clonotypic and Vα/Vβ antibodies are unavailable. The recent addition of tetrameric staining adds a new dimension to the visualization and recognition of antigen-specific T cells.

REFERENCES TOP

1. Hall B. Cells mediating allograft rejection. Transplantation 1991; 51(6): 1141.
[Medline Link] [Context Link]

2. Wood K. New concepts in tolerance. Clin Transplant 1996; 10(1 Pt 2): 93.
[Context Link]

3. McHeyzer-Williams M, Altman JD, Davis MM. Tracking antigen-specific helper T cell responses. Curr Opin Immunol 1996; 8(2): 278.
[Medline Link] [CrossRef] [Context Link]

4. Pape K, Kearney ER, Khoruts A, et al. Use of adoptive transfer of T-cell-antigen-receptor-transgenic T cell for the study of T-cell activation in vivo. Immunol Rev 1997; 156: 67.
[Fulltext Link] [Medline Link] [Context Link]

5. Kupfer A, Swain SL, Janeway CA Jr, Singer SJ. The specific direct interaction of helper T cells and antigen-presenting B cells. Proc Natl Acad Sci U S A 1986; 83(16): 6080.
[Medline Link] [Context Link]

6. Kupfer A, Singer SJ, Janeway CA Jr, Swain SL. Coclustering of CD4 (L3T4) molecule with the T-cell receptor is induced by specific direct interaction of helper T cells and antigen-presenting cells. Proc Natl Acad Sci USA 1987; 84(16): 5888.
[Medline Link] [Context Link]

7. Poo W, Conrad L, Janeway CA Jr. Receptor-directed focusing of lymphokine release by helper T cells. Nature 1988; 332(6162): 378.
[Medline Link] [CrossRef] [Context Link]

8. Monks C, Freiberg BA, Kupfer H, Sciaky N, Kupfer A. Three-dimensional segregation of supramolecular activation clusters in T cells. Nature 1998; 395(6697): 82.
[Medline Link] [CrossRef] [Context Link]

9. Linsley P, Bradshaw J, Greene J, Peach R, Bennett KL, Mittler RS. Intracellular trafficking of CTLA-4 and focal localization towards sites of TCR engagement. Immunity 1996; 4(6): 535.
[CrossRef] [Context Link]

10. Mueller D, Jenkins MK, Schwartz RH. Clonal expansion versus functional clonal inactivation: a costimulatory signalling pathway determines the outcome of T cell antigen receptor occupancy. Annu Rev Immunol 1989; 7: 445.
[Medline Link] [CrossRef] [Context Link]

11. Dustin M, Springer TA. T-cell receptor cross-linking transiently stimulates adhesiveness through LFA-1. Nature 1989; 34(6243): 619.
[Context Link]

12. van Kooyk Y, van de Wiel-van Kemenade P, Weder P, Kuijpers TW, Figdor CG. Enhancement of LFA-1-mediated cell adhesion by triggering through CD2 or CD3 on T lymphocytes. Nature 1989; 342(6251): 811.
[Medline Link] [CrossRef] [Context Link]

13. Wulfing C, Sjaastad MD, Davis MM. Visualizing the dynamics of T cell activation: intracellular adhesion molecule 1 migrates rapidly to the T cell/B cell interface and acts to sustain calcium levels. Proc Natl Acad Sci USA 1998; 95(11): 6302.
[Medline Link] [CrossRef] [Context Link]

14. Fink P, Matis LA, McElligott DL, Bookman M, Hedrick SM. Correlations between T-cell specificity and the structure of the antigen receptor. Nature 1986; 321(6067): 219.
[Medline Link] [CrossRef] [Context Link]

15. Seder R, Paul WE, Davis MM, Fazekas de St Groth B. The presence of interleukin 4 during in vitro priming determines the lymphokine-producing potential of CD4+ T cells from T cell receptor transgenic mice. J Exp Med 1992; 176(4): 1091.
[Medline Link] [CrossRef] [Context Link]

16. Valitutti S, Muller S, Cella M, Padovan E, Lanzavecchia A. Serial triggering of many T-cell receptors by a few peptide-MHC complexes. Nature 1995; 375(6527): 148.
[Medline Link] [CrossRef] [Context Link]

17. Harding F, McArthur JG, Gross JA, Raulet DH, Allison JP. CD28-mediated signalling co-stimulates murine T cells and prevents induction of anergy in T-cell clones. Nature 1992; 356(6370): 607.
[Medline Link] [CrossRef] [Context Link]

18. Lenschow D, Walunas TL, Bluestone JA. CD28/B7 system of T cell costimulation. Annu Rev Immunol

1996; 14: 233.
[Context Link]

19. Wells A, Gudmundsdottir H, Turka LA. Following the fate of individual T cells throughout activation and clonal expansion. Signals from T cell receptor and CD28 differentially regulate the induction and duration of a proliferative response. J Clin Invest 1997; 100(12): 3173.
[Context Link]

20. Festenstein H. Immunogenetic and biological aspects of in vitro lymphocyte allotransformation (MLR) in the mouse. Transplant Rev 1973; 15: 62.
[Medline Link] [Context Link]

21. Kappler J, Staerz U, White J, Marrack PC. Self-tolerance eliminates T cells specific for Mls-modified products of the major histocompatibility complex. Nature 1988; 332(6159): 35.
[Medline Link] [CrossRef] [Context Link]

22. MacDonald H, Schneider R, Lees RK, et al. T-cell receptor V beta use predicts reactivity and tolerance to Mlsa-encoded antigens. Nature 1988; 332(6159): 40.
[Context Link]

23. Bruno L, Kirberg J, von Boehmer H. On the cellular basis of immunological T cell memory. Immunity 1995; 2(1): 37.
[Medline Link] [CrossRef] [Context Link]

24. Schonrich G, Alferink J, Klevenz A, et al. Tolerance induction as a multi-step process. Eur J Immunol 1994; 24(2): 285.
[Medline Link] [Context Link]

25. Kurts C, Heath WR, Carbone FR, Allison J, Miller JF, Kosaka H. Constitutive class I-restricted exogenous presentation of self antigens in vivo. J Exp Med 1996; 184(3): 923.
[Medline Link] [CrossRef] [Context Link]

26. Heath W, Miller JF. Expression of two alpha chains on the surface of T cells in T cell receptor transgenic mice. J Exp Med 1993; 178(5): 1807.
[Medline Link] [CrossRef] [Context Link]

27. Kearney E, Pape KA, Loh DY, Jenkins MK. Visualization of peptide-specific T cell immunity and peripheral tolerance induction in vivo. Immunity 1994; 1(4): 327.
[Medline Link] [CrossRef] [Context Link]

28. Murphy K, Heimberger AB, Loh DY. Induction by antigen of intrathymic apoptosis of CD4+CD8+TCRlo thymocytes in vivo. Science 1990; 250(4988): 1720.
[Context Link]

29. Haskins K, Kubo R, White J, Pigeon M, Kappler J, Marrack P. The major histocompatibility complex-restricted antigen receptor on T cells. I. Isolation with a monoclonal antibody. J Exp Med 1983; 157(4): 1149.
[Medline Link] [CrossRef] [Context Link]

30. Garside P, Ingulli E, Merica RR, Johnson JG, Noelle RJ, Jenkins MK. Visualization of specific B and T lymphocyte interactions in the lymph node. Science 1998; 281(5373): 96.
[Medline Link] [CrossRef] [Context Link]

31. Goodnow C, Crosbie J, Adelstein S, et al. Altered immunoglobulin expression and functional silencing of self-reactive B lymphocytes in transgenic mice. Nature 1988; 334(6184): 676.
[Context Link]

32. Lyons A, Parish CR. Determination of lymphocyte division by flow cytometry. J Immunol Methods 1994; 171(1): 131.
[Medline Link] [CrossRef] [Context Link]

33. Kubbies M, Goller, B, Van Bockstaele, DR. Improved BrdUrd-Hoechst bivariate cell kinetic analysis by helium-cadmium single laser excitation. Cytometry 1992; 13(7): 782.
[Medline Link] [Context Link]

34. Fulcher D, Lyons AB, Korn SL, et al. The fate of self-reactive B cells depends primarily on the degree of antigen receptor engagement and availability of T cell help. J Exp Med 1996; 183(5): 2313.
[Medline Link] [CrossRef] [Context Link]

35. Oehen S, Brduscha-Riem K, Oxenius A, Odermatt B. A simple method for evaluating the rejection of grafted spleen cells by flow cytometry and tracing adoptively transferred cells by light microscopy. J Immunol Methods 1997; 207(1): 33.
[Medline Link] [CrossRef] [Context Link]

36. Weston S, Parish CR. New fluorescent dyes for lymphocyte migration studies. Analysis by flow cytometry and fluorescence microscopy. J Immunol Methods 1990; 133(1): 87.
[Medline Link] [CrossRef] [Context Link]

37. Hara M, Gilot BJ, Jones ND, et al. In vivo cytokine production by allospecific CD8+ transgenic T cells after heart transplantation. Transplant Proc 1999; 31(1-2): 91.
[CrossRef] [Context Link]

38. Jones N, van Maurik A, Hara M, Gilot BJ, Morris PJ, Wood KJ. T cell activation, proliferation and memory following cardiac transplantation in vivo. Ann Surg 1999; 229(4): 570.
[Fulltext Link] [Medline Link] [CrossRef] [Context Link]

39. Sponaas A, Tomlinson PD, Schulz R, et al. Tolerance induction by elimination of subsets of self-reactive thymocytes. Int Immunol 1994; 6(10): 1593.
[Medline Link] [Context Link]

40. Hua C, Boyer C, Buferne M, Schmitt-Verhulst Am. Monoclonal antibodies against an H-2Kb-specific cytotoxic T cell clone detect several clone-specific molecules. J Immunol 1986; 136(6): 1937.
[Medline Link] [Context Link]

41. Auphan N, Curnow J, Guimezanes A, et al. The degree of CD8 dependence of cytolytic T cell precursors is determined by the nature of the T cell receptor (TCR) and influences negative selection in TCR-transgenic mice. Eur J Immunol 1994; 24(7): 1572.
[Medline Link] [Context Link]

42. Sponaas A, Tomlinson PD, Antoniou J, et al. Induction of tolerance to self MHC class I molecules expressed under the control of milk protein or beta-globin gene promoters. Int Immunol 1994; 6(2): 277.
[Context Link]

43. Hua C, Boyer C, Guimezanes A, Albert F, Schmitt-Verhulst Am. Analysis of T cell activation requirements with the use of alloantigens or an anti-clonotypic monoclonal antibody. J Immunol 1986; 136 (6): 1927.
[Medline Link] [Context Link]

44. Buferne M, Luton F, Letourneur F, et al. Role of CD3 delta in surface expression of the TCR/CD3 complex and in activation for killing analyzed with a CD3 delta-negative cytotoxic T lymphocyte variant. J Immunol 1992; 148(3): 657.
[Medline Link] [Context Link]

45. Chen H, Luo H, Xu D, et al. Impaired signaling in alloantigen-specific CD8+ T cells tolerized in vivo: employing a model of Ld-specific TCR transgenic mice transplanted with allogenic hearts under the cover of a short-term rapamycin treatment. J Immunol 1996; 157(10): 4297.
[Context Link]

46. Kedl R, Mescher MF. Migration and activation of antigen-specific CD8+ T cells upon in vivo stimulation with allogeneic tumor. J Immunol 1997; 159(2): 650.
[Medline Link] [Context Link]

47. Matsui K, Boniface JJ, Steffner P, Reay PA, Davis MM. Kinetics of T-cell receptor binding to peptide/I-Ek complexes: correlation of the dissociation rate with T-cell responsiveness. Proc Natl Acad Sci USA 1994; 91(26): 12862.
[Medline Link] [Context Link]

48. Altman J, Moss PAH, Goulder PJR, et al. Phenotypic analysis of antigen-specific T lymphocytes. Science 1996; 274(5284): 94.
[Medline Link] [CrossRef] [Context Link]

49. McMichael A, O'Callaghan CA. A new look at T cells. J Exp Med 1998; 187(9): 1367.
[Medline Link] [CrossRef] [Context Link]

50. McHeyzer-Williams M, Altman JD, Davis MM. Enumeration and characterization of memory cells in the TH compartment. Immunol Rev 1996; 150: 5.
[Fulltext Link] [Medline Link] [Context Link]

51. Murali-Krishna K, Altman JD, Suresh M, et al. Counting antigen-specific CD8 T cells: a reevaluation of bystander activation during viral infection. Immunity 1998; 8(2): 177.
[Medline Link] [CrossRef] [Context Link]

52. Gallimore A, Glithero A, Godkin A, et al. Induction and exhaustion of lymphocytic choriomeningitis virus-specific cytotoxic T lymphocytes visualized using soluble tetrameric major histocompatibility complex class I-peptide complexes. J Exp Med 1998; 187(9): 1383.
[Medline Link] [CrossRef] [Context Link]

53. Butz E, Bevan MJ. Massive expansion of antigen-specific CD8+ T cells during an acute virus infection. Immunity 1998; 8(2): 167.
[Medline Link] [CrossRef] [Context Link]

54. Callan M, Tan L, Annels N, et al. Direct visualization of antigen-specific CD8+ T cells during the primary immune response to Epstein-Barr virus in vivo. J Exp Med 1998; 187(9): 1395.
[Medline Link] [CrossRef] [Context Link]

55. Shoskes DA, Wood KJ. Indirect presentation of MHC antigens in transplantation. Immunol Today 1994; 15(1): 32.
[Context Link]

56. Ossevoort M, De Bruijn ML, Van Veen KJ, Kast WM, Melief CJ. Peptide specificity of alloreactive CD4 positive T lymphocytes directed against a major histocompatibility complex class I disparity. Transplantation 1996; 62(10): 1485.
[Fulltext Link] [Medline Link] [CrossRef] [Context Link]

*Abbreviations used: APC, antigen presenting cell; BrDu, 5-bromodeoxyuridine. CFSE, 5-(and-6)-carboxyfluorescein diacetate, succinimidyl ester; cOVA, chicken ovalbumin; ELISPOT, enzyme-linked immunospot assay; FITC, fluorescein isothiocyanate; GFP, green fluorescent protein; HEL, hen egg lysozyme; ICAM-1 intercellular adhesion molecule 1; IL, interleukin; LCMV, lymphocytic choriomeningitis; LFA-1, lymphocyte function-associated antigen 1; Mls, minor lymphocyte stimulatory; TCR, T cell receptor. [Context Link]

Connecting via Winsock to STN

Welcome to STN International! Enter x:x

LOGINID:ssspta1644pnh

PASSWORD:
TERMINAL (ENTER 1, 2, 3, OR ?):2

* * * * * * * * * * Welcome to STN International * * * * * * * * * *

NEWS	1		Web Page URLs for STN Seminar Schedule - N. America
NEWS	2		"Ask CAS" for self-help around the clock
NEWS	3	FEB 28	PATDPAFULL - New display fields provide for legal status data from INPADOC
NEWS	4	FEB 28	BABS - Current-awareness alerts (SDIs) available
NEWS	5	MAR 02	GBFULL: New full-text patent database on STN
NEWS	6	MAR 03	REGISTRY/ZREGISTRY - Sequence annotations enhanced
NEWS	7	MAR 03	MEDLINE file segment of TOXCENTER reloaded
NEWS	8	MAR 22	KOREAPAT now updated monthly; patent information enhanced
NEWS	9	MAR 22	Original IDE display format returns to REGISTRY/ZREGISTRY
NEWS	10	MAR 22	PATDPASPC - New patent database available
NEWS	11	MAR 22	REGISTRY/ZREGISTRY enhanced with experimental property tags
NEWS	12	APR 04	EPFULL enhanced with additional patent information and new fields
NEWS	13	APR 04	EMBASE - Database reloaded and enhanced
NEWS	14	APR 18	New CAS Information Use Policies available online
NEWS	15	APR 25	Patent searching, including current-awareness alerts (SDIs), based on application date in CA/CAplus and USPATFULL/USPAT2 may be affected by a change in filing date for U.S. applications.
NEWS	16	APR 28	Improved searching of U.S. Patent Classifications for U.S. patent records in CA/CAplus
NEWS	17	MAY 23	GBFULL enhanced with patent drawing images
NEWS	18	MAY 23	REGISTRY has been enhanced with source information from CHEMCATS
NEWS	19	JUN 06	The Analysis Edition of STN Express with Discover! (Version 8.0 for Windows) now available
NEWS	20	JUN 13	RUSSIAPAT: New full-text patent database on STN
NEWS	21	JUN 13	FRFULL enhanced with patent drawing images
NEWS	22	JUN 27	MARPAT displays enhanced with expanded G-group definitions and text labels
NEWS	23	JUL 01	MEDICONF removed from STN
NEWS	24	JUL 07	STN Patent Forums to be held in July 2005
NEWS	25	JUL 13	SCISEARCH reloaded
NEWS	26	JUL 20	Powerful new interactive analysis and visualization software, STN AnaVist, now available
NEWS	27	AUG 11	Derwent World Patents Index(R) web-based training during August
NEWS	28	AUG 11	STN AnaVist workshops to be held in North America

NEWS EXPRESS JUNE 13 CURRENT WINDOWS VERSION IS V8.0, CURRENT MACINTOSH VERSION IS V6.0c(ENG) AND V6.0Jc(JP), AND CURRENT DISCOVER FILE IS DATED 13 JUNE 2005

NEWS HOURS	STN Operating Hours Plus Help Desk Availability
NEWS INTER	General Internet Information
NEWS LOGIN	Welcome Banner and News Items
NEWS PHONE	Direct Dial and Telecommunication Network Access to STN
NEWS WWW	CAS World Wide Web Site (general information)

Enter NEWS followed by the item number or name to see news on that specific topic.

All use of STN is subject to the provisions of the STN Customer agreement. Please note that this agreement limits use to scientific research. Use for software development or design or implementation of commercial gateways or other similar uses is prohibited and may result in loss of user privileges and other penalties.

* * * * * * * * * * * * * * STN Columbus * * * * * * * * * * * * * * * *

FILE 'HOME' ENTERED AT 09:42:42 ON 12 AUG 2005

=> file medline embase biosis scisearch caplus
COST IN U.S. DOLLARS SINCE FILE ENTRY TOTAL SESSION
FULL ESTIMATED COST 0.21 0.21

FILE 'MEDLINE' ENTERED AT 09:43:16 ON 12 AUG 2005

FILE 'EMBASE' ENTERED AT 09:43:16 ON 12 AUG 2005
COPYRIGHT (C) 2005 Elsevier Inc. All rights reserved.

FILE 'BIOSIS' ENTERED AT 09:43:16 ON 12 AUG 2005
Copyright (c) 2005 The Thomson Corporation

FILE 'SCISEARCH' ENTERED AT 09:43:16 ON 12 AUG 2005
Copyright (c) 2005 The Thomson Corporation

FILE 'CAPLUS' ENTERED AT 09:43:16 ON 12 AUG 2005
USE IS SUBJECT TO THE TERMS OF YOUR STN CUSTOMER AGREEMENT.
PLEASE SEE "HELP USAGETERMS" FOR DETAILS.
COPYRIGHT (C) 2005 AMERICAN CHEMICAL SOCIETY (ACS)

=> s corneal graft
L1 4650 CORNEAL GRAFT

=> s l1 and survival
L2 1161 L1 AND SURVIVAL

=> s l2 and indolinone
L3 0 L2 AND INDOLINONE

=> s l2 and kinase inhibitor
L4 1 L2 AND KINASE INHIBITOR

=> d l4 cbib abs

L4 ANSWER 1 OF 1 CAPLUS COPYRIGHT 2005 ACS on STN
2003:696673 Document No. 139:207829 Methods of extending **corneal graft survival** using VEGFR-3 inhibitors which inhibit lymphangiogenesis. De Vries, Gerald W. (Allergan, Inc., USA). PCT Int. Appl. WO 2003072029 A2 20030904, 84 pp. DESIGNATED STATES: W: AE, AG, AL, AM, AT, AU, AZ, BA, BB, BG, BR, BY, BZ, CA, CH, CN, CO, CR, CU, CZ, DE, DK, DM, DZ, EC, EE, ES, FI, GB, GD, GE, GH, GM, HR, HU, ID, IL, IN, IS, JP, KE, KG, KP, KR, KZ, LC, LK, LR, LS, LT, LU, LV, MA, MD, MG, MK, MN, MW, MX, MZ, NO, NZ, OM, PH, PL, PT, RO, RU, SC, SD, SE, SG, SK, SL, TJ, TM, TN, TR, TT, TZ, UA, UG, UZ, VC, VN, YU, ZA, ZM, ZW; RW: AT, BE, BF, BJ, CF, CG, CH, CI, CM, CY, DE, DK, ES, FI, FR, GA, GB, GR, IE, IT, LU, MC, ML, MR, NE, NL, PT, SE, SN, TD, TG, TR. (English). CODEN: PIXXD2. APPLICATION: WO 2003-US5125 20030220. PRIORITY: US 2002-81126 20020222.

AB The present invention provides a method of extending **corneal graft survival** following corneal transplantation in a

patient by administering to the patient an effective amount of a pharmaceutical composition containing a vascular endothelial growth factor receptor-3 (VEGFR-3) inhibitor, whereby lymphangiogenesis is suppressed in the cornea of the patient. More specifically, the VEGFR-3 inhibitor is a dominant neg. VEGFR-3 receptor, a nucleic acid encoding a dominant neg. VEGFR-3 receptor, a VEGFR-3 **kinase inhibitor**, an ATP analog, a VEGFR-3 binding mol., or a sequence-specific RNase.

=> s l2 and angiogenic inhibitor
L5 0 L2 AND ANGIOGENIC INHIBITOR

=> s l2 and review
L6 71 L2 AND REVIEW

=> dup reomve l6
ENTER REMOVE, IDENTIFY, ONLY, OR (?):remove
'REOMVE' IS NOT VALID. VALID FILE NAMES ARE 'MEDLINE, EMBASE, BIOSIS, SCISEARCH, CAPLUS'
You have entered a file name of duplicates to keep that is not referenced by any of the L#s specified for this DUPLICATE command.
The file names of duplicates that can be kept are listed above.
Please enter one of these file names.

=> dup remove l6
PROCESSING COMPLETED FOR L6
L7 33 DUP REMOVE L6 (38 DUPLICATES REMOVED)

=> d l7 1-33 cbib abs

L7 ANSWER 1 OF 33 MEDLINE on STN DUPLICATE 1
2005178938. PubMed ID: 15812772. **Corneal graft** rejection after penetrating keratoplasty for keratoconus in Turner's syndrome. Pinna A; Salvo M; Dore S; Carta F. (Institute of Ophthalmology, University of Sassari, Sassari--Italy.. apinna@uiss.it) . European journal of ophthalmology, (2005 Mar-Apr) 15 (2) 271-3. Journal code: 9110772. ISSN: 1120-6721. Pub. country: Italy. Language: English.

AB PURPOSE: To report a patient with Turner's syndrome who developed graft rejection after penetrating keratoplasty (PK) for keratoconus and to **review** the ophthalmic literature on the association between keratoconus and Turner's syndrome. METHODS: A woman with bilateral keratoconus and Turner's syndrome (45,XO) was referred for progressive visual loss in the right eye. Best-corrected visual acuity was 20/400 in the right eye. Slit-lamp examination revealed corneal thinning with ectatic protrusion of the central cornea and Vogt's striae in the right eye. The patient underwent PK in the right eye in January 2001. She developed graft rejection in April 2003 and visual acuity dropped to hand motion. After treatment with topical and systemic steroids and systemic cyclosporine A, visual acuity recovered to 20/80 in July 2003. RESULTS: The authors know of only three other reported patients (six eyes) with keratoconus in Turner's syndrome. Five eyes underwent PK with good visual rehabilitation, but one developed immunologic graft rejection 7 years after surgery. On the whole, considering the current report and the other cases described in the literature, graft rejection occurred in 2 out of 6 eyes (33.3%). The graft **survival** rate was 80% after 2 years and 40% after 7 years. CONCLUSIONS: The results suggest that grafts for keratoconus in patients with Turner's syndrome might have an increased risk of immunologic rejection. **Corneal grafts** in Turner's syndrome need to be monitored closely. Early detection of graft rejection and aggressive treatment with topical and systemic steroids and systemic cyclosporine A can save the graft and restore useful vision.

L7 ANSWER 2 OF 33 EMBASE
on STN DUPLICATE 2
2004306894 EMBASE Gene therapy approaches to prolonging corneal allograft

survival. Williams K.A.; Jessup C.F.; Coster D.J.. K.A. Williams, Department of Ophthalmology, Flinders Univ. of South Australia, Flinders Medical Centre, GPO Box 2100, Adelaide, SA 5042, Australia. keryn.williams@flinders.edu.au. Expert Opinion on Biological Therapy Vol. 4, No. 7, pp. 1059-1071 2004.
Refs: 112.
ISSN: 1471-2598. CODEN: EOBTA2
Pub. Country: United Kingdom. Language: English. Summary Language: English.
ED Entered STN: 20040819
AB Irreversible immunological rejection is the major cause of human corneal allograft failure and occurs despite the use of topical glucocorticoid immunosuppression. Systemic pharmacological interventions have not found widespread favour in corneal transplantation because of associated morbidities and inadequate demonstration of efficacy. Gene therapy offers tantalising prospects for improving corneal allograft **survival**, especially in those recipients at high risk of graft rejection. Donor corneas can be gene-modified ex vivo, while in storage prior to implantation, and the relative isolation of the transplanted cornea from the circulation decreases the risk of potential systemic complications. A wide variety of vectors have been found suitable for gene transfer to the cornea. The mechanisms involved in **corneal graft** rejection have been placed on a relatively secure footing over the past decade and in consequence a number of transgenes with promise for modulating rejection have been identified. However, relatively few studies have thus far demonstrated significant prolongation of corneal allograft **survival** after gene transfer to the donor cornea. In these instances, the therapeutic protein almost certainly acted at a proximal level in the afferent immune response, within the ocular environs.

L7 ANSWER 3 OF 33 MEDLINE on STN DUPLICATE 3
2004336305. PubMed ID: 14739919. Penetrating keratoplasty in adults with congenital glaucomas. Ramchandani M; Mohammed S; Mirza S; McDonnell P J. (Birmingham and Midland Eye Centre, City Hospitals NHS Trust, Birmingham, UK.) Eye (London, England), (2004 Jul) 18 (7) 703-8. Journal code: 8703986. ISSN: 0950-222X. Pub. country: England: United Kingdom. Language: English.
AB PURPOSE: To report the problems and outcomes of penetrating keratoplasty (PKP) in patients with corneal oedema due to congenital glaucoma. METHOD: Case note **review** of nine such consecutive patients treated with PKP. A Kaplan - Meir **survival** curve was plotted for the series. RESULTS: Nine patients, ranging in age from 27 to 71 years at the time of their surgery were followed up for a mean of 28 months. All had undergone previous surgery for glaucoma. Preoperatively all patients had controlled intraocular pressures, and four were on ocular hypotensives. Two patients developed **corneal graft** failure at 15 and 41 months postoperative. Raised pressure was the cause in both. Final visual acuity improved in five patients, was the same in three, and deteriorated in only one. Complications included raised intraocular pressure, cataract, retinal detachment, and endophthalmitis secondary to an infected Molteno implant. CONCLUSION: Despite multiple impediments to good postoperative vision including previous surgery and pre-existing glaucomatous damage, a successful outcome was achieved by careful patient selection, and an awareness of, and meticulous attention to postoperative complications.

L7 ANSWER 4 OF 33 MEDLINE on STN
2005020230. PubMed ID: 15646495. [Corneal transplantation--immunological mechanisms of rejection episode]. Immunologiczne aspekty reakcji odrzucania przeszczepow rogowek. Cwalina Lukasz; Mrukwa-Kominek Ewa. (Z Katedry i Kliniki Okulistyki Slaskiej Akademii Medycznej w Katowicach.) Klinika oczna, (2004) 106 (4-5) 686-90. Ref: 49. Journal code: 0376614. ISSN: 0023-2157. Pub. country: Poland. Language: Polish.
AB Organ transplantation including cornea is often only the one method of

treatment in case of their irreversible destruction. The genetic difference between donor and graft recipient makes the immunological system recognizes foreign antigens and triggers off a rejection episode. This article **reviews corneal graft** rejection immunology and indicates possible future options for the clinical evaluation of more specific therapeutic agents that modulate the immunological mechanisms of allograft rejection. It discusses also the role of HLA matching in the **survival** of **corneal grafts** especially in "high risk" eyes.

L7 ANSWER 5 OF 33 MEDLINE on STN DUPLICATE 4

2004319934. PubMed ID: 15219876. The role of chemokines and their receptors in ocular disease. Wallace Graham R; John Curnow S; Wloka Kaska; Salmon Mike; Murray Philip I. (The Birmingham and Midland Eye Centre, Sandwell and West Birmingham Hospitals NHS Trust, The University of Birmingham, City Hospital, Dudley Road, Birmingham B18 7QU, UK.. g.r.wallace@bham.ac.uk) . Progress in retinal and eye research, (2004 Jul) 23 (4) 435-48. Ref: 116. Journal code: 9431859. ISSN: 1350-9462. Pub. country: England: United Kingdom. Language: English.

AB The migration and infiltration of cells into the eye whether blood-borne leucocytes, endothelial or epithelial cells occurs in many ocular diseases. Dysregulation of this process is apparent in chronic inflammation, **corneal graft** rejection, allergic eye disease and other sight-threatening conditions. Under normal and inflammatory conditions, chemokines and their receptors are important contributors to cell migration. To date, 47 chemokines and 19 chemokine receptors have been identified and characterised. In recent years, investigations into the role of chemokines and their receptors in ocular disease have generated an increasing number of publications. In the eye, the best understood action of these molecules has arisen from the study of their ability to control the infiltration of leucocytes in uveitis. However, the involvement of chemokines in angiogenesis in several ocular conditions and in the **survival** of corneal transplants demonstrates the multifaceted nature of their effects. Interestingly, the constitutive expression of chemokines and their receptors in ocular tissues suggests that certain chemokines have a homeostatic function. In this **review**, we discuss the nature and function of chemokines in health and disease, and describe the role of chemokines in the pathogenesis of different ocular conditions.

L7 ANSWER 6 OF 33 MEDLINE on STN DUPLICATE 5

2004248172. PubMed ID: 15097133. Cataract extraction following penetrating keratoplasty. Nagra Parveen K; Rapuano Christopher J; Laibson Peter L; Kunimoto Derek Y; Kay Michael; Cohen Elisabeth J. (Cornea Service, Wills Eye Hospital, 840 Walnut Street, Philadelphia, PA 19107, USA.) Cornea, (2004 May) 23 (4) 377-9. Journal code: 8216186. ISSN: 0277-3740. Pub. country: United States. Language: English.

AB OBJECTIVE: To assess the safety of cataract extraction following penetrating keratoplasty for **corneal graft survival** and to evaluate visual and refractive outcomes in **corneal graft** patients undergoing cataract extraction. METHODS: Retrospective chart **review** of 29 eyes of 24 patients with **corneal grafts** who underwent cataract extraction from January 1, 1993 to December 31, 2002, followed on the Cornea Service at Wills Eye Hospital. RESULTS: The mean time from penetrating keratoplasty to cataract extraction was 8.4 years (range 2 months to 36 years). Following cataract extraction, the **corneal grafts** remained clear in all but 1 eye (3%), during an average follow-up time of 44.5 months (range 3-118 months). All of the remaining patients benefited from improved visual acuity, with 15 of 28 patients having a postoperative best-corrected visual acuity of 20/30 or better. Patients also benefited from decreased absolute spherical refractive error, with a preoperative mean value of 6.6 +/- 3.4 D compared with 2.4 +/- 1.6 D postoperatively, while cylindrical refractive error remained relatively stable at 3.2 +/- 2.9 D preoperatively and 2.8 +/- 2.4

postoperatively. The patient who developed graft failure had 3 episodes of preoperative endothelial rejection and a clear **corneal graft** at the time of cataract surgery. CONCLUSIONS: Cataract surgery following penetrating keratoplasty is a safe and effective procedure, with a low but definite risk of **corneal graft** failure. In patients with clear grafts and visually significant cataracts, cataract extraction alone is preferred over repeat penetrating keratoplasty and cataract extraction.

L7 ANSWER 7 OF 33 CAPLUS COPYRIGHT 2005 ACS on STN
2004:194806 Document No. 140:263367 Medical care in keratoplasty. Present and future. Inoue, Yoshitsugu (Sch. Med., Tottori Univ., Yonago, 683-8504, Japan). Atarashii Ganka, 21(2), 179-185 (Japanese) 2004. CODEN: ATGAEX. ISSN: 0910-1810. Publisher: Medikaru Aoi Shuppan.
AB A **review** on the prevention and treatment of graft rejection by steroids, pathol. and treatment of infectious diseases after keratoplasty, treatment of dry eye with eye drops, steroid-induced glaucoma, and future prospect of the medical care in corneal transplantation. Effects of cyclosporin, FK506, cytokines (IL-4, IL-10, IL-1 receptor antagonists, etc.), various immunotherapies, and angiogenesis inhibition on the **corneal graft survival** and their possible clin. application are discussed.

L7 ANSWER 8 OF 33 MEDLINE on STN DUPLICATE 6
2003335729. PubMed ID: 12867398. Long-term graft **survival** after penetrating keratoplasty. Thompson Robert W Jr; Price Marianne O; Bowers Patrick J; Price Francis W Jr. (Price Vision Group, Indianapolis, Indiana, USA.) Ophthalmology, (2003 Jul) 110 (7) 1396-402. Journal code: 7802443. ISSN: 0161-6420. Pub. country: United States. Language: English.
AB PURPOSE: To determine long-term graft **survival** rates and causes of secondary graft failures for a large series of penetrating keratoplasties (PKPs). DESIGN: Retrospective, noncomparative case series. PARTICIPANTS: Longitudinal **review** of 3992 consecutive eyes that underwent PKP at a large tertiary care referral center from 1982 through 1996. Data were collected retrospectively from August 1982 through December 1988 and prospectively thereafter. INTERVENTION: Three thousand six hundred forty primary grafts and 352 regrafts. MAIN OUTCOME MEASURES: **Corneal graft survival** and etiology of graft failures. Patients were evaluated preoperatively and at 1, 3, 6, 9, 12, 18, and 24 months after transplant, then at yearly intervals. RESULTS: Mean recipient age was 67 years (range, 1-98 years). The predominant indications for PKP were pseudophakic bullous keratopathy (32%) and Fuchs' dystrophy (23%). Graft failure occurred in 10% (385) of the eyes. The most common causes of secondary graft failure were endothelial failure (29%) or immunologic endothelial rejection (27%). **Survival** of first time grafts was 90% at 5 years and 82% at 10 years. Initial regrafts had significantly lower 5-year and 10-year **survival** rates, 53% and 41%, respectively. The highest 5-year and 10-year **survival** rates were noted in primary grafts for eyes with a preoperative diagnosis of keratoconus (97% and 92%, respectively), or Fuchs' dystrophy (97% and 90%, respectively). Primary grafts for aphakic bullous keratopathy without intraocular lens placement had the lowest 5-year **survival** rate, 70%. CONCLUSIONS: The 5-year and 10-year **survival** rates in this series demonstrate that PKP is a safe and effective treatment for the corneal diseases commonly transplanted in the United States. However, endothelial failure and immunologic graft rejection were persistent risks over the long term, supporting the need for continued patient follow-up. Regrafts, aphakic eyes without intraocular lens placement at the time of transplant, and corneas with deep stromal vascularization had reduced graft **survival** rates. Pseudophakic bullous keratopathy grafts with a retained posterior chamber intraocular lens were at increased risk of endothelial failure compared with primary grafts done for other causes or compared with pseudophakic bullous keratopathy grafts done with intraocular lens exchange.

L7 ANSWER 9 OF 33 MEDLINE on STN DUPLICATE 7
2003446938. PubMed ID: 14507748. Penetrating keratoplasty in children: visual and graft outcome. McClellan K; Lai T; Grigg J; Billson F. (Department of Clinical Ophthalmology and Save Sight Institute, University of Sydney, GPO Box 4337, Sydney NSW 2001, Australia.. kathy@eye.usyd.edu.au) . British journal of ophthalmology, (2003 Oct) 87 (10) 1212-4. Journal code: 0421041. ISSN: 0007-1161. Pub. country: England: United Kingdom. Language: English.

AB AIMS: To **review** factors affecting graft **survival** and determinants of visual acuity after penetrating keratoplasty in children. METHODS: All cases of penetrating keratoplasty performed in an ophthalmic unit, in children aged less than 15 years at the time of operation, for the period 1984 to 2002 were included. RESULTS: 19 penetrating keratoplasties were done in 18 eyes of 16 children, age range 2 weeks to 14 years 8 months (mean 9.24 years), with mean follow up 6.6 years. 73.7% of grafts have remained clear for up to 14 years. Postoperative visual acuity among congenital indications for graft was better than 6/60 in only 14.2% of cases, but was better than or equal to 6/12 in all cases of keratoconus. CONCLUSION: This series shows that prolonged **corneal graft survival** can be achieved in children, but successful restoration of visual acuity depends upon a period of normal visual development before the onset of corneal opacification.

L7 ANSWER 10 OF 33 MEDLINE on STN
2004007915. PubMed ID: 14704816. [Immunomodulation in penetrating keratoplasty. Current status and perspectives]. Immunmodulation bei perforierender Keratoplastik. Stand und Perspektiven. Pleyer U. (Augenklinik, Charite, Universitatsmedizin Berlin, Campus Virchow Klinikum, Berlin.. uwe.pleyer@charite.de) . Der Ophthalmologe : Zeitschrift der Deutschen Ophthalmologischen Gesellschaft, (2003 Dec) 100 (12) 1036-44. Ref: 87. Journal code: 9206148. ISSN: 0941-293X. Pub. country: Germany: Germany, Federal Republic of. Language: German.

AB The immune privileged nature of the cornea contributes to the favourable outcome in **corneal grafts.** However, preventive measures are necessary to reduce allograft rejection particular in "high-risk" cases. Although corticosteroids are still a major component of our immunopharmacological armentarium, they might be supplemented by other more specific immunomodulating agents. The spectrum includes agents such as azathioprin, methotrexate or more specific calcineurin inhibitors affecting T-cells (cyclosporin A, FK506) and highly selective monoclonal antibodies directed against T-cell subpopulations and other targets. In order to better evaluate the risks and benefit of these agents, the properties of established and forthcoming agents are presented. In addition, this **review** attempts to address some new concepts of tolerance induction following penetrating keratoplasty.

L7 ANSWER 11 OF 33 MEDLINE on STN DUPLICATE 8
2004007913. PubMed ID: 14704814. [Tissue typing in perforating corneal transplantation]. Gewebetypisierung bei der perforierenden Keratoplastik. Wachtlin J; Khaireddin R; Hoffmann F. (Augenklinik, Charite, Universitatsmedizin Berlin, Campus Benjamin Franklin, Berlin.. wachtlin@ukbf.fu-berlin.de) . Der Ophthalmologe : Zeitschrift der Deutschen Ophthalmologischen Gesellschaft, (2003 Dec) 100 (12) 1021-30. Ref: 81. Journal code: 9206148. ISSN: 0941-293X. Pub. country: Germany: Germany, Federal Republic of. Language: German.

AB The demand for matched **corneal grafts** has risen rapidly over the last years. One reason for this is the change in the judgement of the value of tissue and especially HLA typing for prevention of an immune reaction in perforating corneal transplantation. Besides HLA or major antigens, there are other immunologically relevant tissue surface molecules such as the non-MHC antigens of which blood groups and minor antigens are the most important. With regard to effective cost-benefit and waiting time-benefit analyses, differentiated matching strategies are needed to assure optimized utilization and allocation of the still unsatisfactory number of available **corneal grafts.**

With special matching strategies, such as the calculation of the individual waiting time, the consideration of split, non-MHC and HLA antigens, additional HLA loci as well as so-called "permissible" and "taboo" mismatches, much more has to be taken into account in the future than just the numerical correspondence of HLA antigens. This will make it possible to turn from a pure numerical approach to a functional matching strategy. This **review** summarizes the discussion and different matching strategies, possibilities and limitations of HLA and tissue typing in perforating corneal transplantation.

L7 ANSWER 12 OF 33 SCISEARCH COPYRIGHT (c) 2005 The Thomson Corporation on STN

2003:1050730 The Genuine Article (R) Number: 747BY. Cyclosporine A delivery to the eye: A pharmaceutical challenge. Lallemand F; Felt-Baeyens O; Besseghir K; Behar-Cohen F; Gurny R (Reprint). Univ Geneva, Sch Pharm, 30 Quai E Ansermet, CH-1211 Geneva 4, Switzerland (Reprint); Univ Geneva, Sch Pharm, CH-1211 Geneva 4, Switzerland; Debiopharm SA, Lausanne, Switzerland; INSERM, U 450, Paris, France. EUROPEAN JOURNAL OF PHARMACEUTICS AND BIOPHARMACEUTICS (NOV 2003) Vol. 56, No. 3, pp. 307-318. ISSN: 0939-6411. Publisher: ELSEVIER SCIENCE BV, PO BOX 211, 1000 AE AMSTERDAM, NETHERLANDS. Language: English.

ABSTRACT IS AVAILABLE IN THE ALL AND IALL FORMATS

AB Systemic administration of cyclosporine A (CsA) is commonly used in the treatment of local ophthalmic conditions involving cytokines, such as **corneal graft** rejection, autoimmune uveitis and dry eye syndrome. Local administration is expected to avoid the various side effects associated with systemic delivery. However, the currently available systems using oils to deliver CsA topically are poorly tolerated and provide a low bioavailability. These difficulties may be overcome through formulations aimed at improving CsA water solubility (e.g. cyclodextrins), or those designed to facilitate tissue drug penetration using penetration enhancers. The use of colloidal carriers (micelles, emulsions, liposomes and nanoparticles) as well as the approach using hydrosoluble prodrugs of CsA have shown promising results. Solid devices such as shields and particles of collagen have been investigated to enhance retention time on the eye surface. Some of these topical formulations have shown efficacy in the treatment of extraocular diseases but were inefficient at reaching intraocular targets. Microspheres, implants and liposomes have been developed to be directly administered subconjunctivally or intravitreally in order to enhance CsA concentration in the vitreous. Although progress has been made, there is still room for improvement in CsA ocular application, as none of these formulations is ideal.

L7 ANSWER 13 OF 33 MEDLINE on STN DUPLICATE 9

2003142021. PubMed ID: 12658081. Graft **survival** and glaucoma outcome after simultaneous penetrating keratoplasty and ahmed glaucoma valve implant. Al-Torbak Abdullah. (Department of Ophthalmology, Al-Qasseem Medical College, King Saud University, Buraidah, Saudi Arabia.. atorbaq@health.net.sa) . Cornea, (2003 Apr) 22 (3) 194-7. Journal code: 8216186. ISSN: 0277-3740. Pub. country: United States. Language: English.

AB PURPOSE: To investigate the success of **corneal graft** and intraocular pressure (IOP) control after simultaneous penetrating keratoplasty (PKP) and Ahmed glaucoma valve implant in patients with coexisting corneal opacity and glaucoma. METHODS: A retrospective **review** was undertaken of adult patients at King Khaled Eye Specialist Hospital, Riyadh, Saudi Arabia, who underwent simultaneous PKP and Ahmed glaucoma valve implant between January 1994 and September 1999.RESULTS: Twenty-five eyes of 25 patients were included in the study. Cumulative probabilities of success by Kaplan-Meier analysis showed 92% and 50% graft success and 92% and 86% IOP control at 1 and 3 years, respectively. The main postoperative complication was graft failure in 10 of 25 cases, and the majority of those failures resulted from immunologic graft rejection and tube endothelial touch.CONCLUSION: Ahmed glaucoma valve implant is effective in controlling IOP in a majority of eyes during

a 3-year time span. However, **corneal graft** success continues to pose challenges.

L7 ANSWER 14 OF 33 EMBASE COPYRIGHT 2005 ELSEVIER INC. ALL RIGHTS RESERVED. on STN DUPLICATE 10

2004015319 EMBASE The immune privilege of **corneal grafts.**
Niederkorn J.Y.. J.Y. Niederkorn, Department of Ophthalmology, Univ. of Texas SW. Medical Center, 5323 Harry Hines Blvd., Dallas, TX 75093, United States. jerry.niederkorn@utsouthwestern.edu. Journal of Leukocyte Biology Vol. 74, No. 2, pp. 167-171 2003.
Refs: 54.
ISSN: 0741-5400. CODEN: JLBIE7
Pub. Country: United States. Language: English. Summary Language: English.

ED Entered STN: 20040129

AB Keratoplasty is the oldest and one of the most successful forms of solid tissue transplantation. In the United States, over 33,000 corneal transplants are performed each year. Unlike other forms of tissue transplantation, keratoplasties are routinely performed without the aid of tissue typing or systemic immunosuppressive drugs. In spite of this, 90% of the first-time corneal transplants will succeed-a condition that demonstrates the immune privilege of keratoplasties. The avascular nature of the corneal allograft bed led many to suspect that **corneal grafts** were sequestered from the immune apparatus. Although pleasing in its simplicity, this explanation has given way to a more comprehensive hypothesis that embodies multiple, interdependent mechanisms, which promote the long-term **survival** of corneal allografts. These mechanisms conspire to interrupt the transmission of immunogenic stimuli to peripheral lymphoid tissues; induce the generation of a deviated immune response; and neutralize immune effector elements at the host-graft interface. This paradigm is analogous to a three-legged stool. Disassembly of any one of the three components results in the collapse of immune privilege. Strategies to re-establish corneal immune privilege may have clinical application for high-risk hosts who have rejected previous corneal allografts.

L7 ANSWER 15 OF 33 EMBASE COPYRIGHT 2005 ELSEVIER INC. ALL RIGHTS RESERVED. on STN DUPLICATE 11

2003147708 EMBASE The potential of antibody-based immunosuppressive agents for corneal transplantation. Thiel M.A.; Coster D.J.; Williams K.A.. Dr. K.A. Williams, Department of Ophthalmology, Flinders Medical Centre, Bedford Park, SA 5042, Australia. keryn.williams@flinders.edu.au. Immunology and Cell Biology Vol. 81, No. 2, pp. 93-105 2003.
Refs: 205.
ISSN: 0818-9641. CODEN: ICBIEZ
Pub. Country: Australia. Language: English. Summary Language: English.

ED Entered STN: 20030424

AB Corneal transplantation is a sight-restorative procedure but its success is limited by irreversible graft rejection, which accounts for up to 50 per cent of failures. The normal eye is an immune-privileged site. Multiple mechanisms maintain ocular privilege, including the blood-eye barrier, the lack of blood vessels and lymphatics in the normal cornea, the relative paucity of mature antigen-presenting cells in the central cornea, the presence of immunomodulatory factors in ocular fluids, and the constitutive expressive of CD95L (Fas ligand) within the eye. However, privilege can be eroded by the sequelae of inflammation and neovascularization. **Corneal graft** rejection in humans is currently suppressed with topical glucocorticosteroids, which are moderately effective. Systemically administered immunosuppressive therapy is of limited efficacy and may be accompanied by unacceptable morbidity. Alternative therapies are needed to improve outcomes. **Corneal graft** rejection is primarily a cell-mediated response controlled by the CD4(+) T cell, and thus CD4 and costimulatory molecule blockade are appealing targets for new therapeutic interventions. A number of monoclonal antibodies have shown promise as immunosuppressants to prolong **corneal graft survival** in experimental animal

models, and may eventually prove to be useful adjuncts to corticosteroids.

L7 ANSWER 16 OF 33 MEDLINE on STN DUPLICATE 12
2003011406. PubMed ID: 12517252. Recent developments in the pharmacological treatment and prevention of **corneal graft** rejection. Banerjee Sanjiv; Dick Andrew D. (Division of Ophthalmology, School of Medical Sciences, University Walk, Bristol, BS8 1TD, UK.) Expert opinion on investigational drugs, (2003 Jan) 12 (1) 29-37. Ref: 93. Journal code: 9434197. ISSN: 1354-3784. Pub. country: England: United Kingdom. Language: English.
AB At present, given the high initial success rate of corneal transplantation (although late **survival** is poor), immunosuppression is often reserved for 'high-risk' patients. Despite immune privilege, **corneal graft** rejection remains the leading cause of corneal allograft failure. Interpreting the limited and also restricted design of most trials, immunosuppressive therapy has not enjoyed the success seen in solid organ grafts. This **review** discusses the limited data available whilst proposing newer therapies that have developed as a result of our increased understanding of the immunobiology of **corneal graft** rejection.

L7 ANSWER 17 OF 33 EMBASE on STN
2003286669 EMBASE **Corneal graft** rejection after posterior capsulotomy. Yucel I.; Akar Y.. Dr. Y. Akar, Akdeniz Univ. Hastanesi Goz Host ABD, 07070 Antalya, Turkey. dryakar@yahoo.com. Asian Journal of Ophthalmology Vol. 5, No. 1, pp. 15-16 2003.
Refs: 15.
ISSN: 1560-2133. CODEN: AJOSBK
Pub. Country: Hong Kong. Language: English. Summary Language: English.
ED Entered STN: 20030731
AB This report **reviews** 3 patients with pseudophakia who developed **corneal graft** rejection after undergoing Q-switched neodymium:yttrium-aluminum-garnet laser posterior capsulotomy for posterior capsular opacification. All patients had previously undergone a combined procedure of extracapsular cataract extraction with posterior chamber intraocular lens implantation in the capsular bag. Both the beneficial optical effects and the potential adverse effects should be carefully considered prior to performing neodymium:yttrium-aluminum-garnet laser posterior capsulotomy in patients with **corneal graft.** It is suggested that all efforts should be made for meticulous control and early intensive treatment of the inflammation and the intraocular pressure increment in patients with pseudophakia with **corneal graft** who require neodymium:yttrium-aluminum-garnet laser capsulotomies to improve the outcome of **corneal grafts.**

L7 ANSWER 18 OF 33 BIOSIS on STN
2003:554737 Document No.: PREV200300551995. POST KERATOPLASTY EMERGENCY VISITS - A PROSPECTIVE **REVIEW** OF 100 CONSECUTIVE VISITS. Gnanaraj, L. [Reprint Author]; Sandhu, S. [Reprint Author]; Figueiredo, F. C. [Reprint Author]. Ophthalmology, Royal Victoria Infirmary, Newcastle Upon Tyne, UK. ARVO Annual Meeting Abstract Search and Program Planner, (2003) Vol. 2003, pp. Abstract No. 4696. cd-rom.
Meeting Info.: Annual Meeting of the Association for Research in Vision and Ophthalmology. Fort Lauderdale, FL, USA. May 04-08, 2003. Association for Research in Vision and Ophthalmology.
Language: English.
AB Purpose: Pre operative counselling for penetrating keratoplasty should include awareness of symptoms of possible complications as early presentation can enhance long term success. In our corneal transplantation service, all patients are instructed to arrange a same day emergency visit through a dedicated telephone line if they experience redness, sensitivity to light, vision loss, pain (R.S.V.P) or any other

symptoms in eyes that have undergone keratoplasty. This study was designed to evaluate the reason for presentation, management outcome of each visit and the efficiency of the system in management of post keratoplasty complications. Methods: A prospective **review** of one hundred consecutive emergency visits by post penetrating keratoplasty patients was included. Results: Sixty-two patients from a cohort of 350, with a mean age of 62.8 years (range 18 ?92) presented between May 2001 and July 2002. 68% were male, with varied preoperative diagnosis. Sixteen visits were during the first month after surgery and forty visits within the first year. Ten patients (16%) sought consultation more than twice during the study period with one patient presenting 5 times. Pain and grittiness were the main presenting complaints (68%). Loose corneal suture (25%) necessitating removal was the most common diagnosis. Sixteen patients (26%) needed in-patient treatment. This group included graft rejection (13%), graft infection (8%), a case each of retinal detachment, increased intra ocular pressure and Bells palsy. Early intervention and successful management ensured graft **survival** and preservation of visual acuity in all our patients. Conclusions: Presentation with short duration of symptoms and gross reduction in postoperative visual acuity invariably indicate a serious complication. Most corneal surgeons educate their patient to seek prompt treatment for symptoms such as R.S.V.P as early intervention of any sight threatening complication increase the chance for graft **survival** and improvement of vision. This **review** shows a simple open access system helps early presentation and successful management of post graft complications.

L7 ANSWER 19 OF 33 EMBASE on STN

2002212469 EMBASE The outcome of corneal grafting in patients with stromal keratitis of herpetic and non-herpetic origin. Halberstadt M.; Machens M.; Gahlenbek K.-A.; Bohnke M.; Garweg J.G.. Dr. J.G. Garweg, Department of Ophthalmology, University of Bern, Inselspital, CH-3010 Bern, Switzerland. justus.garweg@insel.ch. British Journal of Ophthalmology Vol. 86, No. 6, pp. 646-652 2002.
Refs: 63.
ISSN: 0007-1161. CODEN: BJOPAL
Pub. Country: United Kingdom. Language: English. Summary Language: English.

ED Entered STN: 20020627

AB Aim: To evaluate the outcome of corneal grafting in patients with stromal keratitis of herpetic (HSK) and non-herpetic origin, using predefined diagnostic criteria and standardised postoperative therapeutic strategies. Methods: 384 adult immunocompetent recipients of a **corneal graft** for herpetic (n = 186) or non-herpetic (n = 198) keratitis were followed up prospectively for up to 5 years. Results: The herpetic group displayed significantly more corneal vascularisation (p = 0.013), more epithelial defects (p = 0.049), lower corneal sensitivity (p<0.001), more graft rejection episodes (p = 0.002), and required larger grafts (p<0.001). However, the postoperative course of visual acuity, endothelial cell numerical density, and rate of graft failures were similar in both groups. After 5 years, cumulative probability of graft **survival** in HSK patients (40.85%) was similar to that observed in individuals with non-herpetic keratitis (50.15%; log rank = 0.874; relative risk: 1.04). Conclusion: Despite a markedly higher preoperative risk profile in herpetic eyes, the functional outcomes of grafts in individuals with keratitis of herpetic or non-herpetic origin were similar. Probably the most important contribution is a consequent close follow up and a therapeutic strategy including systemic prophylaxis of viral recurrence and of graft rejection by well adopted local steroid therapy.

L7 ANSWER 20 OF 33 BIOSIS on STN

2003:154341 Document No.: PREV200300154341. Recurrence of Corneal Stromal Dystrophies after Penetrating Keratoplasty. Marcon, A. S. [Reprint

Author]; Rapuano, C. J. [Reprint Author]; Laibson, P. R. [Reprint Author]; Cohen, E. J. [Reprint Author]. Cornea Service, Wills Eye Hospital - Thomas Jefferson University, Philadelphia, PA, USA. ARVO Annual Meeting Abstract Search and Program Planner, (2002) Vol. 2002, pp. Abstract No. 1723. cd-rom.
Meeting Info.: Annual Meeting of the Association For Research in Vision and Ophthalmology. Fort Lauderdale, Florida, USA. May 05-10, 2002.
Language: English.

AB Purpose: The objective of this study is to assess the rate of recurrence of stromal dystrophies in **corneal grafts.** Methods: We conducted a retrospective **review** of Wills Eye Hospital records from 1984 to 2001, identifying all patients with stromal dystrophies who had penetrating keratoplasties. Recurrence is defined as any clinical findings compatible with recurrence of the disease in the graft button. Clinically significant recurrence is defined as ocurring in the visual axis causing decreased visual acuity (loss of two lines or more, or worse than 20/40) or causing recurrent erosion symptoms. Factors to be analyzed include age, gender, time to recurrence and time to clinically significant recurrence. Results will be analyzed using Kaplan-Meier **survival** curves. Results: Preliminary results are as follow. Forty-eight patients (77 eyes) were included in this study. Twenty-one patients (35 eyes) were diagnosed with lattice dystrophy (mean follow-up time of 139 months), 10 patients (17 eyes) with dystrophy of Bowman's membrane (152 months), 8 patients (14 eyes) with macular dystrophy (86 months), 5 patients (7 eyes) with granular dystrophy (145 months), 4 patients (4 eyes) with Schnyder's crystalline dystrophy (52 months). The mean time for the dystrophy of Bowman's membrane eyes to show signs of any recurrence (14 eyes) was 34 months and to show signs of clinically significant recurrence (11 eyes) was 52 months. One eye, with a follow-up period of at least 36 months, failed to present with signs of recurrent disease. Of the eyes with granular dystrophy the mean time for any recurrence (3 eyes) was 35 months and 81 months for clinically significant recurrence (2 eyes). Four eyes, with a follow-up period of at least 36 months, did not have signs of recurrence. The mean time for the lattice dystrophy eyes to present with signs of any recurrence was 87 months (21 eyes) and 114 months for clinically significant recurrence (17 eyes). All eyes had evidence of some recurrence during the study period. Of the 14 eyes diagnosed with macular dystrophy only 1 presented with signs of any recurrence, 190 months after the surgery. None of the 4 eyes with Schnyder's crystalline dystrophy had signs of recurrence during the study period. Conclusion: The corneal dystrophies studied can be successfully treated with penetrating keratoplasty but some degree of recurrence of the original disease in the graft should be expected eventually. Dystrophy of the Bowman's membrane and granular dystrophy are likely to recur earlier than other stromal dystrophies.

L7 ANSWER 21 OF 33 SCISEARCH COPYRIGHT (c) 2005 The Thomson Corporation on STN

2001:508263 The Genuine Article (R) Number: 442MF. Corneal allograft rejection: Current understanding I. Immunobiology and basic mechanisms. Pleyer U (Reprint); Dannowski H; Volk H D; Ritter T. Humboldt Univ, Dept Ophthalmol, Charite, Augustenburger Pl 1, D-13353 Berlin, Germany (Reprint); Humboldt Univ, Dept Ophthalmol, Charite, D-13353 Berlin, Germany; Humboldt Univ, Inst Med Immunol, Charite, D-13353 Berlin, Germany . OPHTHALMOLOGICA (JUL-AUG 2001) Vol. 215, No. 4, pp. 254-262. ISSN: 0030-3755. Publisher: KARGER, ALLSCHWILERSTRASSE 10, CH-4009 BASEL, SWITZERLAND. Language: English.
ABSTRACT IS AVAILABLE IN THE ALL AND IALL FORMATS

AB Allograft rejection remains the single largest impediment to success in corneal transplantation. This article briefly **reviews** our current understanding of some fundamental aspects of corneal immunology and the pathogenetic mechanisms underlying **corneal graft** rejection. As knowledge increases, it is hoped that a better understanding of the immunobiology may result in improved preventive and therapeutic measures.

L7 ANSWER 22 OF 33 MEDLINE on STN DUPLICATE 13

2001301989. PubMed ID: 11248813. **Corneal graft** outcome study. Sit M; Weisbrod D J; Naor J; Slomovic A R. (Faculty of Medicine, University of Toronto, Canada.) Cornea, (2001 Mar) 20 (2) 129-33. Journal code: 8216186. ISSN: 0277-3740. Pub. country: United States. Language: English.

AB PURPOSE: To determine overall 2- and 5-year **corneal graft survival** rates and to identify risk factors for **corneal graft** failure in our patient population. METHODS: A retrospective chart **review** of 696 patients undergoing corneal transplantation performed by a single surgeon at The Toronto Western Hospital over a 7.5-year period. RESULTS: A total of 468 eyes met the inclusion criteria for this study. Overall, the 2- and 5-year graft **survival** rates were 78.8% and 64.5%, respectively. In a univariate analysis, patient age, gender, history of glaucoma, preoperative diagnosis, type of operative procedure, and postoperative factors all were shown to be significantly associated with graft **survival.** In a multivariate analysis, six independent predictors of graft failure were identified: preoperative diagnosis, neovascularization of the graft, the presence of peripheral anterior synechiae, gender, occurrence of one or more rejection episodes, and age of the recipient at the time of corneal transplantation. CONCLUSIONS: Risk of graft failure can vary substantially within a population of patients receiving a corneal transplant. The outcomes of this study concur with the risk factors for **corneal graft** failure in the literature and can be used as prognostic guidelines for both surgeons and patients.

L7 ANSWER 23 OF 33 MEDLINE on STN

2003509242. PubMed ID: 14585142. Molecular mechanisms of immunity in corneal allotransplantation and xenotransplantation. Qian Y; Dana M R. (Laboratory of Immunology, Schepens Eye Research Institute, Harvard Medical School, 20 Staniford Street, Boston, MA 02114, USA.. yqian@vision.eri.harvard.edu) . Expert reviews in molecular medicine [electronic resource], (2001 Jul 16) 2001 1-21. Electronic Publication: 2001-07-16. Journal code: 100939725. ISSN: 1462-3994. Pub. country: England: United Kingdom. Language: English.

AB Corneal allotransplantation is the most common and successful form of solid organ transplantation in humans. In uncomplicated cases, the two-year graft **survival** rate is over 90%. This extraordinary success can be attributed in part to various features of the normal cornea and anterior segment that together account for their 'immune-privileged' status. However, despite this success, a significant number of **corneal grafts** fail and immunological rejection remains by far the leading cause of graft failure. Studies on animal models of corneal transplantation have yielded a wealth of information on the molecular and cellular features of graft rejection, and have established that this process is mediated primarily by CD4+ T cells of the T helper 1 (Th1) phenotype. In addition, studies have elucidated that certain facets of allosensitisation differ between corneal and other solid organ transplants. On the basis of these findings, novel experimental strategies selectively targeting the afferent or efferent arms of corneal alloimmunity have provided promising results in preventing corneal allograft rejection in the laboratory. Finally, because of the global shortage of human donor corneas, there is currently renewed interest in the possibility of using corneas from other species for transplantation into human eyes (xenotransplantation). Preliminary studies on animal models of corneal xenotransplantation have documented both antibody-mediated and cell-mediated responses that might play important roles in the accelerated rejection observed in corneal xenotransplants. This **review** synthesises the principal concepts emerging from studies of the molecular mechanisms in corneal transplant immunology.

L7 ANSWER 24 OF 33 CAPLUS COPYRIGHT 2005 ACS on STN

2001:758173 Document No. 136:165572 Molecular mechanisms of immunity in corneal allotransplantation and xenotransplantation. Qian, Ying; Reza, Dana M. (Lab. Immunology, Schepens Eye Res. Inst., Harvard Medical School, Boston, MA, 01114, USA). Expert Reviews in Molecular Medicine [online computer file] No pp. given (English) 2001. CODEN: ERMMFS. ISSN: 1462-3994. URL: http://www-ermm.cbcu.cam.ac.uk/01003246a.pdf Publisher: Cambridge University Press.

AB A **review.** Corneal allotransplantation is the most common and successful form of solid organ transplantation in humans. In uncomplicated cases, the two-year graft **survival** rate is over 90%. This extraordinary success can be attributed in part to various features of the normal cornea and anterior segment that together account for their immune privileged status. However, despite this success, a significant number of **corneal grafts** fail and immunol. rejection remains by far the leading cause of graft failure. Studies on animal models of corneal transplantation have yielded a wealth of information on the mol. and cellular features of graft rejection, and have established that this process is mediated primarily by CD4+ T cells of the T helper 1 (Th1) phenotype. In addition, studies have elucidated that certain facets of allosensitization differ between corneal and other solid organ transplants. On the basis of these findings, novel exptl. strategies selectively targeting the afferent or efferent arms of corneal alloimmunity have provided promising results in preventing corneal allograft rejection in the laboratory Finally, because of the global shortage of human donor corneas, there is currently renewed interest in the possibility of using corneas from other species for transplantation into human eyes (xenotransplantation). Preliminary studies on animal models of corneal xenotransplantation have documented both antibody-mediated and cell-mediated responses that might play important roles in the accelerated rejection observed in corneal xenotransplants. This **review** synthesizes the principal concepts emerging from studies of the mol. mechanisms in corneal transplant immunol.

L7 ANSWER 25 OF 33 MEDLINE on STN DUPLICATE 14

1999215794. PubMed ID: 10201611. Long-term results of **corneal graft survival** in infants and children with peters anomaly. Yang L L; Lambert S R; Lynn M J; Stulting R D. (Emory Eye Center, Emory University, Atlanta, Georgia 30322, USA.) Ophthalmology, (1999 Apr) 106 (4) 833-48. Journal code: 7802443. ISSN: 0161-6420. Pub. country: United States. Language: English.

AB OBJECTIVE: To determine the long-term results of **corneal graft survival** after penetrating keratoplasty for Peters anomaly and to identify risk factors for graft failure. DESIGN: Noncontrolled interventional case series: a single-center retrospective **review** of a consecutive surgical series. PARTICIPANTS: The records of all children 12 years of age or younger who underwent penetrating keratoplasty for Peters anomaly between January 1971 and December 1992 were reviewed. All study eyes had completed a minimum of 3 years of follow-up from the date of first keratoplasty and had undergone most of their corneal surgery at Emory University. INTERVENTION: Characteristics of the recipient, the eye, the donor, and the surgical procedure were analyzed for their influence on **survival** of the first graft. **Survival** probabilities were estimated using the Kaplan-Meier method. Multivariate regression analysis was performed to estimate relative risks and adjusted **survival** probabilities. MAIN OUTCOME MEASURE: Graft clarity. RESULTS: One hundred forty-four penetrating keratoplasties were performed in 72 eyes of 47 patients. The median age at first keratoplasty was 4.4 months. The median follow-up was 11.1 years. Fifty-four percent of eyes received one graft, 18% received two grafts, and 28% received three or more grafts. The overall probability of maintaining a clear first graft was 56% at 6 months, 49% at 12 months, 44% at 3 years, and 35% at 10 years. The probability of second or subsequent grafts surviving for 3 years was less than 10%. Thirty-nine percent of eyes had a clear graft at the time of **review**; 36% of eyes had a clear first graft. Multivariate analysis identified disease

severity, donor cornea size, coexisting central nervous system abnormalities, and quadrants of anterior synechiae as the strongest risk factors for graft failure. Supplemental multivariate analysis, restricted to observable preoperative variables, identified stromal vessels, total limbal opacification, and preoperative glaucoma as independent preoperative predictors of graft failure. Allograft rejection was the most frequently identified cause of graft failure. Major complications after keratoplasty were phthisis, retinal detachment, cataract, and glaucoma. CONCLUSIONS: The overall long-term probability of maintaining a clear graft after initial penetrating keratoplasty for Peters anomaly is 35% +/- 0.06%, with subsequent grafts rarely surviving. Eyes with severe disease, larger donor corneas, coexisting central nervous system abnormalities, and anterior synechiae have significantly poorer outcomes than eyes without these factors. These data should be carefully considered before recommending corneal transplantation for Peters anomaly, particularly after previous graft failure.

L7 ANSWER 26 OF 33 SCISEARCH COPYRIGHT (c) 2005 The Thomson Corporation on STN

1999:727371 The Genuine Article (R) Number: 240BM. Tacrolimus (FK 506). Letko E; Bhol K; Pinar V; Foster C S; Ahmed A R (Reprint). Harvard Univ, Sch Dent Med, Dept Oral Med, 188 Longwood Ave, Boston, MA 02115 USA (Reprint); Harvard Univ, Sch Dent Med, Dept Oral Med, Boston, MA 02115 USA; Harvard Univ, Massachusetts Eye & Ear Infirm, Sch Med, Dept Ophthalmol, Boston, MA USA. ANNALS OF ALLERGY ASTHMA & IMMUNOLOGY (SEP 1999) Vol. 83, No. 3, pp. 179-189. ISSN: 1081-1206. Publisher: AMER COLL ALLERGY ASTHMA IMMUNOLOGY, 85 WEST ALGONQUIN RD SUITE 550, ARLINGTON HTS, IL 60005 USA. Language: English.

ABSTRACT IS AVAILABLE IN THE ALL AND IALL FORMATS

AB Objective: The focus of this **review** is to summarize the mechanism of action, animal and clinical studies, and adverse effects of tacrolimus (FK 506) in treatment after solid organ transplantation and in treatment of autoimmune diseases.

Data sources: A detailed search of the literature was done. Both human and animal studies considered relevant and important were used.

Study selection: Material was taken only from peer reviewed journals.

Results: FK 506 is a macrolide lactone antibiotic with potent immunosuppressive activity. It acts primarily on CD4+ T helper lymphocytes by inhibiting the production of lymphokines, which are required for cell growth and differentiation, principally interleukin-2, at the transcriptional level. It was first clinically used in patients after liver transplantation. Tacrolimus-based immunosuppression has been proven to be beneficial in prolonging the **survival** of liver, kidney, heart, lung, pancreas, pancreatic islet, and intestinal allografts. Autoimmune diseases in which the immunosuppressive efficacy of tacrolimus has been tested experimentally include arthritis, systemic lupus erythematosus, uveitis, type-1 diabetes, thyroiditis, autoimmune renal disorders, experimental autoimmune encephalomyelitis, myocarditis, myasthenia gravis, colitis, and alopecia areata. Tacrolimus has been used for treatment of selected human diseases, such as psoriasis, uveitis, corticosteroid-resistant nephrotic syndrome, recalcitrant pyoderma gangrenosum, new onset type 1 diabetes, autoimmune chronic active hepatitis, pediatric autoimmune enteropathy, Crohn's disease and atopic dermatitis.

Conclusion: Tacrolimus is a potent immunosuppressive drug in treatment of patients after solid organ transplantation and in selected autoimmune diseases. Further studies are necessary to better understand intracellular mechanism of action and specify therapeutic indications.

L7 ANSWER 27 OF 33 CAPLUS COPYRIGHT 2005 ACS on STN

2000:242539 Document No. 133:265238 The immunology of corneal transplantation. Niederkorn, Jerry Y. (Department of Ophthalmology, University of Texas Southwestern Medical Center, Dallas, TX, USA). Developments in Ophthalmology, 30(Immuno-Ophthalmology), 129-140 (English) 1999. CODEN: DEOPDB. ISSN: 0250-3751. Publisher: Karger.

AB A **review** with 53 refs. is presented on the immunol. aspects of **corneal graft** failure. Topics discussed include the immune privilege of corneal allografts, the role of Langerhans cells in eliciting alloimmune responses and **corneal graft** rejection, efferent blockage of corneal allograft rejection by FasL, the role of anterior chamber-associated immune deviation in corneal allograft **survival**, and the mechanisms of corneal allograft rejection.

L7 ANSWER 28 OF 33 EMBASE COPYRIGHT 2005 ELSEVIER INC. ALL RIGHTS RESERVED. on STN

97365934 EMBASE Document No.: 1997365934. Rethinking immunological privilege: Implications for corneal and limbal stem cell transplantation. Williams K.A.; Coster D.J.. Dr. K.A. Williams, Department of Ophthalmology, Flinders Univ. of South Australia, Flinders Medical Centre, Bedford Park, SA 5042, Australia. Molecular Medicine Today Vol. 3, No. 11, pp. 495-501 1997.
Refs: 44.
ISSN: 1357-4310. CODEN: MMTOFK
S 1357-4310(97)01122-2. Pub. Country: United Kingdom. Language: English. Summary Language: English.

ED Entered STN: 971218

AB Immunological privilege operates within the normal eye by multiple passive and active mechanisms, including antigen sequestration, maintenance of an immunosuppressive local environment and induction of apoptotic death in infiltrating cells of the immune system. Ocular privilege might have developed to protect the eye from the collateral damage associated with an inflammatory response to invading pathogens. Nevertheless, **corneal grafts** do undergo irreversible immunological rejection and, furthermore, **corneal graft** rejection is very similar at a histological level to the rejection processes that operate in vascularized organ grafts. Ocular privilege is thus relative. The question arises as to how **corneal grafts** are rejected in the face of so many mechanisms designed to prevent immune responses from operating inside the eye-a question that is still essentially unanswered.

L7 ANSWER 29 OF 33 MEDLINE on STN DUPLICATE 15

96014793. PubMed ID: 7556726. Immunosuppression in corneal transplantation. Hill J C. (Department of Ophthalmology, Groote Schuur Hospital, Cape Town, South Africa.) Eye (London, England), (1995) 9 (Pt 2) 247-53. Journal code: 8703986. ISSN: 0950-222X. Pub. country: ENGLAND: United Kingdom. Language: English.

AB This paper **reviews** the clinical post-operative management of keratoplasty and the management of **corneal graft** rejection. In both instances corticosteroids remain the mainstay of treatment; however, the literature shows a wide range for both route and frequency of administration. Grafts at 'high risk' require more immunosuppressive therapy, but no universally accepted definition of high risk exists and consequently different treatment regimens are difficult to compare and evaluate. Studies using univariate and multivariate **survival** analysis suggest that recipient corneas can be divided into low, medium and high risk depending on the number of quadrants of vascularisation (avascular, 1-2 quadrants and 3+ quadrants respectively). This wider classification would make the devising and comparing of treatment regimens more consistent. In high-risk cases, corticosteroids alone provide insufficient immunosuppression and systemic cyclosporine is needed in exceptional cases. When managing rejection episodes, a severe reaction involving the endothelium often does not respond to topical steroids alone, and systemic corticosteroids are required. Instead of oral steroids, we now prefer to use an intravenous 'pulse' of 500 mg methylprednisolone: this is at least as effective, avoids prolonged medication, and may confer some long-term benefit.

L7 ANSWER 30 OF 33 SCISEARCH COPYRIGHT (c) 2005 The Thomson Corporation on STN

1995:327072 The Genuine Article (R) Number: QX094. THE MECHANISMS OF **CORNEAL GRAFT** FAILURE IN THE RAT. KATAMI M (Reprint). KITASATO UNIV, SCH MED, DEPT OPHTHALMOL, 1-15-1 KITASATO, KANAGAWA 228, JAPAN (Reprint). EYE (1995) Vol. 9, Part 2, pp. 197-207. ISSN: 0950-222X. Publisher: ROYAL COLL OPHTHALMOLOGISTS, 17 CORNWALL TERRACE, LONDON, ENGLAND NW1 4QW. Language: English.
ABSTRACT IS AVAILABLE IN THE ALL AND IALL FORMATS

AB The success rate of corneal transplantation is very similar to that of other organ transplantations because corneal transplants can induce an allograft rejection similar to other organ transplants. Only the centre of the cornea can be considered an immunologically privileged site. The reasons for this are considered in this **review** of experimental corneal grafting which has led to an understanding the immunological mechanisms behind **corneal graft** rejection. The topics discussed include the role of antigen presenting cells (APCs) in experimental **corneal graft** rejection and their distribution in the cornea.

L7 ANSWER 31 OF 33 MEDLINE on STN DUPLICATE 16

91208970. PubMed ID: 2019116. **Corneal graft survival** in HLA-A- and HLA-B-matched transplantations in high-risk cases with retrospective **review** of HLA-DR compatibility. Beekhuis W H; van Rij G; Renardel de Lavalette J G; Rinkel-van Driel E; Persijn G; D'Amaro J. (Cornea Service, Rotterdam Eye Hospital, The Netherlands.) Cornea, (1991 Jan) 10 (1) 9-12. Journal code: 8216186. ISSN: 0277-3740. Pub. country: United States. Language: English.

AB In 107 HLA-A- and HLA-B-matched corneal transplantations performed in high-risk patients, the 3-year graft **survival** was 60.5%. The criteria used for the definition of high risk were vascularization of the recipient cornea and/or one or more previous failed grafts; they were also the indications for HLA typing and matching. Donor/recipient compatibility was defined by the presence of only 0 or 1 HLA-A or HLA-B mismatches. When non-immunological factors leading to graft failure were excluded, the 3-year **survival** was 76.3%. During that follow-up period, a total of 33 grafts failed; in 13 cases, the cause was allograft rejection. When only first transplants were considered, a 3-year graft **survival** of 81.0% was observed. Retrospective DR typing was possible in 33 cases. Because only three graft rejections occurred in that group, we were unable to assess the importance of DR compatibility on the **survival** of corneal allografts.

L7 ANSWER 32 OF 33 MEDLINE on STN DUPLICATE 17

90076586. PubMed ID: 2591598. Large **corneal grafts** can be successful. Kirkness C M; Ficker L A; Rice N S; Steele A D. (Corneal Clinic, Moorfields Eye Hospital, London.) Eye (London, England), (1989) 3 (Pt 1) 48-55. Journal code: 8703986. ISSN: 0950-222X. Pub. country: ENGLAND: United Kingdom. Language: English.

AB Seventeen grafts of 10 mm in diameter or larger have been performed on 16 eyes of 15 patients. The major indications for surgery were infections or perforations or both. Follow-up has ranged from 8-54 months (mean 26.4). The 4 year **survival** probability was 0.64. Although the procedure was successful in saving all but one eye and restored useful vision in the majority, complications including cataract, glaucoma, graft rejection episodes and infections were encountered. The management of these complications is described. At final **review**, 13 eyes had clear grafts including those in whom regraft had been performed. These results have only been achieved by close co-operation between patients and the medical team responsible for their care.

L7 ANSWER 33 OF 33 MEDLINE on STN DUPLICATE 18

85019312. PubMed ID: 6385606. The effect of prospective HLA-A and -B matching in 288 penetrating keratoplasties for herpes simplex keratitis. Volker-Dieben H J; Kok-van Alphen C C; D'Amaro J; de Lange P. Acta ophthalmologica, (1984 Aug) 62 (4) 513-23. Journal code: 0370347. ISSN: 0001-639X. Pub. country: Denmark. Language: English.

AB A retrospective **review** of 288 penetrating keratoplasties (PKP) for herpes simplex keratitis demonstrated a 60.4% **survival** rate of clear grafts at 3 years. A highly significant difference in **corneal graft survival** in severely vascularized corneas (57.1% at 3 years) versus non- or slightly vascularized corneas (82.8% at 3 years) was observed (P = 0.009). Prospectively HLA-A and -B matched grafts in vascularized corneas revealed a significantly improved graft **survival** when compared to unmatched grafts (P = 0.035). **Corneal graft survival** in eyes grafted 'a chaud' was not significantly below the graft **survival** of vascularized corneas with a clinically non-active herpetic corneal disease. Recurrence of herpes simplex in the graft was observed in an earlier postoperative period in HLA-A and -B matched grafts (P = 0.0004).

=> s l2 and ATP analog
L8 1 L2 AND ATP ANALOG

=> d l8 cbib abs

L8 ANSWER 1 OF 1 CAPLUS COPYRIGHT 2005 ACS on STN
2003:696673 Document No. 139:207829 Methods of extending **corneal graft survival** using VEGFR-3 inhibitors which inhibit lymphangiogenesis. De Vries, Gerald W. (Allergan, Inc., USA). PCT Int. Appl. WO 2003072029 A2 20030904, 84 pp. DESIGNATED STATES: W: AE, AG, AL, AM, AT, AU, AZ, BA, BB, BG, BR, BY, BZ, CA, CH, CN, CO, CR, CU, CZ, DE, DK, DM, DZ, EC, EE, ES, FI, GB, GD, GE, GH, GM, HR, HU, ID, IL, IN, IS, JP, KE, KG, KP, KR, KZ, LC, LK, LR, LS, LT, LU, LV, MA, MD, MG, MK, MN, MW, MX, MZ, NO, NZ, OM, PH, PL, PT, RO, RU, SC, SD, SE, SG, SK, SL, TJ, TM, TN, TR, TT, TZ, UA, UG, UZ, VC, VN, YU, ZA, ZM, ZW; RW: AT, BE, BF, BJ, CF, CG, CH, CI, CM, CY, DE, DK, ES, FI, FR, GA, GB, GR, IE, IT, LU, MC, ML, MR, NE, NL, PT, SE, SN, TD, TG, TR. (English). CODEN: PIXXD2. APPLICATION: WO 2003-US5125 20030220. PRIORITY: US 2002-81126 20020222.
AB The present invention provides a method of extending **corneal graft survival** following corneal transplantation in a patient by administering to the patient an effective amount of a pharmaceutical composition containing a vascular endothelial growth factor receptor-3 (VEGFR-3) inhibitor, whereby lymphangiogenesis is suppressed in the cornea of the patient. More specifically, the VEGFR-3 inhibitor is a dominant neg. VEGFR-3 receptor, a nucleic acid encoding a dominant neg. VEGFR-3 receptor, a VEGFR-3 kinase inhibitor, an **ATP analog**, a VEGFR-3 binding mol., or a sequence-specific RNase.

=> s l1 and ATP analog
L9 1 L1 AND ATP ANALOG

=> d l9 cbib abs

L9 ANSWER 1 OF 1 CAPLUS COPYRIGHT 2005 ACS on STN
2003:696673 Document No. 139:207829 Methods of extending **corneal graft** survival using VEGFR-3 inhibitors which inhibit lymphangiogenesis. De Vries, Gerald W. (Allergan, Inc., USA). PCT Int. Appl. WO 2003072029 A2 20030904, 84 pp. DESIGNATED STATES: W: AE, AG, AL, AM, AT, AU, AZ, BA, BB, BG, BR, BY, BZ, CA, CH, CN, CO, CR, CU, CZ, DE, DK, DM, DZ, EC, EE, ES, FI, GB, GD, GE, GH, GM, HR, HU, ID, IL, IN, IS, JP, KE, KG, KP, KR, KZ, LC, LK, LR, LS, LT, LU, LV, MA, MD, MG, MK, MN, MW, MX, MZ, NO, NZ, OM, PH, PL, PT, RO, RU, SC, SD, SE, SG, SK, SL, TJ, TM, TN, TR, TT, TZ, UA, UG, UZ, VC, VN, YU, ZA, ZM, ZW; RW: AT, BE, BF, BJ, CF, CG, CH, CI, CM, CY, DE, DK, ES, FI, FR, GA, GB, GR, IE, IT, LU, MC, ML, MR, NE, NL, PT, SE, SN, TD, TG, TR. (English). CODEN: PIXXD2. APPLICATION: WO 2003-US5125 20030220. PRIORITY: US 2002-81126 20020222.

AB The present invention provides a method of extending **corneal graft** survival following corneal transplantation in a patient by administering to the patient an effective amount of a pharmaceutical composition containing a vascular endothelial growth factor receptor-3 (VEGFR-3) inhibitor, whereby lymphangiogenesis is suppressed in the cornea of the patient. More specifically, the VEGFR-3 inhibitor is a dominant neg. VEGFR-3 receptor, a nucleic acid encoding a dominant neg. VEGFR-3 receptor, a VEGFR-3 kinase inhibitor, an **ATP analog**, a VEGFR-3 binding mol., or a sequence-specific RNase.

=> s (devries g?/au)
L10 965 (DEVRIES G?/AU)

=> s l10 and graft
L11 2 L10 AND GRAFT

=> dup remove l11
PROCESSING COMPLETED FOR L11
L12 2 DUP REMOVE L11 (0 DUPLICATES REMOVED)

=> d l12 1-2 cbib abs

L12 ANSWER 1 OF 2 SCISEARCH COPYRIGHT (c) 2005 The Thomson Corporation on STN
1996:788096 The Genuine Article (R) Number: VP210. Hypospadias repair by laser tissue soldering: Intraoperative results and follow-up in 30 children. Kirsch A J (Reprint); **deVries G M**; Chang D T; Olsson C A; Connor J P; Hensle T W. COLUMBIA UNIV, COLL PHYS & SURG, DEPT UROL, SQUIER UROL CLIN, NEW YORK, NY; COLUMBIA UNIV, COLL PHYS & SURG, BABIES & CHILDRENS HOSP NEW YORK, NEW YORK, NY. UROLOGY (OCT 1996) Vol. 48, No. 4, pp. 616-623. ISSN: 0090-4295. Publisher: CAHNERS PUBL CO, 249 WEST 17 STREET, NEW YORK, NY 10011. Language: English.
ABSTRACT IS AVAILABLE IN THE ALL AND IALL FORMATS
AB Objectives. We examined the use of laser tissue soldering (LTS) as an adjunct to suturing of, as well as a primary means of, tissue closure in urethral reconstruction.

Methods. Since June 1994, 26 boys ranging in age from 3 months to 14 years (mean 3.0 years) underwent hypospadias repair using LTS techniques. The classification of hypospadias was subcoronal in 13, midpenile in 5, penoscrotal in 7, and scrotal in 1. Laser tissue soldering was used in an additional 4 patients: tunica vaginalis patch **graft** corporoplasty in 2 (scrotal hypospadias), epispadias fistulae in 1, and urethral diverticulum in 1. Of these cases, 5 hypospadias repairs were completely sutureless. An intraoperative comparision was made between suturing and LTS with respect to operative time and degree of difficulty in performing LTS. Postoperatively, patients were examined to determine complications, including stricture, fistula, or impaired wound healing. An unselected group of 25 consecutive boys undergoing hypospadias repair between 1991 and 1992 served as a historical control group.

Results. No intraoperative complications resulted from laser activation. In 5 of the 30 procedures (16.6%), suture disruption was noted to occur, with a higher incidence seen with finer, dyed suture material. For hypospadias repair, the average time to suture was 6.7 min/cm (n = 23), whereas it was 3.1 min/cm for adjunctive LTS (n = 25) and 1.4 min/cm for sutureless urethroplasty (n = 3). Follow-up ranged from 3 to 22 months (average 9.6). four fistulae were noted (I onlay, 2 skin tube **grafts**, 1 Thiersch tube) each following penoscrotal or scrotal hypospadias repair; a fifth fistula developed following a traumatic catheterization in a sutureless repair. The overall complication rate in the LTS group was 19% (5 of 26) versus 24% (6 of 25) for controls, whereas that for the distal forms of hypospadias was 11% (2 of 18) and 13.6% (3 of 22), respectively.

Conclusions. Tissue soldering with laser and chromophore-doped

solder is feasible, safe, and easy to perform. Laser tissue soldering may be an alternative to standard microsuture technique for hypospadias repair.

L12 ANSWER 2 OF 2 SCISEARCH COPYRIGHT (c) 2005 The Thomson Corporation on STN
1992:29476 The Genuine Article (R) Number: GX499. FIBER OUTGROWTH FROM FETAL VASOPRESSIN NEURONS OF THE SUPRACHIASMATIC NUCLEUS, BED NUCLEUS OF THE STRIA TERMINALIS, AND MEDIAL AMYGDALOID NUCLEUS TRANSPLANTED INTO ADULT BRATTLEBORO RATS. ALSHAMMA H A (Reprint); **DEVRIES G J.** UNIV MASSACHUSETTS, DEPT PSYCHOL, PROGRAM NEUROSCI & BEHAV, AMHERST, MA 01003 (Reprint). DEVELOPMENTAL BRAIN RESEARCH (17 DEC 1991) Vol. 64, No. 1-2, pp. 200-204. ISSN: 0165-3806. Publisher: ELSEVIER SCIENCE BV, PO BOX 211, 1000 AE AMSTERDAM, NETHERLANDS. Language: English.
ABSTRACT IS AVAILABLE IN THE ALL AND IALL FORMATS
AB Outgrowth of fibers from different types of vasopressin (AVP) neurons was compared in the brains of AVP-deficient Brattleboro rats. Fetal **grafts** of the suprachiasmatic nucleus (SCN), the bed nucleus of the stria terminalis (BST), and the medial amygdaloid nucleus (MA) were implanted into the lateral ventricle. AVP-immunoreactive fibers from all **grafts** entered the host tissue in the lateral septum. SCN fibers were confined to the lateral margin of the septum. In contrast, MA and BST fibers formed equally dense networks spanning the width of the lateral septum. The data suggest that these transplanted neurons show specific outgrowth, and that the phylogenetically related BST and MA neurons follow similar cues to reach their targets.

=> s l10 and ATP analog
L13 0 L10 AND ATP ANALOG

=> s l10 and VEGF receptor
L14 2 L10 AND VEGF RECEPTOR

=> dup remove l14
PROCESSING COMPLETED FOR L14
L15 2 DUP REMOVE L14 (0 DUPLICATES REMOVED)

=> d l15 1-2 cbib abs

L15 ANSWER 1 OF 2 SCISEARCH COPYRIGHT (c) 2005 The Thomson Corporation on STN
1997:233047 The Genuine Article (R) Number: WN186. Expression of vascular endothelial growth factor (**VEGF**) **receptors** and cDNA cloning of KDR/Flk-1 in normal rat retina. Wen Y (Reprint); Edelman J L; **DeVries G W**; Sachs G. W LOS ANGELES VET AFFAIRS MED CTR, LOS ANGELES, CA 90073; UNIV CALIF LOS ANGELES, SCH MED, LOS ANGELES, CA; ALLERGAN PHARMACEUT INC, IRVINE, CA 92715. INVESTIGATIVE OPHTHALMOLOGY & VISUAL SCIENCE (15 MAR 1997) Vol. 38, No. 4, Part 1, pp. 1677-1677. ISSN: 0146-0404. Publisher: LIPPINCOTT-RAVEN PUBL, 227 EAST WASHINGTON SQ, PHILADELPHIA, PA 19106. Language: English.

L15 ANSWER 2 OF 2 SCISEARCH COPYRIGHT (c) 2005 The Thomson Corporation on STN
1996:385434 The Genuine Article (R) Number: UK861. Cloning of a **VEGF receptor** from bovine choroidal and retinal endothelial cells.. Friant S (Reprint); Andrews K; **DeVries G W.** ALLERGAN PHARMACEUT INC, DEPT BIOL SCI, IRVINE, CA 92715. FASEB JOURNAL (30 APR 1996) Vol. 10, No. 6, pp. 1435-1435. ISSN: 0892-6638. Publisher: FEDERATION AMER SOC EXP BIOL, 9650 ROCKVILLE PIKE, BETHESDA, MD 20814-3998. Language: English.

=> dup remove l10
PROCESSING COMPLETED FOR L10
L16 558 DUP REMOVE L10 (407 DUPLICATES REMOVED)

=> s l16 and inhibitor
L17 29 L16 AND INHIBITOR

=> s l17 and retina
L18 1 L17 AND RETINA

=> d l18 cbib abs

L18 ANSWER 1 OF 1 EMBASE COPYRIGHT 2005 ELSEVIER INC. ALL RIGHTS RESERVED. on STN
90280482 EMBASE Document No.: 1990280482. Regulation of cyclic AMP levels in mammalian **retina**: Effects of depolarizing agents and transmitters. Blazynski C.; **DeVries G.**; Geary K.; Cohen A.I.; Ferrendelli J.A.. Deptartment of Biochemistry, Box 8231 Washington Univ., School of Medicine, 660 S. Euclid,St. Louis, MO 63110, United States. Neurochemistry International Vol. 17, No. 3, pp. 425-433 1990. ISSN: 0197-0186. CODEN: NEUIDS
Pub. Country: United Kingdom. Language: English. Summary Language: English.
ED Entered STN: 911213
AB Cellular depolarization in brain results in a modulation of cAMP levels by releasing neurotransmitters having receptors linked via GTP-binding proteins to adenylate cyclase. In order to determine the transmitters regulating cAMP during cellular depolarization in mammalian **retina**, the modulation of cAMP by depolarizing media was investigated. Cyclic AMP levels in light adapted **retinas** increased following exposure to depolarizing media, but levels in dark adapted **retinas** remained unaltered. The depolarization-induced modulation of cAMP levels persisted in dystrophic **retinas**, suggesting that the response occurred in the inner **retina.** In microdissected discrete retinal layers from rabbit, levels of cAMP were increased following perfusion with depolarizing medium in the outer plexiform and inner nuclear layers, consistent with the observation seen with mouse **retinas.** To begin to identify transmitters released by cellular depolarization, a variety of transmitters and/or antagonists were included in the incubation medium. Haloperidol reduced the depolarization induced increase in cAMP levels by 25% in normal mouse **retinas**, and 75% in dystrophic **retinas.** Dopamine elevated cAMP levels in normal and dystrophic mouse **retinas**, and when combined with depolarizing medium, additive increases were observed. The effects of various neurotransmitters on retinal cAMP levels in the absence of any phosphodiesterase **inhibitors** were assessed, and both dopamine and norepinephrine were found to increase cAMP levels in normal and dystrophic **retinas.** Phentolamine antagonized the increase elicited by norepinephrine. When dopamine and norepinephrine were combined non-additive increases were observed. Serotonin, GABA, acetylcholine, histamine and adenosine had little or no significant effect on the retinal levels of cAMP in either normal or dystrophic mouse **retinas.** These results indicate that depolarizing media increase cAMP levels partially by releasing dopamine. The processes regulating cAMP levels in **retina** are both different and similar to those in brain.

=> d l17 1-29 cbib abs

L17 ANSWER 1 OF 29 MEDLINE on STN
2005028655. PubMed ID: 15602756. Schwann cell lines derived from malignant peripheral nerve sheath tumors respond abnormally to platelet-derived growth factor-BB. Dang Ian; **DeVries George H.** (Research Service, Hines VA Hospital, Hines, IL 60141, USA.. george.devries@med.va.gov) . Journal of neuroscience research, (2005 Feb 1) 79 (3) 318-28. Journal code: 7600111. ISSN: 0360-4012. Pub. country: United States. Language: English.

AB Neurofibromatosis type 1 (NF1) is a genetic disease caused by the loss of neurofibromin, which can lead to formation of highly invasive malignant peripheral nerve sheath tumors (MPNST). We characterized platelet-derived growth factor-beta (PDGF-beta) receptor expression levels and signal transduction pathways in NF1 MPNST cell lines and compared them with the expression of PDGF-beta receptors in normal human Schwann cells (nhSC). As examined by Western blotting, PDGF-beta receptor expression levels were similar in nhSC and NF1 MPNST cell lines. MAPK and Akt also were phosphorylated in both cell types to a similar degree in response to PDGF B chains (PDGF-BB). However, increased intracellular calcium (Ca2+) levels in response to PDGF-BB were observed only in the NF1 MPNST cell lines; nhSC did not show any increase in intracellular calcium when stimulated with PDGF-BB. The calcium response in NF1 MPNST cell lines was blocked with thapsigargin, suggesting that the PDGF-BB-stimulated increases in intracellular calcium originated in the internal compartment of the cell rather than reflecting influx of calcium from the extracellular compartment. Calmodulin kinase II (CAMKII) is phosphorylated in response to PDGF-BB in the NF1 MPNST cell lines, whereas no phosphorylation of CAMKII was observed in nhSCs. The decreased growth of NF1 MPNST cell lines after treatment with a CAMKII **inhibitor** is consistent with the view that aberrant activation of the calcium-signaling pathway by PDGF-BB contributes to the formation of MPNST in NF1 patients.

L17 ANSWER 2 OF 29 MEDLINE on STN

2004148596. PubMed ID: 15042580. Prostaglandin E(2) and 6-keto-prostaglandin F(1alpha) production is elevated following traumatic injury to sciatic nerve. Muja Naser; **DeVries George H.** (Neuroscience Graduate Program, Neurobiology, and Anatomy Loyola University of Chicago, Maywood, Illinois, USA.) Glia, (2004 Apr 15) 46 (2) 116-29. Journal code: 8806785. ISSN: 0894-1491. Pub. country: United States. Language: English.

AB Sciatic nerve explants cultured either alone or in the presence of peritoneal macrophages were used to study prostaglandin E(2) (PGE(2)) and 6-keto-PGF(1alpha) production following traumatic peripheral nerve injury. Although barely detectable at early time points (1-3 h in vitro), the production of PGE(2) and 6-keto-PGF(1alpha) by sciatic nerve explants increased significantly after 18 h and remained elevated for up to 96 h. The cyclooxygenase-2 (COX-2) selective **inhibitor**, NS-398, inhibited PGE(2) and 6-keto-PGF(1alpha) production by injured sciatic nerve in a dose-dependent manner. Consistent with the observed effect of NS-398, peripheral nerve explants, as well as Schwann cells and perineural fibroblasts cultured from neonatal sciatic nerve, each contained COX-2 immunoreactivity after 24 h in vitro. Both Schwann cells and perineural fibroblasts produced significant amounts of PGE(2) and 6-keto-PGF(1alpha); but only in the presence of arachidonic acid. As observed for injured sciatic nerve, the production of PGE(2) and 6-keto-PGF(1alpha) by primary Schwann cells and perineural fibroblasts was completely inhibited by NS-398. Compared to macrophages cultured alone, macrophages cultured in the presence of sciatic nerve explants produced large amounts of PGE(2), whereas the level of 6-keto-PGF(1alpha) was unchanged. In contrast, macrophages treated with adult sciatic nerve homogenate did not produce significant amounts of either PGE(2) or 6-keto-PGF(1alpha) during the entire course of treatment. We conclude that injured sciatic nerves produce PGE(2) and 6-keto-PGF(1alpha) by a mechanism involving COX-2 activity and that macrophages produce large amounts of PGE(2) in response to soluble factors produced by injured nerve but not during the phagocytosis of peripheral nerve debris.

L17 ANSWER 3 OF 29 MEDLINE on STN

2002738337. PubMed ID: 12499280. SPARC is a key Schwannian-derived **inhibitor** controlling neuroblastoma tumor angiogenesis. Chlenski Alexandre; Liu Shuqing; Crawford Susan E; Volpert Olga V; **DeVries George H**; Evangelista Amy; Yang Qiwei; Salwen Helen R; Farrer Robert; Bray James; Cohn Susan L. (The Robert H. Lurie Comprehensive Cancer

Center, Northwestern University, Feinberg School of Medicine, Chicago, Illinois 60611, USA.) Cancer research, (2002 Dec 15) 62 (24) 7357-63. Journal code: 2984705R. ISSN: 0008-5472. Pub. country: United States. Language: English.

AB Neuroblastoma (NB), a common pediatric neoplasm, consists of two main cell populations: neuroblastic/ganglionic cells and Schwann cells. NB tumors with abundant Schwannian stroma display a more benign clinical behavior than stroma-poor tumors. Recent studies suggest that Schwann cells influence NB tumor growth via secreted factors that induce differentiation, suppress proliferation, and inhibit angiogenesis. Two angiogenesis **inhibitors**, pigment epithelium-derived factor and tissue **inhibitor** of metalloproteinase-2, have been detected in Schwann cell secretions. Here, we isolated another Schwann cell-derived secreted **inhibitor** of angiogenesis, a 43-kDa protein identified as SPARC (secreted protein acidic and rich in cysteine), an extracellular matrix protein. We found SPARC to be critical for the antiangiogenic phenotype of cultured Schwann cells. We also show that purified SPARC potently inhibits angiogenesis and significantly impairs NB tumor growth in vivo. SPARC may be an effective candidate for the treatment of children with clinically aggressive, Schwannian stroma-poor NB tumors.

L17 ANSWER 4 OF 29 MEDLINE on STN

2001453679. PubMed ID: 11483647. Identification and functional characterization of thromboxane A2 receptors in Schwann cells. Muja N; Blackman S C; Le Breton G C; **DeVries G H.** (Neuroscience Graduate Program, and Department of Cell Biology, Neurobiology and Anatomy, Loyola University of Chicago, Maywood, Illinois, USA.) Journal of neurochemistry, (2001 Aug) 78 (3) 446-56. Journal code: 2985190R. ISSN: 0022-3042. Pub. country: United States. Language: English.

AB Previous reports have demonstrated the presence of functional thromboxane A2 (TP) receptors in astrocytes and oligodendrocytes. In these experiments, the presence and function of TP receptors in primary rat Schwann cells (rSC) and a neurofibrosarcoma-derived human Schwann cell line (T265) was investigated. Immunocytochemical and immunoblot analyses using polyclonal anti-TP receptor antibodies demonstrate that both cell types express TP receptors. Treatment with the stable thromboxane A2 mimetic U46619 (10 microM) did not stimulate intracellular calcium mobilization in rSC, whereas T265 cells demonstrated a calcium response that was inhibited by prior treatment with TP receptor antagonists. U46619 also stimulated CREB phosphorylation on Ser133 in T265 cells and, to a lesser extent, in rSC. To identify potential mechanisms of CREB phosphorylation in rSC, we monitored intracellular cAMP levels following U46619 stimulation. Elevated levels of cAMP were detected in both rSC (20-fold) and T265 (15-fold) cells. These results demonstrate that TP receptor activation specifically stimulates CREB phosphorylation in T265 cells, possibly by a calcium- and/or cAMP-dependent mechanism. In contrast, TP receptor activation in rSC stimulates increases in cAMP and CREB phosphorylation but does not elicit changes in intracellular calcium.

L17 ANSWER 5 OF 29 MEDLINE on STN

1999235517. PubMed ID: 10220111. Phosphorylation of CREB in axon-induced Schwann cell proliferation. Lee M M; Badache A; **DeVries G H.** (Mental Retardation Research Center, Department of Neurobiology, University of California School of Medicine, Los Angeles, USA.) Journal of neuroscience research, (1999 Mar 15) 55 (6) 702-12. Journal code: 7600111. ISSN: 0360-4012. Pub. country: United States. Language: English.

AB Axonal contact regulates Schwann cell (SC) proliferation during development. However, the intracellular signal transduction pathways involved in the axon-induced proliferation of SC have not been described. We have previously shown that SC proliferation induced by axolemma-enriched fractions (AEF) is accompanied by increased expression of cyclic AMP-responsive element binding protein, CREB. We now report the AEF and dorsal root ganglion neuritic-induced signal transduction pathway(s) which regulate the phosphorylation of CREB that correlate with the SC proliferative response. The phosphorylated form of CREB was

significantly increased after 16 hr of axonal stimulation, continued to increase for 48 hr, and subsequently decreased as monitored by immunocytochemistry and Western blot analysis. Treatment with protein kinase A (PKA) **inhibitor**, H89, completely abolished both the CREB activation and SC proliferation. In contrast, treatment with protein kinase C (PKC) **inhibitor** (bisindolylmaleimide) inhibited AEF-induced SC proliferation, but did not immediately affect CREB phosphorylation. These data are consistent with the view that PKA and PKC pathways are essential for AEF-induced SC proliferation. Since PKC can influence SC proliferation without initially affecting CREB phosphorylation, PKC may regulate SC proliferation at pathways distal to the immediate CREB activation.

L17 ANSWER 6 OF 29 MEDLINE on STN

97220699. PubMed ID: 9067861. Immunolocalization of cytoplasmic and myelin mcalpain in transfected Schwann cells: I. Effect of treatment with growth factors. Neuberger T; Chakrabarti A K; Russell T; **DeVries G H**; Hogan E L; Banik N L. (Department of Neurology, Medical University of South Carolina, Charleston.) Journal of neuroscience research, (1997 Mar 1) 47 (5) 521-30. Journal code: 7600111. ISSN: 0360-4012. Pub. country: United States. Language: English.

AB We have examined the effect of growth factors on the activity and localization of calpain in transfected Schwann cells (tSc). Axolemma-enriched fraction, cAMP, or NGF showed concentration-dependent inhibition of both mu calpain and mcalpain activity. In contrast, both acidic FGF and basic FGF stimulated mu calpain (37%) and mcalpain (58%) of tSC while PDGF-aa and PDGF-bb inhibited both calpain activities. The **inhibitor** (calpastatin) activity was approximately 90% following treatment with NGF, cAMP, PDGF-aa, and PDGF-bb compared to control while this activity was 40% with FGF-treated samples. Immunofluorescence studies indicated localization of cytoplasmic calpain in the nuclear region following growth factor treatment in the cytoplasm. Growth factor treatment caused a decrease in the intensity of calpain immunoreactivity. Treatment with cAMP or FGF resulted in strong immunoreactivity of mcalpain in the nuclear region and cytoplasm compared to untreated. The growth factors did not cause translocation of calpain to the outer surface of the cell membrane. The increased immunoreactivity seen with myelin calpain antibody was greater than cytosolic antibody. The changes seen in calpain activity and immunoreactivity following treatment with growth factors suggest that these factors may regulate calpain-calpastatin expression and translocation to the membrane for interaction with lipids for enzyme activation.

L17 ANSWER 7 OF 29 MEDLINE on STN

96263364. PubMed ID: 8847737. Two mitogenic regions of myelin basic protein interact with different receptors to induce Schwann cell proliferation in a cAMP dependent process. Tzeng S F; Deibler G E; Neuberger T J; **DeVries G H.** (Department of Biochemistry and Molecular Biophysics, Medical College of Virginia, Richmond, USA.) Journal of neuroscience research, (1995 Dec 15) 42 (6) 758-67. Journal code: 7600111. ISSN: 0360-4012. Pub. country: United States. Language: English.

AB Previous studies have shown that myelin basic protein (MBP) is mitogenic for Schwann cells (SCs) in the presence of elevated intracellular cAMP. Two mitogenic regions of MBP have been identified: one mitogenic region within the first 44 residues of the aminoterminus (1-44) and the other mitogenic region within the terminal 15 residues of the carboxyl end of the molecule (152-167). Unlike the mitogenic effect of a myelin enriched fraction (MEF), the mitogenic effect of MBP was not reduced by the addition of the lysosomal **inhibitor**, ammonium chloride. These data indicate that MBP causes SC proliferation by direct interaction of MBP with a surface receptor. Using Scatchard analysis of the binding of MBP to SCs, we report that treatment with forskolin does not cause the upregulation of receptors for MBP. Moreover, MBP blocks the cross-linking of 125I-bFGF with two fibroblast growth factor (FGF) receptors having

apparent molecular weights of 140 kDa and 120 kDa, respectively. Since neither TGF-beta nor PDGF-BB displaced cell surface bound 125I-MBP, we conclude that MBP binds to the FGF receptor rather than other growth factor receptors. Furthermore, only MBP interacted with ganglioside GM1, whereas MBP did not interact with this ganglioside. These results are consistent with the view that ganglioside GM1 mediates the mitogenic effects of MBP, while the FGF receptor mediates the mitogenic effect of MBP. Intracellular cAMP of SCs was transiently increased after the addition of macrophage conditioned medium, suggesting that macrophages may produce factors in vivo which can transiently elevate intracellular cAMP levels, allowing a wave of SC proliferation in response to MBP-related mitogens.

L17 ANSWER 8 OF 29 MEDLINE on STN

95305025. PubMed ID: 7785500. Poster discussion lipid mediators--new agents. **DeVries G W**; Jacobs R S. (Allergan, Inc., Irvine, CA 92715, USA.) Agents and actions. Supplements, (1995) 47 203-5. Journal code: 7801014. ISSN: 0379-0363. Pub. country: Switzerland. Language: English.

L17 ANSWER 9 OF 29 MEDLINE on STN

94254452. PubMed ID: 7515130. Mitochondrial schwannopathy and peripheral myelinopathy in a rabbit model of dideoxycytidine neurotoxicity. Anderson T D; Davidovich A; Feldman D; Sprinkle T J; Arezzo J; Brosnan C; Calderon R O; Fossom L H; DeVries J T; **DeVries G H.** (Department of Toxicology and Pathology, Hoffmann-La Roche Inc., Nutley, New Jersey.) Laboratory investigation; a journal of technical methods and pathology, (1994 May) 70 (5) 724-39. Journal code: 0376617. ISSN: 0023-6837. Pub. country: United States. Language: English.

AB BACKGROUND: The reverse transcriptase **inhibitor**, 2',3'-dideoxycytidine (ddC), causes a dose-limiting peripheral neuropathy in humans, the mechanism of which is unknown. Rabbits given ddC develop peripheral myelinopathy and axonopathy, but it has not been determined if either the myelin or axonal changes are primary or if they occur concurrently. EXPERIMENTAL DESIGN: To characterize sequential development of the ddC-induced neuropathy, 40 rabbits were given either vehicle or ddC by oral intubation at a dose of 35 mg/kg per day for 24 weeks. Electrophysiologic studies, pathologic examination of peripheral and central nervous system and skeletal muscle, and biochemical analysis of the sciatic nerve were performed at baseline (electrophysiology only) and after 8, 12, 16, 20, and 24 weeks of treatment. RESULTS: Neuropathologic changes in peripheral nerves were first evident at 16 weeks and were more pronounced at 20 and 24 weeks; onset of paresis occurred at week 20, whereas clear electrophysiologic deficits were seen only at week 24. Electrophysiologic changes were prolonged F-waves (measure of proximal motor conduction) and minor changes in distal conduction measurements. Pathologic changes included myelin splitting, intramyelinic edema, demyelination, and remyelination of the largest diameter nerve fibers in the ventral root and sciatic nerve. Axonal degeneration and reduction in axonal diameter were seen. Enlarged mitochondria with abnormal ultrastructure were present in Schwann cells of those animals with a myelinopathy. Mitochondrial abnormalities or other signs of degeneration were not seen in neurons of the dorsal root ganglia or in skeletal muscle. Significant changes were not present in myelin protein composition, myelin lipid composition, or activity of the myelin-specific enzyme 2',3'-cyclic nucleotide 3'-phosphohydrolase. Major reductions in levels of protein zero (P0, the homophilic adhesion protein of myelin) were not seen; however, the turnover rate of P0 was reduced as P0 messenger RNA expression in ddC-treated sciatic nerves decreased to 30 to 50% of control values. CONCLUSIONS: The peripheral neuropathy caused by ddC in rabbits is characterized as a myelinopathy of the proximal portion of the nerve fibers and as an axonopathy involving both proximal and distal fibers. The myelinopathy was associated with enlarged and abnormally shaped mitochondria in Schwann cells and is consistent with an effect of ddC on structure and function of Schwann cell mitochondria. Altered Schwann cell

metabolism was evident by reduced levels of P0 messenger RNA, loss of homophilic myelin adhesion at the intraperiod line, and subsequent intramyelinic edema. Because axonal degeneration occurred concurrently with the myelin changes, it could not be determined if axonal changes were secondary to serve myelinic edema or if they represented a primary effect of ddC on neurons.

L17 ANSWER 10 OF 29 MEDLINE on STN

92015367. PubMed ID: 1656060. Calcium-activated neutral proteinase (CANP; calpain) activity in Schwann cells: immunofluorescence localization and compartmentation of mu- and mCANP. Banik N L; **DeVries G H**; Neuberger T; Russell T; Chakrabarti A K; Hogan E L. (Department of Neurology, Medical University of South Carolina, Charleston 29425.) Journal of neuroscience research, (1991 Jul) 29 (3) 346-54. Journal code: 7600111. ISSN: 0360-4012. Pub. country: United States. Language: English.

AB Calcium-activated neutral proteinase (CANP) activity was determined in cytosolic and membranous subcellular fractions of transformed Schwann cells (tSc). The muM and mM Ca(2+)-sensitive (mu- and mCANP) forms of CANP were separated by DEAE and phenyl Sepharose column chromatography, the latter step enabling removal of the endogenous **inhibitor** calpastatin. The tSc contained more muCANP than the mM isoform. More than 75% of mCANP activity was membrane-associated and 20% was cytosolic. In contrast, approximately 80% of muCANP was cytosolic and 15% was membranous. Triton X-100 stimulated activity of the whole homogenate and of the membrane pellet but did not stimulate CANP activity in the cytosolic fraction. Immunohistochemical distribution of mM enzyme was studied in both fixed and permeabilized tSc with cytosolic (anti-cyt-mCANP) and myelin (anti-my-mCANP) antibodies. Live cells (non-permeabilized) stained with anti-my-mCANP had a single filamentous ring circumscribing individual cells. Permeabilized cells treated with anti-my-mCANP had immunoreactive deposits throughout the intracellular space but sparing the perinuclear region. No immunohistochemical staining was detected when live cells were exposed to anti-cyt-mCANP whereas permeabilized cells had extensive intracellular staining with the most intense immunoreactivity in the perinuclear region. Our results indicate that both forms of CANP are present in tSc and that the activity of most of the muCANP is cytosolic while mCANP is particulate.

L17 ANSWER 11 OF 29 MEDLINE on STN

91073437. PubMed ID: 1979353. Properties of acetylcholinesterase in axolemma-enriched fractions isolated from bovine splenic nerve. Hannesson H H; **DeVries G H.** (Department of Biochemistry and Molecular Biophysics, Medical College of Virginia, Virginia Commonwealth University 23298-0614.) Journal of neuroscience research, (1990 Sep) 27 (1) 84-8. Journal code: 7600111. ISSN: 0360-4012. Pub. country: United States. Language: English.

AB The properties of acetylcholinesterase (AChE) in axolemma-enriched fractions (AEF) from bovine splenic nerve were investigated to see if they differed in any way from those of the AChE in diaphragm muscle. The axolemmal enzyme had a low Km for acetylthiocholine (ca. 90 microM), exhibited substrate inhibition, and had a well-defined optimum of substrate concentration of 1 mM. The rate of hydrolysis of substrate decreased with increasing acyl chain length (acetyl- greater than propionyl- greater than butyryl-). The AChE **inhibitors** eserine and hexamethonium were competitive **inhibitors** of the membrane-bound enzyme, whereas lidocaine was a noncompetitive **inhibitor**; these results were comparable to the effect of these **inhibitors** on diaphragm muscle AChE. The axolemmal enzyme was more efficiently solubilized and more stable in nonionic detergents such as Triton X-100 and Tween 20 than charged detergents such as lysolecithin and zwitterionic detergents. These results indicate that the AChE present in bovine splenic nerve AEF is identical to the previously characterized AChE from other sources.

L17 ANSWER 12 OF 29 MEDLINE on STN

89374890. PubMed ID: 2775530. Protein kinase C from chicken gizzard: characterization and detection of an **inhibitor** and endogenous substrates. **DeVries G**; Fraser E D; Walsh M P. (Department of Medical Biochemistry, Faculty of Medicine, University of Calgary, Alta., Canada.) Biochemistry and cell biology = Biochimie et biologie cellulaire, (1989 Jun) 67 (6) 260-70. Journal code: 8606068. ISSN: 0829-8211. Pub. country: Canada. Language: English.

AB Protein kinase C was purified from the cytosolic fraction of chicken gizzard by Ca2+ -dependent hydrophobic interaction chromatography, anion-exchange chromatography, and hydrophobic chromatography. The molecular weight was estimated as 61,500 by gel filtration and 80,000 by denaturing gel electrophoresis, indicating that the native enzyme is a monomer. Using the mixed micellar assay, with histone III-S as the substrate, protein kinase C required Ca2+, phospholipid, and diacylglycerol for activity, with half-maximal activation at approximately 5 x 10(-7) M Ca2+ in the presence of L-alpha-phosphatidyl-L-serine and 1,2-diolein. No activation by Ca2+ was observed in the absence of diacylglycerol. Protein kinase C requires free Mg2+, in addition to the MgATP2- substrate, for activity. The Km for ATP was determined to be 20 microM. Activity was sensitive to ionic strength, with half-maximal inhibition at 70 mM NaCl. Using the liposomal assay, phosphorylation of platelet P47 protein and smooth muscle vinculin was more strongly dependent on Ca2+ and lipids than was histone phosphorylation. Partial digestion of protein kinase C with trypsin yielded a constitutively active fragment. A heat-stable **inhibitor** and three major endogenous protein substrates of protein kinase C were also detected in chicken gizzard smooth muscle.

L17 ANSWER 13 OF 29 MEDLINE on STN

89215830. PubMed ID: 2540277. Role of intracellular pH in the axolemma- and myelin-induced proliferation of Schwann cells. Saunders R D; Brandon Y W; **DeVries G H.** (Department of Biochemistry and Molecular Biophysics, Virginia Commonwealth University, Medical College of Virginia, Richmond.) Journal of neurochemistry, (1989 May) 52 (5) 1576-81. Journal code: 2985190R. ISSN: 0022-3042. Pub. country: United States. Language: English.

AB In order to provide additional information on the biochemical events that interact to cause Schwann cells to proliferate, we have monitored the intracellular pH of Schwann cells that have been stimulated to divide with myelin-enriched fractions (MEF) or axolemma-enriched fractions (AEF). The intracellular pH of Schwann cells was monitored using 2',7'-bis(carboxymethyl)-5(6)-carboxyfluorescein (BCECF), which displays an increase in fluorescence upon alkalinization. Both AEF and MEF caused dose-dependent increases in the intracellular fluorescence of the Schwann cell cultures. At their maximum doses, AEF and MEF stimulation resulted in a 260 and 300% increase in intracellular fluorescence, respectively. The increase in intracellular fluorescence was abolished when cells were stimulated in Na+-free media, suggesting a role for the Na+/H+ exchanger. Mitotic stimulation required integrity of the Na+/H+ exchanger, as inhibition of the Na+/H+ exchanger for periods up to 1 h after addition of mitogen caused a significant inhibition of subsequent mitosis. Phorbol esters, which can potentiate AEF- and MEF-induced Schwann cell proliferation, increased intracellular fluorescence fivefold, an effect which was also dependent upon the presence of Na+ in the culture media. The specificity of the increase in intracellular pH for AEF and MEF was tested by incubating Schwann cells with liver microsomes and a biologically inactive phorbol alcohol, neither of which is significantly mitogenic for Schwann cells. Neither liver microsomes nor phorbol alcohol had a significant effect on intracellular pH. The implications of the increase in intracellular pH in Schwann cells with respect to inositol phospholipid metabolism, protein kinase C activation, and cellular proliferation are discussed.(ABSTRACT TRUNCATED AT 250 WORDS)

L17 ANSWER 14 OF 29 MEDLINE on STN

89139577. PubMed ID: 2918026. Cerebellar granule cells contain a membrane

mitogen for cultured Schwann cells. Mason P W; Bigbee J W; **DeVries G H.** (Department of Biochemistry and Molecular Biophysics, Medical College of Virginia, Virginia Commonwealth University, Richmond 23298.) Journal of cell biology, (1989 Feb) 108 (2) 607-11. Journal code: 0375356. ISSN: 0021-9525. Pub. country: United States. Language: English.

AB Proliferation of Schwann cells is one of the first events that occurs after contact with a growing axon. To further define the distribution and properties of this axonal mitogen, we have (a) cocultured cerebellar granule cells, which lack glial ensheathment in vivo with Schwann cells; and (b) exposed Schwann cell cultures to isolated granule cell membranes. Schwann cells cocultured with granule cells had a 30-fold increase in the labeling index over Schwann cells cultured alone, suggesting that the mitogen is located on the granule cell surface. Inhibition of granule cell proteoglycan synthesis caused a decrease in the granule cells' ability to stimulate Schwann cell proliferation. Membranes isolated from cerebellar granule cells when added to Schwann cell cultures caused a 45-fold stimulation in [3H]thymidine incorporation. The granule cell mitogenic signal was heat and trypsin sensitive and did not require lysosomal processing by Schwann cells to elicit its proliferative effect. The ability of granule cells and their isolated membranes to stimulate Schwann cell proliferation suggests that the mitogenic signal for Schwann cells is a ubiquitous factor present on all axons regardless of their ultimate state of glial ensheathment.

L17 ANSWER 15 OF 29 MEDLINE on STN

88061452. PubMed ID: 3681350. Morphological and proliferative responses of cultured Schwann cells following rapid phagocytosis of a myelin-enriched fraction. Bigbee J W; Yoshino J E; **DeVries G H.** (Department of Anatomy, Medical College of Virginia, Richmond 23298.) Journal of neurocytology, (1987 Aug) 16 (4) 487-96. Journal code: 0364620. ISSN: 0300-4864. Pub. country: ENGLAND: United Kingdom. Language: English.

AB Cultured Schwann cells were found to phagocytose exogenously applied myelin membranes within 1 h. However, the resulting proliferative response required an additional 9 h of incubation. Treatment with ammonium chloride, a lysosomal **inhibitor**, delayed the appearance of the proliferative response to the myelin membranes by 12 h. Processing of myelin within the Schwann cells was followed by the appearance of immunocytochemically detectable myelin basic protein which was first visible at 4 h. Similar to the proliferative response, the appearance of immunoreactive material was delayed by the addition of ammonium chloride. Schwann cells were observed initially to ingest myelin fragments at their distal-most tips after which time the myelin phagosomes collected in the perinuclear region and fused with lysosomes. Phagocytic Schwann cells had a notable increase in Golgi membranes and microfilaments and contained widely dilated, rough endoplasmic reticulum cisternae. In purified cell cultures, Schwann cells phagocytosed myelin slower than macrophages, but displayed phagocytic abilities much greater than fibroblasts. The ability of cultured Schwann cells to phagocytose myelin rapidly suggests that these cells may aid in the breakdown and removal of myelin during Wallerian degeneration. These data further confirm the mitogenic effect of myelin and its possible role during nerve regeneration.

L17 ANSWER 16 OF 29 MEDLINE on STN

86061756. PubMed ID: 3934342. Differential proliferative responses of cultured Schwann cells to axolemma and myelin-enriched fractions. II. Morphological studies. Meador-Woodruff J H; Yoshino J E; Bigbee J W; Lewis B L; **Devries G H.** Journal of neurocytology, (1985 Aug) 14 (4) 619-35. Journal code: 0364620. ISSN: 0300-4864. Pub. country: ENGLAND: United Kingdom. Language: English.

AB Axolemma-enriched and myelin-enriched fractions were prepared from bovine CNS white matter and conjugated to fluorescein isothiocyanate (FITC). Both unlabelled and FITC-labelled axolemma and myelin were mitogenic for cultured rat Schwann cells. Treatment of Schwann cells with the FITC-labelled mitogens for up to 24 h resulted in two distinct morphological appearances. FITC-myelin-treated cells were filled with

numerous round, fluorescent-labelled intracellular vesicles, while FITC-axolemma-treated cells appeared to be coated with a patchy, ill-defined fluorescence, primarily concentrated around the cell body but extending onto the cell processes. These observations were corroborated under phase microscopy. Electron microscopy revealed multiple, membrane-bound, membrane-containing phagosomes within myelin-treated cells and to a far lesser extent in axolemma-treated cells. The effect on the expression of the myelin-mediated and axolemma-mediated mitogenic signal when Schwann cells were treated with the lysosomal **inhibitors**, ammonium chloride and chloroquine, was evaluated. The mitogenicity of myelin was reduced 70-80% by these agents whereas the mitogenicity of axolemma was not significantly altered under these conditions. These results suggest that axolemma and myelin stimulate the proliferation of cultured Schwann cells by different mechanisms. Myelin requires endocytosis and lysosomal processing for expression of its mitogenic signal; in contrast, the mitogenicity of axolemma may be transduced at the Schwann cell surface.

L17 ANSWER 17 OF 29 MEDLINE on STN

85055166. PubMed ID: 6501427. Differential proliferative responses of cultured Schwann cells to axolemma- and myelin-enriched fractions. I. Biochemical studies. Yoshino J E; Dinneen M P; Lewis B L; Meador-Woodruff J H; **Devries G H.** Journal of cell biology, (1984 Dec) 99 (6) 2309-13. Journal code: 0375356. ISSN: 0021-9525. Pub. country: United States. Language: English.

AB Cultured rat Schwann cells were treated for 72 h with axolemma- and myelin-enriched fractions prepared from rat brainstem. [3H]Thymidine was added to the cultures 48 h before the termination of the experiment. Although, both fractions produced a dose-dependent uptake of label into Schwann cells, the shape of the dose response curves and rates at which [3H]thymidine was incorporated were different. The axolemma-enriched fraction produced a sigmoid dose response curve with a Hill coefficient of 2.05. The dose response curve for myelin rose sharply and saturated at a level that was approximately 50% of the maximal response observed with axolemma. Schwann cells that had been treated with axolemma exhibited little change in the rate of [3H]thymidine incorporation from 36-72 h after the addition of the membranes. In contrast, Schwann cells accumulated label three times faster during the 48-72-h period following the addition of myelin to the cultures when compared with the rate during the preceding 12-h interval. Furthermore, the mitogenic activity of the myelin-enriched fraction was decreased by the addition of ammonium chloride, a lysosomal **inhibitor**, whereas the activity of the axolemmal fraction was not impaired.

L17 ANSWER 18 OF 29 MEDLINE on STN

84256813. PubMed ID: 6331451. Cyclic AMP and calcium as potential mediators of stimulation of cultured Schwann cell proliferation by axolemma-enriched and myelin-enriched membrane fractions. Meador-Woodruff J H; Lewis B L; **DeVries G H.** Biochemical and biophysical research communications, (1984 Jul 18) 122 (1) 373-80. Journal code: 0372516. ISSN: 0006-291X. Pub. country: United States. Language: English.

AB The roles of cyclic AMP and calcium in the transduction of the mitogenic effects of central nervous system axolemma and myelin-enriched fractions on cultured Schwann cells were examined. Cyclic AMP levels were not elevated in axolemma or myelin-stimulated Schwann cells, but were increased when stimulated with cholera toxin, an adenyl cyclase activator. The mitogenicity of axolemma and myelin was markedly reduced by 2.5 mM citrate, a calcium chelator, and 10 uM trifluoroperazine, an **inhibitor** of calmodulin. Treatment of Schwann cells with several tumor-promoting phorbol esters caused significant enhancement of the mitogenicity of the axolemma and myelin preparations. These data suggest that the mitogenic effects of axolemma and myelin are not mediated by cyclic AMP, but may be mediated by calcium ions.

L17 ANSWER 19 OF 29 MEDLINE on STN

72235910. PubMed ID: 4339795. 3-Hydroxy-N-acetylneuraminic acid: synthesis and inhibitory properties. **DeVries G H**; Binkley S B. Archives of biochemistry and biophysics, (1972 Jul) 151 (1) 243-50. Journal code: 0372430. ISSN: 0003-9861. Pub. country: United States. Language: English.

L17 ANSWER 20 OF 29 MEDLINE on STN
72235909. PubMed ID: 4339794. N-acetylneuraminic acid aldolase of Clostridium perfringens: purification, properties and mechanism of action. **DeVries G H**; Binkley S B. Archives of biochemistry and biophysics, (1972 Jul) 151 (1) 234-42. Journal code: 0372430. ISSN: 0003-9861. Pub. country: United States. Language: English.

L17 ANSWER 21 OF 29 EMBASE on STN
90280482 EMBASE Document No.: 1990280482. Regulation of cyclic AMP levels in mammalian retina: Effects of depolarizing agents and transmitters. Blazynski C.; **DeVries G.**; Geary K.; Cohen A.I.; Ferrendelli J.A.. Deptartment of Biochemistry, Box 8231 Washington Univ., School of Medicine, 660 S. Euclid,St. Louis, MO 63110, United States. Neurochemistry International Vol. 17, No. 3, pp. 425-433 1990.
ISSN: 0197-0186. CODEN: NEUIDS
Pub. Country: United Kingdom. Language: English. Summary Language: English.
ED Entered STN: 911213
AB Cellular depolarization in brain results in a modulation of cAMP levels by releasing neurotransmitters having receptors linked via GTP-binding proteins to adenylate cyclase. In order to determine the transmitters regulating cAMP during cellular depolarization in mammalian retina, the modulation of cAMP by depolarizing media was investigated. Cyclic AMP levels in light adapted retinas increased following exposure to depolarizing media, but levels in dark adapted retinas remained unaltered. The depolarization-induced modulation of cAMP levels persisted in dystrophic retinas, suggesting that the response occurred in the inner retina. In microdissected discrete retinal layers from rabbit, levels of cAMP were increased following perfusion with depolarizing medium in the outer plexiform and inner nuclear layers, consistent with the observation seen with mouse retinas. To begin to identify transmitters released by cellular depolarization, a variety of transmitters and/or antagonists were included in the incubation medium. Haloperidol reduced the depolarization induced increase in cAMP levels by 25% in normal mouse retinas, and 75% in dystrophic retinas. Dopamine elevated cAMP levels in normal and dystrophic mouse retinas, and when combined with depolarizing medium, additive increases were observed. The effects of various neurotransmitters on retinal cAMP levels in the absence of any phosphodiesterase **inhibitors** were assessed, and both dopamine and norepinephrine were found to increase cAMP levels in normal and dystrophic retinas. Phentolamine antagonized the increase elicited by norepinephrine. When dopamine and norepinephrine were combined non-additive increases were observed. Serotonin, GABA, acetylcholine, histamine and adenosine had little or no significant effect on the retinal levels of cAMP in either normal or dystrophic mouse retinas. These results indicate that depolarizing media increase cAMP levels partially by releasing dopamine. The processes regulating cAMP levels in retina are both different and similar to those in brain.

L17 ANSWER 22 OF 29 BIOSIS on STN
2002:3972 Document No.: PREV200200003972. Elevated prostaglandin release from degenerating sciatic nerve explants: Contribution of cyclooxygenase 2. Muja, N. [Reprint author]; **DeVries, G. H.** [Reprint author]. Neuroscience Program, Loyola University of Chicago, Maywood, IL, USA. Society for Neuroscience Abstracts, (2001) Vol. 27, No. 2, pp. 2387. print.
Meeting Info.: 31st Annual Meeting of the Society for Neuroscience. San Diego, California, USA. November 10-15, 2001.

ISSN: 0190-5295. Language: English.

AB Schwann cells express prostanoid receptors coupled to the cAMP mediated signaling cascade. To identify physiologic sources of prostanoids for Schwann cells, we determined the extent of prostaglandin release from explants of sciatic nerve. PGE2 and PGI2 levels in the conditioned medium of sciatic nerve explants increased rapidly between 18 and 24 hours and remained elevated for up to 96 hours. Medium from primary Schwann cells and perineural fibroblasts treated with arachidonic acid (0.001-1 muM) also contained significant levels of both PGE2 and PGI2. The production of PGE2 and PGI2 by sciatic nerve explants and primary cultured cells was inhibited by the COX-2 specific **inhibitor** NS-398 (EC50=5 nM). Compared to medium from quiescent macrophages, medium from macrophages cultured in the presence of adult sciatic nerve explants contained significant amounts of PGE2 whereas the level of PGI2 production was not changed. Similar trends in PGE2 and PGI2 production were observed following treatment of cultured macrophages with conditioned medium from either primary Schwann cells or perineural fibroblasts. In contrast, macrophages treated with a homogenate of adult sciatic nerve (1-25 mug/ml) did not produce significant levels of either PGE2 or PGI2 over the entire course of treatment. We conclude that Schwann cells and perineural fibroblasts are significant physiologic sources of prostanoids within 24 hours of traumatic peripheral nerve injury and that recruited macrophages may be a secondary source of prostanoids, particularly PGE2, at the injury site.

L17 ANSWER 23 OF 29 BIOSIS COPYRIGHT (c) 2005 The Thomson Corporation on STN

1997:527109 Document No.: PREV199799826312. Effects of the serotonin reuptake **inhibitor** fluoxetine on social behaviors in male and female prairie voles. Villalba, C.; Boyle, P. A.; **Devries, G. J.**. Neuroscience Behavior Program, Dep. Psychology, Univ. Mass., Amherst, MA 01003-7710, USA. Society for Neuroscience Abstracts, (1997) Vol. 23, No. 1-2, pp. 1087.
Meeting Info.: 27th Annual Meeting of the Society for Neuroscience. New Orleans, Louisiana, USA. October 25-30, 1997.
ISSN: 0190-5295. Language: English.

L17 ANSWER 24 OF 29 BIOSIS COPYRIGHT (c) 2005 The Thomson Corporation on STN

1991:434396 Document No.: PREV199192090561; BA92:90561. CALCIUM-ACTIVATED NEUTRAL PROTEINASE CANP CALPAIN ACTIVITY IN SCHWANN CELLS IMMUNOFLUORESCENCE LOCALIZATION AND COMPARTMENTATION OF MU-CANP AND MCANP. BANIK N L [Reprint author]; **DEVRIES G H**; NEUBERGER T; RUSSELL T; CHAKRABARTI A K; HOGAN E L. MED UNIV SC, DEP NEUROL, 171 ASHLEY AVE, CHARLESTON, SC 29425, USA. Journal of Neuroscience Research, (1991) Vol. 29, No. 3, pp. 345-354.
CODEN: JNREDK. ISSN: 0360-4012. Language: ENGLISH.

AB Calcium-activated neutral proteinase (CANP) activity was determined in cytosolic and membranous subcellular fractions of transformed Schwann cells (tSc). The μM and mM Ca2+-sensitive (μ- and mCANP) forms of CANP were separated by DEAE and phenyl Sepharose column chromatography, the latter step enabling removal of the endogenous **inhibitor** calpastatin. The tSc contained more μCANP than the mM isoform. More than 75% of mCANP activity was membrane-associated and 20% was cytosolic. In contrast, approximately 80% of μCANP was cytosolic and 15% was membranous. Triton X-100 stimulated activity of the whole homogenate and of the membrane pellet but did not stimulate CANP activity in the cytosolic fraction. Immunohistochemical distribution of mM enzyme was studied in both fixed and permeabilized tSc with cytosolic (anti-cyt-mCANP) and myelin (anti-my-mCANP) antibodies. Live cells (non-permeabilized) stained with anti-my-mCANP had a single filamentous ring circumscribing individual cells. Permeabilized cells treated with anti-my-mCANP had immunoreactive deposits throughout the intracellular space but sparing the perinuclear region. No immunohistochemical staining was detected when live cells were exposed to anti-cyt-mCANP whereas

permeabilized cells had extensive intracellular staining with the most intense immunoreactivity in the perinuclear region. Our results indicate that both forms of CANP are present in tSc and that the activity of most of the μCANP is cytolic while mCANP is particulate.

L17 ANSWER 25 OF 29 BIOSIS COPYRIGHT (c) 2005 The Thomson Corporation on STN

1990:257857 Document No.: PREV199038124445; BR38:124445. **INHIBITORS** OF CALCIUM MOBILIZATION ARE POTENTIAL **INHIBITORS** OF EPIDERMAL DIFFERENTIATION. TONG P [Reprint author]; LEE G; **DEVRIES G**; SYAGE E; CHANDRARATNA R; GARST M; WHEELER L. ALLERGEN INC/HERBERT LABS, IRVINE, CALIF, USA. Journal of Investigative Dermatology, (1990) Vol. 94, No. 4, pp. 585.
Meeting Info.: EUROPEAN SOCIETY FOR DERMATOLOGICAL RESEARCH (ESDR), JAPANESE SOCIETY FOR INVESTIGATIVE DERMATOLOGY (JSID) AND SOCIETY FOR INVESTIGATIVE DERMATOLOGY (SID) TRICONTINENTAL MEETING, WASHINGTON, D.C., USA, MAY 2-5, 1990. J INVEST DERMATOL.
CODEN: JIDEAE. ISSN: 0022-202X. Language: ENGLISH.

L17 ANSWER 26 OF 29 SCISEARCH COPYRIGHT (c) 2005 The Thomson Corporation on STN

1991:561628 The Genuine Article (R) Number: GJ048. AGN 190383, A NOVEL PHOSPHOLIPASE **INHIBITOR** WITH TOPICAL ANTIINFLAMMATORY ACTIVITY. **DEVRIES G W (Reprint)**; LEE G; AMDAHL L; WENZEL M; GARST M; WHEELER L A. ALLERGAN PHARMACEUT INC, DEPT BIOL SCI, 2525 DUPONT DR, IRVINE, CA 92715 (Reprint); ALLERGAN PHARMACEUT INC, DEPT CHEM SCI, 2525 DUPONT DR, IRVINE, CA 92715. AGENTS AND ACTIONS (SEP 1991) Vol. 34, No. 1-2, pp. 70-72. ISSN: 0065-4299. Publisher: BIRKHAUSER VERLAG AG, PO BOX 133 KLOSTERBERG 23, CH-4010 BASEL, SWITZERLAND. Language: English.
ABSTRACT IS AVAILABLE IN THE ALL AND IALL FORMATS

AB AGN 190383 is a 5-hydroxy-2(5H)-furanone ring analog of the marine natural product manoalide. When applied topically, AGN 190383 inhibits phorbol ester induced mouse ear edema. It is a potent **inhibitor** of bee venom phospholipase A2 and blocks the release of arachidonic acid from calcium ionophore A23187 stimulated human neutrophils. AGN 190383 also inhibits both hormone-operated and depolarization-dependent calcium mobilization in GH3 cells, as well as fMLP stimulated increases in free cytosolic calcium in human PMNs. Furthermore, it is also able to block the release of the neutral protease elastase from stimulated neutrophils. The effects of AGN 190383 on arachidonic acid metabolism and leukocyte function may account, in part, for its anti-inflammatory activity in vivo.

L17 ANSWER 27 OF 29 SCISEARCH COPYRIGHT (c) 2005 The Thomson Corporation on STN

1990:231073 The Genuine Article (R) Number: CZ244. **INHIBITORS** OF CALCIUM MOBILIZATION ARE POTENTIAL **INHIBITORS** OF EPIDERMAL DIFFERENTIATION. TONG P (Reprint); LEE G; **DEVRIES G**; SYAGE E; CHANDRARATNA R; GARST M; WHEELER L. ALLERGAN PHARMACEUT INC, HERBERT LABS, IRVINE, CA. CLINICAL RESEARCH (APR 1990) Vol. 38, No. 2, pp. A668-A668. ISSN: 0009-9279. Publisher: SLACK INC, 6900 GROVE RD, THOROFARE, NJ 08086. Language: English.

L17 ANSWER 28 OF 29 CAPLUS COPYRIGHT 2005 ACS on STN

2004:652623 Document No. 141:150978 Method of inhibiting angiogenesis and neuroblastoma growth with α and β isoforms of neu differentiation factor (NDF α and NDF β). **DeVries, George H.**; Crawford, Susan E. (U. S. Department of Veterans Affairs, USA). U.S. Pat. Appl. Publ. US 2004157770 A1 20040812, 10 pp. (English).
CODEN: USXXCO. APPLICATION: US 2003-360720 20030210.

AB The invention relates to the inhibition of angiogenesis and neuroblastoma growth. In particular, the invention relates to the treatment of angiogenesis-dependent and angiogenesis-associated diseases, such as neural crest-derived tumors, using the α and β isoforms of neu differentiation factor (NDF), which have the following effects: (1) prevention of blood vessel formation; (2) induction of differentiation of

neuroblastoma cells, which prevents proliferation and stops tumor growth; and (3) induction of programmed cell death (apoptosis) in neuroblastoma cells, which further inhibits tumor growth.

L17 ANSWER 29 OF 29 CAPLUS COPYRIGHT 2005 ACS on STN
1977:5870 Document No. 86:5870 Analysis and purification of 2-hydroxyethyl methacrylate by means of thin-layer chromatography. Brinkman, U. A. T.; Van Schaik, T. A. M.; **DeVries, G.**; DeVisser, A. C. (Dep. Anal. Chem., Free Reformed Univ., Amsterdam, Neth.). ACS Symposium Series, 31(Hydrogels Med. Relat. Appl., Symp., 1975), 105-18 (English) 1976. CODEN: ACSMC8. ISSN: 0097-6156.
AB Thin layer chromatog. was used for anal. and small-scale preparation of 2-hydroxyethyl methacrylate [868-77-9] on SiO2 gel with hexane-Et2O or hexane-MIBK-octanol saturated with 25% HNO3 as the mobile phase. The preparative work was performed on the H2SO4-impregnated SiO2 gel and developed with hexane-Et2O. **Inhibitors** were detected by thin layer chromatog. and a drop test procedure using diazotized sulfanilic acid.

=>

---Logging off of STN---

=>
Executing the logoff script...

=> LOG Y

COST IN U.S. DOLLARS	SINCE FILE ENTRY	TOTAL SESSION
FULL ESTIMATED COST	172.31	172.52

DISCOUNT AMOUNTS (FOR QUALIFYING ACCOUNTS)	SINCE FILE ENTRY	TOTAL SESSION
CA SUBSCRIBER PRICE	-5.84	-5.84

STN INTERNATIONAL LOGOFF AT 09:50:16 ON 12 AUG 2005